Eur. Phys. J. C (2026) 86:470
https://doi.org/10.1140/epjc/s10052-026-15311-0

THE EUROPEAN PHYSICAL JOURNAL C

Regular Article - Experimental Physics

Precise measurement of the $t\bar{t}$ production cross-section and lepton differential distributions in $e\mu$ dilepton events from $\sqrt{s} = 13$ TeV pp collisions with the ATLAS detector

ATLAS Collaboration[*]

CERN, 1211 Geneva 23, Switzerland

Received: 19 September 2025 / Accepted: 13 January 2026

Abstract The inclusive top quark pair ($t\bar{t}$) cross-section $\sigma_{t\bar{t}}$ has been measured in proton–proton collisions at $\sqrt{s} = 13$ TeV, using 140 fb^{-1} of data collected by the ATLAS experiment at the Large Hadron Collider. Using events with an opposite-charge $e\mu$ pair and b-tagged jets, the cross-section is measured to be:

$\sigma_{t\bar{t}} = 829.3 \pm 1.3\,\text{(stat)} \pm 8.0\,\text{(syst)} \pm 7.3\,\text{(lumi)} \pm 1.9\,\text{(beam)}$ pb,

where the uncertainties reflect the limited size of the data sample, experimental and theoretical systematic effects, the integrated luminosity, and the proton beam energy, giving a total uncertainty of 1.3%. The result is used to determine the top quark pole mass via the dependence of the predicted cross-section on m_t^{pole}, giving $m_t^{\text{pole}} = 172.8^{+1.5}_{-1.7}$ GeV. The same event sample is used to measure absolute and normalised differential cross-sections for the $t\bar{t} \to e\mu\nu\bar{\nu}b\bar{b}$ process as a function of single-lepton and dilepton kinematic variables. Complementary measurements of $e\mu b\bar{b}$ production, treating both $t\bar{t}$ and Wt events as signal, are also provided. Both sets of differential cross-sections are compared to the predictions of various Monte Carlo event generators, demonstrating that the state-of-the-art generators POWHEG MiNNLO and POWHEG *bb4l* describe the data better than POWHEG hvq.

Contents

1 Introduction

The study of top quark-antiquark ($t\bar{t}$) production at the CERN Large Hadron Collider (LHC) allows quantum chromodynamics (QCD) to be probed at some of the highest accessible energy scales, and forms a key part of the experimental programme of the ATLAS experiment [1]. The large mass of the top quark, close to the scale of electroweak symmetry breaking, gives it a unique role in the Standard Model of particle physics, and $t\bar{t}$ production is also a significant background in many searches for physics beyond the Standard Model. Precise measurements of absolute $t\bar{t}$ production rates and differential distributions are therefore vital to fully exploit the discovery potential of the LHC, and to refine theoretical predictions and QCD calculational tools.

The inclusive $t\bar{t}$ production cross-section $\sigma_{t\bar{t}}$ in proton–proton (pp) collisions has been calculated at next-to-next-to-leading-order (NNLO) accuracy in the strong coupling constant α_s, including the resummation of next-to-next-to-

[*] e-mail: atlas.publications@cern.ch

Published online: 05 May 2026

leading-logarithmic (NNLL) soft gluon terms [2–7]. The predictions are in excellent agreement with measurements from ATLAS and CMS at centre-of-mass energies $\sqrt{s}$ from 5.02 TeV to 13.6 TeV [8–20]. At $\sqrt{s} = 13$ TeV, assuming a fixed top quark mass of $m_t = 172.5$ GeV, the NNLO+NNLL prediction calculated by the `Top++ 2.0` program [21] is $834 \pm 21^{+21}_{-30}$ pb, i.e. a total uncertainty of $^{+3.5}_{-4.4}$%. The first uncertainty component of the prediction corresponds to parton distribution function (PDF) uncertainties evaluated using the PDF4LHC21 [22] combination of the CT18 [23], MSHT20 [24] and NNPDF3.1 [25] PDF sets. The second represents QCD renormalisation (μ_R) and factorisation (μ_F) scale uncertainties as a proxy for unknown higher-order corrections, evaluated from the envelope of predictions with independent variations of μ_R and μ_F up and down by factors of two from default values of $\mu_R = \mu_F = m_t$, whilst never letting them differ by more than a factor of two [26,27]. The predicted cross-section also depends strongly on m_t, decreasing by 2.7% for a 1 GeV increase in the top quark mass. The mass parameter in the cross-section prediction is the top quark pole mass m_t^{pole}, corresponding to the definition of the mass of a free particle, and allowing $\sigma_{t\bar{t}}$ to be interpreted as a measurement of m_t^{pole}, free of the ambiguities linked to the direct reconstruction of the invariant mass of its decay products [28–31].

In the Standard Model, 99.8% of top quark decays are to a W boson and b-quark [32], making the final-state topologies in $t\bar{t}$ production dependent on the W boson decay modes. The $e^+\mu^-$ dilepton channel[1] ($t\bar{t} \to W^+bW^-\bar{b} \to e^+\mu^-\nu\bar{\nu}b\bar{b}$) with one or two jets tagged as likely to contain b-hadrons (b-tagged), has been exploited to make increasingly precise ATLAS measurements of $\sigma_{t\bar{t}}$ at $\sqrt{s} = 13$ TeV using progressively larger data samples [33,34], culminating in a measurement using the full 140 fb^{-1} dataset that achieved an uncertainty of 1.8% [12]. The same-flavour dilepton channels ($t\bar{t} \to e^+e^-\nu\bar{\nu}b\bar{b}$ and $t\bar{t} \to \mu^+\mu^-\nu\bar{\nu}b\bar{b}$) in that dataset were used to make a precise test of lepton flavour universality in $W \to e\nu$ and $W \to \mu\nu$ decays [35]. This paper reports a further measurement of $\sigma_{t\bar{t}}$ using the full $\sqrt{s} = 13$ TeV dataset, profiting from the precise calibration of lepton efficiencies used in Ref. [35], together with recent improvements in the modelling of lepton kinematics in $t\bar{t}$ events using the MiNNLO$_{\text{PS}}$ procedure [36] for the computation of $t\bar{t}$ production at NNLO matched to parton shower simulation. The resulting measurement is also used to extract an updated value for m_t^{pole}.

The $e\mu$ + b-tagged jets sample also enables precise measurements of the differential distributions of the leptons produced in $t\bar{t}$ events ($t\bar{t} \to e\mu$). A set of eight one-dimensional and three two-dimensional distributions was measured at $\sqrt{s} = 8$ TeV [37] and with a partial $\sqrt{s} = 13$ TeV sample [34], and a slightly different set of distributions was measured with the full $\sqrt{s} = 13$ TeV dataset [12]. This paper presents more precise measurements of the distributions studied in Ref. [34], namely the absolute and normalised differential cross-sections as functions of the transverse momentum p_{T}^{ℓ} and absolute rapidity $|\eta^{\ell}|$ of the single leptons[2] (combined for electrons and muons), the p_{T}, invariant mass and absolute rapidity of the $e\mu$ system ($p_{\text{T}}^{e\mu}$, $m^{e\mu}$ and $|y^{e\mu}|$), the absolute azimuthal angle $\Delta\phi^{e\mu}$ between the two leptons in the transverse plane, and the scalar sums of the transverse momenta ($p_{\text{T}}^{e} + p_{\text{T}}^{\mu}$) and energies ($E^e + E^{\mu}$) of the two leptons. This set of distributions was shown to have sensitivity to the gluon PDF and m_t^{pole} [37]. Two-dimensional distributions of $|\eta^{\ell}|$, $|y^{e\mu}|$ and $\Delta\phi^{e\mu}$ as functions of $m^{e\mu}$ are also measured, and the single-lepton p_{T}^{ℓ} values are used to form distributions $p_{\text{T}}^{\ell,\text{max}}$ and $p_{\text{T}}^{\ell,\text{min}}$ of the maximum and minimum lepton p_{T} in each event. All these distributions are defined without making any requirements on jets or b-jets. The distributions are compared with the predictions from various next-to-leading-order (NLO) $t\bar{t}$ matrix element generators combined with parton showers, as well as the MiNNLO$_{\text{PS}}$ approach.

In kinematic regions with high lepton p_{T}, the differential cross-section measurements are limited by uncertainties due to the interference that occurs at NLO between $t\bar{t}$ and Wt, the associated production of a W boson and a top quark, which can both lead to $WbW\bar{b}$ and hence $e\mu b\bar{b}$ final states [38–41]. Such final states receive contributions from both $t\bar{t}$-like (doubly resonant) and Wt (singly resonant) processes. A second set of lepton differential cross-sections are measured in this paper by considering the $e\mu b\bar{b}$ final state as the signal region, explicitly requiring the presence of two b-tagged jets. The same set of leptonic differential cross-sections as for $t\bar{t} \to e\mu$ production are measured using this signal region, and compared with the sum of predictions for $t\bar{t}$ and Wt production, and to predictions from the $bb4l$ generator for the full NLO $pp \to \ell^+\ell^-\nu\bar{\nu}b\bar{b}$ process matched to parton showers [42]. These measurements of leptonic distributions are complementary to those also involving the jet kinematics described in Ref. [43].

The event selection, analysis methodology and uncertainty evaluation for the inclusive, $t\bar{t} \to e\mu$ differential and $e\mu b\bar{b}$ differential cross-section measurements are similar.

[1] Charge-conjugate decay modes are implied unless otherwise stated.

[2] ATLAS uses a right-handed coordinate system with its origin at the nominal interaction point in the centre of the detector, and the z axis along the beam line. Pseudorapidity is defined in terms of the polar angle θ as $\eta = -\ln\tan\theta/2$, and transverse momentum and energy are defined relative to the beam line as $p_{\text{T}} = p\sin\theta$ and $E_{\text{T}} = E\sin\theta$. The azimuthal angle around the beam line is denoted by ϕ, and distances in (η, ϕ) space by $\Delta R = \sqrt{(\Delta\eta)^2 + (\Delta\phi)^2}$. The rapidity is defined as $y = \frac{1}{2}\ln\left(\frac{E+p_z}{E-p_z}\right)$, where p_z is the z-component of the momentum and E is the energy of the relevant object or system.

The data and Monte Carlo simulation samples are described in Sect. 2, followed by the event reconstruction and selection in Sect. 3. The measurement techniques are discussed in Sect. 4 and the evaluation of systematic uncertainties in Sect. 5. Inclusive cross-section results are given in Sect. 6, together with the determination of m_t^{pole}. Section 7 presents the $t\bar{t} \to e\mu$ and $e\mu b\bar{b}$ differential cross-section results and comparisons with the predictions of various event generators. Finally, conclusions are drawn in Sect. 8.

2 Data and simulated event samples

The ATLAS detector [44–46] at the LHC covers nearly the entire solid angle around the collision point. It consists of an inner tracking detector surrounded by a thin superconducting solenoid producing a 2T axial magnetic field, electromagnetic and hadronic calorimeters, and an external muon spectrometer incorporating three large toroidal magnet assemblies. The analysis was performed on samples of pp collision data collected at $\sqrt{s} = 13$ TeV in 2015–18, corresponding to an integrated luminosity of $140.1 \pm 1.2\,\text{fb}^{-1}$ after data quality requirements [47,48]. Events were required to satisfy a single-electron or single-muon trigger [49,50], with transverse momentum thresholds that were progressively raised during the data-taking period. The electron trigger reached the efficiency plateau region for electrons with reconstructed $p_{\text{T}} > 25$ GeV in 2015 and for $p_{\text{T}} > 27$ GeV in 2016–18. The corresponding thresholds for the muon trigger are 21 GeV for 2015 and 27.3 GeV thereafter. Each recorded event also includes the signals from on average 33 superimposed inelastic pp collisions, referred to as pileup.

Monte Carlo simulated event samples were used to develop the analysis procedures, to evaluate signal and background contributions, and to compare with data. Samples were processed using either the full ATLAS detector simulation [51] based on GEANT4 [52], or with a faster simulation making use of parameterised showers in the calorimeters [53]. The effects of pileup were simulated by generating additional inelastic pp collisions with PYTHIA8 (v8.186) [54] using the A3 set of parameter values (tune) [55] and overlaying them on the primary simulated events, so as to match the distribution of the number of inelastic events per bunch crossing observed in the data. These combined events were then processed using the same reconstruction and analysis chain as the data [56]. Small corrections were applied to lepton and jet energy scales [57–59], and to lepton and b-tagging efficiencies [60–62], to improve agreement with the response observed in data. Further topology-specific lepton isolation corrections were applied as discussed in Sect. 5.2.

The baseline simulated $t\bar{t}$ sample was generated using the MiNNLO$_{\text{PS}}$ matched NNLO QCD plus parton shower procedure [36], implemented in POWHEG [63–65] with the settings $p_{\text{T,hard}} = 0$ and $p_{\text{T,def}} = 2$ [66,67], using the NNPDF3.0 PDF set [68] in the matrix element and interfaced to PYTHIA8.312 with the A14 tune [69] and NNPDF2.3 PDF set [70] for the parton shower, hadronisation and underlying event modelling. The QCD renormalisation and factorisation scales were set to $\mu_R = \mu_F = H_{\text{T}}^{t\bar{t}}/4$, where $H_{\text{T}}^{t\bar{t}}$ is the sum of the transverse masses ($\sqrt{(m_t^2 + p_{\text{T},t}^2)}$) of the top quark and antiquark. This sample, referred to hereafter as POWHEG MiNNLO+PYTHIA8, predicts a softer top quark p_{T} spectrum in $t\bar{t}$ events than the standard samples based on the NLO `hvq` process in POWHEG BOX v2 [71] interfaced to PYTHIA8 used for the previous $\sqrt{s} = 13$ TeV analyses [12,34], and predicts a lepton p_{T} spectrum closer to that seen in data. For comparisons with data and to study systematic uncertainties, a POWHEG+PYTHIA8 $t\bar{t}$ simulation sample was generated using the `hvq` process, with nominal settings of $p_{\text{T,hard}} = 0$ and the h_{damp} parameter, which gives a cut-off scale for the first gluon emission, set to $h_{\text{damp}} = \frac{3}{2}m_t$ [41]. The renormalisation and factorisation scales were set to the top quark transverse mass. Variations of this sample were generated with $p_{\text{T,hard}} = 1$, with $h_{\text{damp}} = 3m_t$, and using HERWIG 7.1.3 [72,73] instead of PYTHIA8 for the parton shower, hadronisation and underlying event. Further variations were obtained from the POWHEG MiNNLO+PYTHIA8 and nominal POWHEG+PYTHIA8 samples by using event weights to change the QCD renormalisation and factorisation scales, the amounts of initial and final state radiation, and the PDF. In all samples, the top quark mass was set to $m_t = 172.5$ GeV, the $W \to \ell\nu$ branching ratio to the Standard Model prediction of 0.1082 for each lepton flavour (e, μ and τ) [74], and EVTGEN [75] was used to handle the decays of b- and c-flavoured hadrons.

The measured $e\mu b\bar{b}$ cross-sections were also compared with a sample generated with the POWHEG $bb4l$ generator [42], which includes the complete set of $\ell\ell'\nu\bar{\nu}b\bar{b}$ final states, taking into account interference between the $t\bar{t}$ and Wt final states as well as off-shell and non-resonant effects. This sample uses the POWHEG BOX RES framework [76], with matrix elements at NLO in QCD, and resonance-aware matching to the parton shower [77,78], with QCD scales and other configuration parameters set as described in Ref. [43].

Backgrounds in the $\sigma_{t\bar{t}}$ inclusive and $t\bar{t} \to e\mu$ differential cross-section measurements are classified into two types: those with two real prompt leptons (electrons or muons, including those produced via leptonic decays of τ-leptons), and those where at least one of the reconstructed leptons is misidentified, i.e. a non-prompt lepton from the decay of a bottom or charm hadron, an electron from a photon conversion, a hadronic jet misidentified as an electron, or a muon produced from the decay in flight of a pion or kaon. The

background with two real prompt leptons is dominated by Wt production, modelled using POWHEG + PYTHIA8 with the same settings as the corresponding POWHEG hvq $t\bar{t}$ sample. The renormalisation and factorisation scales were set to the dynamic scales $\mu_R = \mu_F = H_T/2$ where H_T is the scalar sum of the p_T of all outgoing partons, giving a better description of data [79] than that obtained from the fixed scales $\mu_R = \mu_F = m_t$ used in previous analyses [12,34]. The interference between $t\bar{t}$ and Wt was modelled using the diagram removal scheme [38,80]. The Wt cross-section was taken to be 79.3 ± 2.2 (PDF) $^{+1.9}_{-1.8}$ (QCD scale) pb, based on an NLO calculation with the addition of third-order corrections resumming NNLL soft gluon contributions [81]. The Wt contribution is part of the signal for the $e\mu b\bar{b}$ cross-section measurement.

In all three measurements, smaller backgrounds with two prompt leptons arise from $Z \to \tau\tau(\to e\mu)$+jets, and from diboson production (WW, WZ and ZZ) in association with jets. The Z+jets background was modelled with SHERPA 2.2.11 [82] for $Z \to ee/\mu\mu$ and SHERPA 2.2.14 for $Z \to \tau\tau$, with NLO matrix elements for up to two partons, and leading-order matrix elements for up to five partons, calculated with the COMIX [83] and OPENLOOPS [84] libraries and matched with the SHERPA parton shower [85] using the MEPS@NLO prescription [86–89]. They were generated using the NNPDF3.0 PDF set and normalised to an NNLO cross-section prediction [90]. Diboson production was simulated using SHERPA 2.2.2 using a similar approach. Production of $t\bar{t}$ in association with a leptonically decaying W, Z or Higgs boson, or an additional $t\bar{t}$ pair, gives a negligible contribution to the opposite-charge dilepton samples, but is significant in the same-charge control samples used to assess the background from misidentified leptons. These processes were modelled at NLO using POWHEG + PYTHIA8, or MADGRAPH5_AMC@NLO (referred to hereafter as AMC@NLO) [91] interfaced to PYTHIA8.

Backgrounds with one real and one misidentified lepton arise from $t\bar{t}$ events with one leptonically decaying and one hadronically decaying W, simulated with POWHEG MiNNLO + PYTHIA8. Similar backgrounds arise from W+jets production, modelled with SHERPA 2.2.11 as for Z+jets, and t-channel single top production, modelled with POWHEG + PYTHIA8. Other backgrounds, including processes with two misidentified leptons, are negligible after the event selections used in the analysis.

3 Event reconstruction and selection

This analysis makes use of reconstructed electrons, muons and b-tagged jets. Electron candidates were reconstructed from a localised cluster of energy deposits in the electromagnetic calorimeter matched to a track in the inner detector, passing the 'Medium' likelihood-based requirement of Ref. [57]. They were required to have transverse momentum $p_T > 20$ GeV and pseudorapidity $|\eta| < 2.47$, excluding the transition region between the barrel and endcap electromagnetic calorimeters, $1.37 < |\eta| < 1.52$, and to be consistent with originating from the signal primary vertex. The latter was defined as the reconstructed vertex with the highest sum of p_T^2 of associated tracks. To reduce background from non-prompt electrons, electron candidates were further required to pass the 'Tight' isolation requirements of Ref. [57], based on the amount of summed calorimeter energy and track transverse momentum close to the electron. Muon candidates were reconstructed by combining tracks from the inner detector with matching tracks reconstructed in the muon spectrometer, and were required to have $p_T > 20$ GeV, $|\eta| < 2.5$ and to satisfy the 'Medium' requirements of Ref. [61]. Muons were also required to be consistent with the signal primary vertex and to satisfy the 'Tight' isolation requirements of Ref. [61].

Jets were reconstructed using the anti-k_t algorithm [92,93] with radius parameter $R = 0.4$, starting from particle-flow objects that combine information from topological clusters of calorimeter energy deposits and inner-detector tracks [94]. After calibration using information from both simulation and data [59], jets were required to have $p_T > 25$ GeV and $|\eta| < 2.5$, and jets with $p_T < 60$ GeV and $|\eta| < 2.4$ were subject to additional pileup rejection criteria using the multivariate jet-vertex tagger (JVT) [95]. To prevent double counting of electron energy deposits as jets, the closest jet to an electron candidate was removed if it was within $\Delta R = 0.2$ of the electron. Furthermore, to reduce the contribution of leptons from heavy-flavour hadron decays inside jets, leptons within $\Delta R = 0.4$ of selected jets were discarded, unless the lepton was a muon and the jet had fewer than three associated tracks, in which case the jet was discarded. Jets likely to contain b-hadrons were tagged using the DL1r algorithm [62,96], a multivariate discriminant based on deep-learning techniques making use of track impact parameters and reconstructed secondary vertices. For the inclusive $\sigma_{t\bar{t}}$ and $t\bar{t} \to e\mu$ differential cross-section measurements, a tagger working point with an efficiency of 70% for tagging b-quark jets from top-quark decays in simulated $t\bar{t}$ events was used, corresponding to rejection factors of about 380 against light quark and gluon jets, and 10 against jets originating from charm quarks. A looser working point with 77% b-tagging efficiency and a factor of two less background rejection was used for the $e\mu b\bar{b}$ measurement.

Selected events were required to have exactly one electron and exactly one muon passing the requirements given above, with at least one of the leptons matched to a corresponding electron or muon trigger. Although the lepton p_T threshold is 20 GeV, the trigger matching requirements imply that at least one lepton must have offline reconstructed

$p_{\mathrm{T}} > 27\,\mathrm{GeV}$ (if an electron) or $p_{\mathrm{T}} > 27.3\,\mathrm{GeV}$ (if a muon) for most of the dataset. However, the lower thresholds in 2015 data give access to the phase space where the two leptons satisfy $(p_{\mathrm{T},1}, p_{\mathrm{T},2}) > (21, 20)\,\mathrm{GeV}$. Events where the electron and muon were separated in angle by $|\Delta\theta| < 0.15$ and $|\Delta\phi| < 0.15$ were rejected. Events with an opposite-charge $e\mu$ pair comprise the main analysis sample, whilst events with a same-charge $e\mu$ pair were used to estimate the background from misidentified leptons.

4 Cross-section measurements

The inclusive $\sigma_{t\bar{t}}$ and $t\bar{t} \to e\mu$ differential cross-sections were measured using the double-tagging technique described in Ref. [34], employing subsets of the opposite-charge $e\mu$ sample with exactly one and exactly two b-tagged jets, as described in Sects. 4.1 and 4.2. The $e\mu b\bar{b}$ differential cross-sections were derived mainly from the two b-tagged jet sample using the 77% efficiency b-tagging working point, and are described in Sect. 4.3. Background estimates are discussed in Sect. 4.4, and the validation of the differential measurements using simulation in Sect. 4.5.

4.1 Inclusive cross-sections

The inclusive $t\bar{t}$ cross-section $\sigma_{t\bar{t}}$ was determined by counting the numbers of opposite-charge $e\mu$ events with exactly one (N_1) and exactly two (N_2) b-tagged jets, using the 70% b-tagging efficiency working point. The two event counts satisfy the tagging equations:

$$\begin{aligned} N_1 &= L\sigma_{t\bar{t}}\,\epsilon_{e\mu} 2\epsilon_b(1 - C_b\epsilon_b) + N_1^{\mathrm{bkg}}, \\ N_2 &= L\sigma_{t\bar{t}}\,\epsilon_{e\mu} C_b {\epsilon_b}^2 + N_2^{\mathrm{bkg}}, \end{aligned} \tag{1}$$

where L is the integrated luminosity of the sample, $\epsilon_{e\mu}$ the efficiency for a $t\bar{t}$ event to pass the opposite-charge $e\mu$ selection, and C_b is a tagging correlation coefficient close to unity. The combined probability for a jet from the quark q in the $t \to Wq$ decay to fall within the acceptance of the detector, be reconstructed as a jet with transverse momentum above the selection threshold, and be tagged as a b-jet, is denoted by ϵ_b. The parameter $C_b = \epsilon_{bb}/{\epsilon_b}^2$, where ϵ_{bb} is the probability to reconstruct and b-tag both b-quark jets from the two top quark decays, accounts for the fact that the tagging probabilities of the two b-quark jets are not completely independent. It was evaluated from simulation as $C_b = 4N_{e\mu}^{t\bar{t}} N_2^{t\bar{t}}/(N_1^{t\bar{t}} + 2N_2^{t\bar{t}})^2$, where $N_{e\mu}^{t\bar{t}}$ is the number of selected $e\mu$ $t\bar{t}$ events and $N_1^{t\bar{t}}$ and $N_2^{t\bar{t}}$ are the numbers of such events with one and two b-tagged jets.[3] In the baseline POWHEG MiNNLO+PYTHIA8 simulation, $\epsilon_{e\mu} \approx 0.89\%$, $\epsilon_b \approx 54\%$ and $C_b \approx 1.009$, indicating a small positive correlation. The backgrounds from sources other than $t\bar{t}$ production are given by the terms N_1^{bkg} and N_2^{bkg}, evaluated using a combination of simulation and data control samples as discussed in Sect. 4.4. The tagging Eq. (1) were then solved to determine $\sigma_{t\bar{t}}$ and ϵ_b.

The selection efficiency $\epsilon_{e\mu}$ can be written as the product of two terms: $\epsilon_{e\mu} = A_{e\mu} G_{e\mu}$. The acceptance $A_{e\mu} \approx 1.7\%$ represents the fraction of simulated $t\bar{t}$ events that have a true opposite-charge $e\mu$ pair from $W \to e/\mu$ decays, with each lepton satisfying $p_{\mathrm{T}} > 20\,\mathrm{GeV}$ and $|\eta| < 2.5$. These requirements define the fiducial region. The contributions via leptonic τ decays ($t \to W \to \tau \to e/\mu$) are included. The lepton four-momenta were evaluated at particle level after final-state radiation, and 'dressed' by including the four-momenta of any photons within a cone of size $\Delta R = 0.1$ around the lepton direction, excluding photons produced from hadron decays or interactions with the detector material. The reconstruction efficiency $G_{e\mu}$ represents the probability that the two leptons are reconstructed and pass all the trigger, identification and isolation requirements. It also corrects for the 0.5% of selected $t\bar{t}$ events that are outside the fiducial region and only selected due to the limited lepton resolution. The fiducial cross-section $\sigma_{t\bar{t}}^{\mathrm{fid}}$ corresponding to the production of $t\bar{t}$ events with a particle-level electron and muon satisfying the requirements on p_{T} and η is $\sigma_{t\bar{t}}^{\mathrm{fid}} = A_{e\mu}\sigma_{t\bar{t}}$, and can be measured by replacing $\sigma_{t\bar{t}}\epsilon_{e\mu}$ with $\sigma_{t\bar{t}}^{\mathrm{fid}} G_{e\mu}$ in Eq. (1). As in Refs. [34,37], this fiducial cross-section definition makes no requirements on the presence of jets, as the tagging formalism allows the number of $t\bar{t}$ events with no reconstructed and b-tagged jets to be inferred from the event counts N_1 and N_2. Measurement of the fiducial cross-section avoids the systematic uncertainties associated with the evaluation of the acceptance.

A total of 1,483,775 events passed the opposite-charge $e\mu$ selection in data. The numbers of observed events with one and two b-tagged jets are shown in Table 1, together with the expected non-$t\bar{t}$ contributions from Wt and dibosons evaluated from simulation, and Z+jets and misidentified leptons evaluated using both data and simulation. The one b-tag sample is expected to be about 88% pure and the two b-tag sample 96% pure in $t\bar{t}$ events, with the largest backgrounds coming from Wt production in both cases. The distribution of the b-tagged jet multiplicity $N_{\mathrm{b-tag}}$ is shown in Fig. 1(a) and compared with the expectation from simulation, broken down into contributions from $t\bar{t}$ events (modelled using the POWHEG MiNNLO+PYTHIA8 sample) and various background processes. The predictions using POWHEG+PYTHIA8

[3] The formula for C_b follows from the definitions of ϵ_b as the number of b-tagged jets divided by the total number of b-jets from $t\bar{t}$ events, i.e. $\epsilon_b = (N_1^{t\bar{t}} + 2N_2^{t\bar{t}})/(2N_{e\mu}^{t\bar{t}})$ and ϵ_{bb} as the number of $t\bar{t}$ events with two b-tagged jets divided by the total number of $t\bar{t}$ events, i.e. $\epsilon_{bb} = N_2^{t\bar{t}}/N_{e\mu}^{t\bar{t}}$.

Table 1 Observed numbers of opposite-charge $e\mu$ events with one (N_1) and two (N_2) b-tagged jets, together with the estimates of backgrounds and associated uncertainties described in Sects. 4.4 and 5

Event counts	N_1	N_2
Data	576,725	314,961
Wt single top	$59{,}100 \pm 3200$	$10{,}200 \pm 1800$
$Z(\to \tau\tau \to e\mu)$+jets	2650 ± 110	204 ± 8
Diboson	1320 ± 270	54 ± 13
Misidentified leptons	3410 ± 910	1250 ± 730
Total background	$66{,}500 \pm 3300$	$11{,}700 \pm 2000$

and POWHEG + HERWIG7 $t\bar{t}$ events are also shown.[4] All predictions are normalised to the same integrated luminosity as the data, using the cross-sections discussed in Sects. 1 and 2. The three $t\bar{t}$ samples have been reweighted to increase the number of events with at least three particle-level b-jets by 50%. As discussed in Sect. 5.1, this reweighting brings the number of events with $N_{\text{b-tag}} \geq 3$ into good agreement with data. The purple dot-dashed line in Fig. 1(a) shows the prediction from POWHEG MiNNLO + PYTHIA8 without this reweighting, which gives a 25% deficit in the number of events with $N_{\text{b-tag}} \geq 3$. Since the predicted value of C_b is sensitive to the production of $t\bar{t}$ with extra heavy quarks, this reweighting was applied to the POWHEG MiNNLO + PYTHIA8 sample throughout the analysis.

Figure 1(b)–(f) show distributions of the p_{T} of the b-tagged jets (one entry per jet), and the p_{T} and $|\eta|$ of the electron and muon, in opposite-charge $e\mu$ events with at least one b-tagged jet. The total simulation prediction is normalised to the same number of selected events as the data, to facilitate shape comparisons. In general, the simulation predictions describe the data well, though the data show softer lepton and b-tagged jet p_{T} distributions than all the simulation predictions, with POWHEG MiNNLO + PYTHIA8 being significantly closer to the data than POWHEG + PYTHIA8 and POWHEG + HERWIG7. The differences in $|\eta|$ distributions between electrons and muons reflect their differing reconstruction efficiencies as a function of lepton η.

4.2 $t\bar{t} \to e\mu$ differential cross-sections

The differential cross-sections as functions of the lepton and dilepton variables defined in Sect. 1 were measured using an extension of Eq. (1), by counting the number of leptons or events with one (N_1^i) or two (N_2^i) b-tagged jets where the lepton(s) fall in bin i of a differential distribution at reconstruction level. There are two counts per event in the single-lepton distributions p_{T}^{ℓ} and $|\eta^{\ell}|$, in the two bins corresponding to the electron and muon. In the dilepton distributions, each event contributes a single count corresponding to the bin in which the appropriate dilepton variable falls. For each bin of each differential distribution, these counts satisfy the tagging equations:

$$\begin{aligned} N_1^i &= L\sigma_{t\bar{t}}^i \, G_{e\mu}^i 2\epsilon_b^i (1 - C_b^i \epsilon_b^i) + N_1^{i,\text{bkg}}, \\ N_2^i &= L\sigma_{t\bar{t}}^i \, G_{e\mu}^i C_b^i (\epsilon_b^i)^2 + N_2^{i,\text{bkg}}, \end{aligned} \tag{2}$$

where $\sigma_{t\bar{t}}^i$ is the absolute fiducial differential cross-section in bin i. The reconstruction efficiency $G_{e\mu}^i$ represents the ratio of the number of reconstructed $e\mu$ events (or leptons for p_{T}^{ℓ} and $|\eta^{\ell}|$) in bin i defined using the reconstructed lepton(s), to the number of true $e\mu$ events (or leptons) in the same bin i at particle level, evaluated using $t\bar{t}$ simulation. In the definition of $G_{e\mu}^i$, the particle-level electron and muon were required to have $p_{\text{T}} > 20\,\text{GeV}$ and $|\eta| < 2.5$, but no requirements were made on reconstructed or particle-level jets, nor on the removal of overlaps between leptons and jets in contrast to Ref. [12] where such overlap requirements were applied. The efficiency $G_{e\mu}^i$ corrects for both the lepton reconstruction efficiency and the effects of event migration, where events in bin j at particle level (or outside the fiducial region) appear in a bin $i \neq j$ at reconstruction level. The integral of any dilepton differential cross-section is equal to the fiducial cross-section $\sigma_{t\bar{t}}^{\text{fid}}$ defined in Sect. 4.1, and the integrals of the single-lepton p_{T}^{ℓ} and $|\eta^{\ell}|$ distributions are equal to $2\sigma_{t\bar{t}}^{\text{fid}}$. The values of $G_{e\mu}^i$ were taken from the POWHEG MiNNLO + PYTHIA8 $t\bar{t}$ simulation, and are generally around 0.4–0.6. The corresponding values of C_b^i are always within 3% of unity, even at the edges of the differential distributions. The background terms $N_1^{i,\text{bkg}}$ and $N_2^{i,\text{bkg}}$ were determined from simulation and data control samples, allowing the tagging Eq. (2) to be solved to give the absolute fiducial differential cross-sections $\sigma_{t\bar{t}}^i$ and associated ϵ_b^i values for each bin i of each differential distribution.

The bin ranges for each differential distribution were based on those used in Ref. [34], splitting or redefining a few bins to profit from the larger data sample. The $\Delta\phi^{e\mu}$ distribution was measured in 20 rather than 10 bins. For other distributions, the bin widths were chosen according to the experimental lepton resolution, in order to keep the fractions of events reconstructed in bin i that do not originate from bin i at particle level at the level of 10% or lower. The chosen bin ranges can be seen in Figs. 12, 13, 14, 15, 16 in Sect. 7.1, and in Ref. [97]. The last bins of the p_{T}^{ℓ}, $p_{\text{T}}^{e\mu}$, $m^{e\mu}$, $p_{\text{T}}^{e} + p_{\text{T}}^{\mu}$, $E^e + E^{\mu}$, $p_{\text{T}}^{\ell,\text{max}}$ and $p_{\text{T}}^{\ell,\text{min}}$ distributions include overflow events falling above the last bin boundary. The normalised fiducial differential cross-sections were calculated from the absolute cross-sections $\sigma_{t\bar{t}}^i$ as discussed in Ref. [34], and are statistically correlated between bins because of the normalisation. The absolute dilepton differential cross-sections are

[4] The names PYTHIA and HERWIG are abbreviated as PY and HW in figure legends and some tables for compactness.

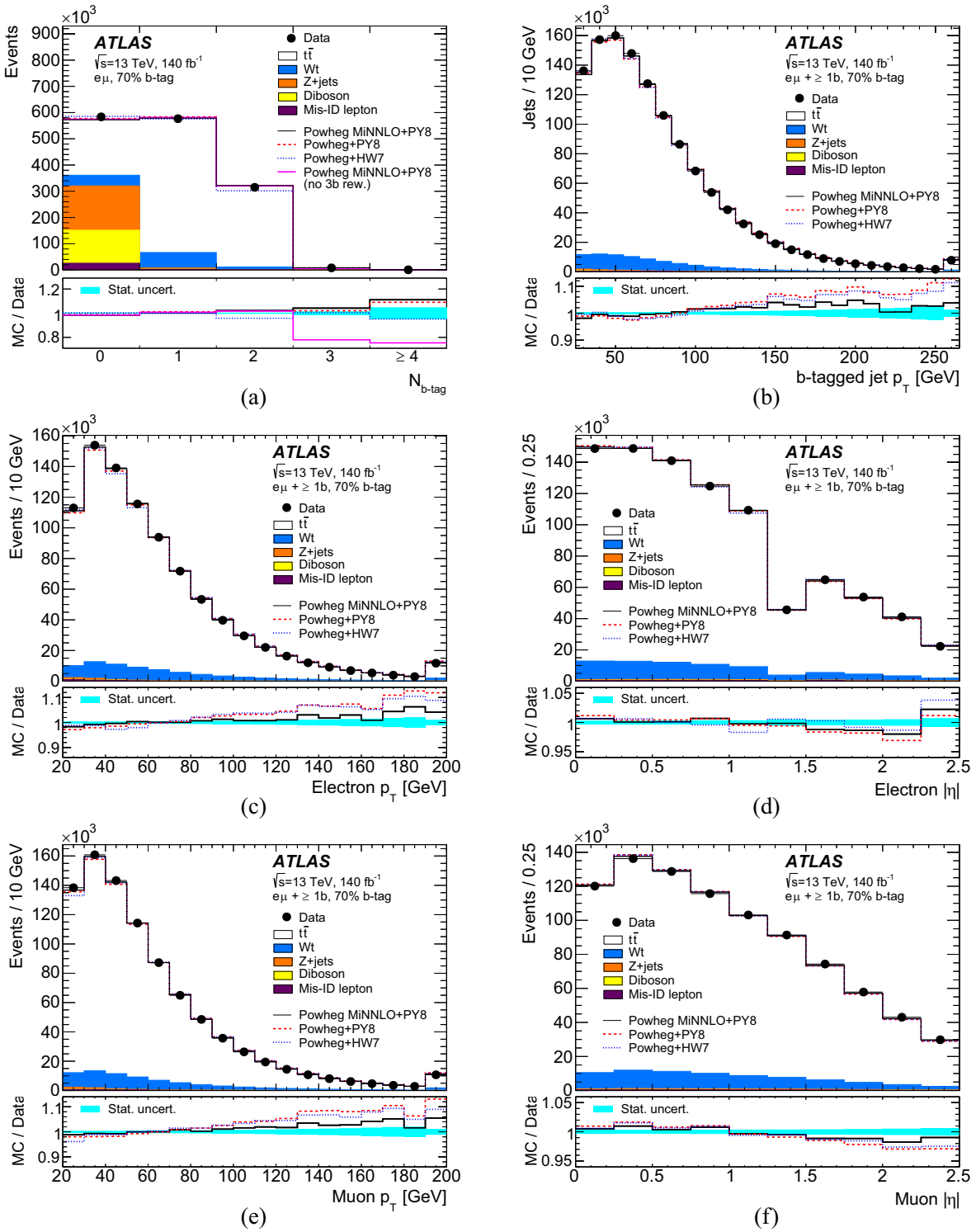

Fig. 1 Distributions of (**a**) the number of b-tagged jets in selected opposite-charge $e\mu$ events; and (**b**) the p_{T} of b-tagged jets, (**c**) the p_{T} of the electron, (**d**) the $|\eta|$ of the electron, (**e**) the p_{T} of the muon and (**f**) the $|\eta|$ of the muon, in events with an opposite-charge $e\mu$ pair and at least one b-tagged jet. The reconstruction-level data are compared with the expectation from simulation, broken down into contributions from $t\bar{t}$ (modelled with POWHEG MiNNLO+PYTHIA8), Wt, Z+jets, dibosons, and events with misidentified electrons or muons. The simulation prediction is normalised to the same integrated luminosity as the data in (**a**) and to the same number of entries as the data in (**b**–**f**). The lower panels show the ratios of simulation to data, using various $t\bar{t}$ simulation samples and with the cyan shaded band indicating the statistical uncertainty. The last bin includes the overflows in panels (**b**), (**c**) and (**e**)

not statistically correlated between bins, but kinematic correlations between the electron and muon within an event introduce small correlations within the absolute single-lepton p_{T}^{ℓ} and $|\eta^{\ell}|$ distributions. Figure 2 shows the reconstructed $p_{\mathrm{T}}^{e\mu}$, $m^{e\mu}$, $|y^{e\mu}|$, $\Delta\phi^{e\mu}$, $p_{\mathrm{T}}^{e}+p_{\mathrm{T}}^{\mu}$ and $E^{e}+E^{\mu}$ distributions for events with at least one b-tagged jet, comparing data with predictions using the same set of $t\bar{t}$ simulation samples as Fig. 1. The predictions are in reasonable qualitative agreement with the data. However there are some significant differences, in particular for $m^{e\mu}$, $\Delta\phi^{e\mu}$ and $p_{\mathrm{T}}^{e}+p_{\mathrm{T}}^{\mu}$, which are discussed quantitatively in terms of the particle-level differential cross-sections in Sect. 7.2.

Two-dimensional distributions with $|\eta^{\ell}|$, $|y^{e\mu}|$ or $\Delta\phi^{e\mu}$ as the first variable, and $m^{e\mu}$ as the second variable, were also measured, using the same binning as Ref. [34]. The excellent resolution in $|\eta^{\ell}|$, $|y^{e\mu}|$ and $\Delta\phi^{e\mu}$ results in migration effects only being significant between the four $m^{e\mu}$ bins, defined as $m^{e\mu} < 80\,\mathrm{GeV}$, $80 < m^{e\mu} < 120\,\mathrm{GeV}$, $120 < m^{e\mu} < 200\,\mathrm{GeV}$ and $m^{e\mu} > 200\,\mathrm{GeV}$. The formalism of Eq. (2) was used, with the index i running over the two-dimensional grid of bins in both variables.

The measured differential cross-sections include contributions where one or both leptons are produced via leptonic decays of τ-leptons ($t \to W \to \tau \to e/\mu$). To enable comparisons with theoretical predictions that only include direct $t \to W \to e/\mu$ decays, a second set of cross-section results was derived with a bin-by-bin multiplicative correction $f^{i}_{\mathrm{no}-\tau}$ to remove the τ contributions:

$$\sigma^{i}_{t\bar{t}}\,(\text{no-}\tau) = f^{i}_{\mathrm{no}-\tau}\,\sigma^{i}_{t\bar{t}} \tag{3}$$

and similarly for the normalised cross-sections. The corrections $f^{i}_{\mathrm{no}-\tau}$ were calculated from $t\bar{t}$ simulation as the fractions of leptons (for the p_{T}^{ℓ} and $|\eta^{\ell}|$ distributions) or events (for the other distributions) in each particle-level bin, that originate from events where neither lepton was produced from a τ-lepton decay. These fractions are typically in the range 0.8–0.9.

4.3 $e\mu b\bar{b}$ differential cross-sections

The $t\bar{t} \to e\mu$ differential cross-sections include leptons from $t\bar{t}$ events only, treating leptons from Wt events as background that is estimated and subtracted using simulation. In some kinematic regions, e.g. those with high lepton or dilepton p_{T}, the interference between $t\bar{t}$ and Wt contributions becomes large and this subtraction has large uncertainties that limit the measurement precision. Recent theoretical work has focused on a combined description of the $t\bar{t}$ and $Wt(b)$ processes, through e.g. the POWHEG $bb4l$ generator [42] that includes the complete set of contributions to $e\mu\nu\bar{\nu}b\bar{b}$ production. To probe this final state, the fiducial cross-section definition was modified to explicitly include a requirement for particle-level b-jets, as well as leptons. An $e\mu b\bar{b}$ fiducial region was therefore defined, requiring at least two particle-level b-jets with $p_{\mathrm{T}} > 25\,\mathrm{GeV}$ and $|\eta| < 2.5$, in addition to the lepton requirements of the $t\bar{t} \to e\mu$ measurement. The particle-level jets were reconstructed with the anti-k_t algorithm with $R = 0.4$ from all truth particles with lifetime $c\tau > 10\,\mathrm{nm}$, excluding leptons and neutrinos from W and Z boson decays. A particle-level jet was assumed to be a b-jet if ghost-associated [98] to at least one weakly decaying b-hadron with $p_{\mathrm{T}} > 5\,\mathrm{GeV}$. The fiducial region was then divided into i bins of lepton or dilepton kinematics, defining the same distributions as in the $t\bar{t} \to e\mu$ measurement but always requiring there to be at least two particle-level b-jets.

The cross-section $\sigma^{i}_{e\mu b\bar{b}}$ in bin i of a kinematic distribution was then determined from:

$$\sigma^{i}_{e\mu b\bar{b}} = \left(\frac{N_2^i - N_2^{i,\mathrm{bkg}}}{L\,G^{i}_{e\mu b\bar{b}}}\right)\cdot S^{2}_{\mathrm{tag}} \tag{4}$$

where N_2^i is the number of data $e\mu$ events with at least two b-tagged jets in lepton kinematic bin i, $N_2^{i,\mathrm{bkg}}$ is the estimated number of background events from Z+jets, dibosons and events with misidentified electrons or muons, and S_{tag} is a b-tagging efficiency scale factor defined below. As the background from events without two true b-jets is very small, the looser 77% b-tagging efficiency working point was used for this measurement. The efficiency $G^{i}_{e\mu b\bar{b}}$ is defined as $G^{i}_{e\mu b\bar{b}} = N^{i,\mathrm{rec}}_{e\mu b\bar{b}}/N^{i,\mathrm{true}}_{e\mu b\bar{b}}$, where $N^{i,\mathrm{rec}}_{e\mu b\bar{b}}$ is the number of selected opposite-charge $e\mu$ events from $t\bar{t}$ or Wt with two b-tagged jets in lepton kinematic bin i, and $N^{i,\mathrm{true}}_{e\mu b\bar{b}}$ is the number of particle-level $t\bar{t}$ and Wt events that pass the fiducial selection on both leptons and b-jets, and are in lepton kinematic bin i at particle level. The efficiency $G^{i}_{e\mu b\bar{b}}$ accounts for the efficiency to b-tag the two b-jets in the $e\mu b\bar{b}$ final state, as well as the lepton efficiencies and migration in and out of kinematic bin i due to both lepton and jet resolution effects. The values of $G^{i}_{e\mu b\bar{b}}$ are around 0.2–0.35, smaller than $G^{i}_{e\mu}$ in the $t\bar{t} \to e\mu$ measurement as $G^{i}_{e\mu b\bar{b}}$ includes the b-tagging efficiency for the two b-jets, evaluated from simulation. The bin-to-bin migration is very similar to that for the $t\bar{t} \to e\mu$ differential cross-sections.

To reduce the sensitivity to the modelling of the b-tagging efficiency in simulation, the second term in Eq. (4) corrects the measured cross-section by the square of the ratio of the values of ϵ_b in simulation (ϵ_b^{MC}) and data ($\epsilon_b^{\mathrm{data}}$), i.e. $S_{\mathrm{tag}} = \epsilon_b^{\mathrm{MC}}/\epsilon_b^{\mathrm{data}}$. These efficiencies were evaluated from the inclusive double-tagging formalism, Eq. (1), applied to the total numbers of events with one and two b-tagged jets using the 77% working point, treating $t\bar{t}$ as signal and Wt as background. Since S_{tag} is calculated inclusively (and not in bins i), it is relatively insensitive to the $t\bar{t}/Wt$ interference

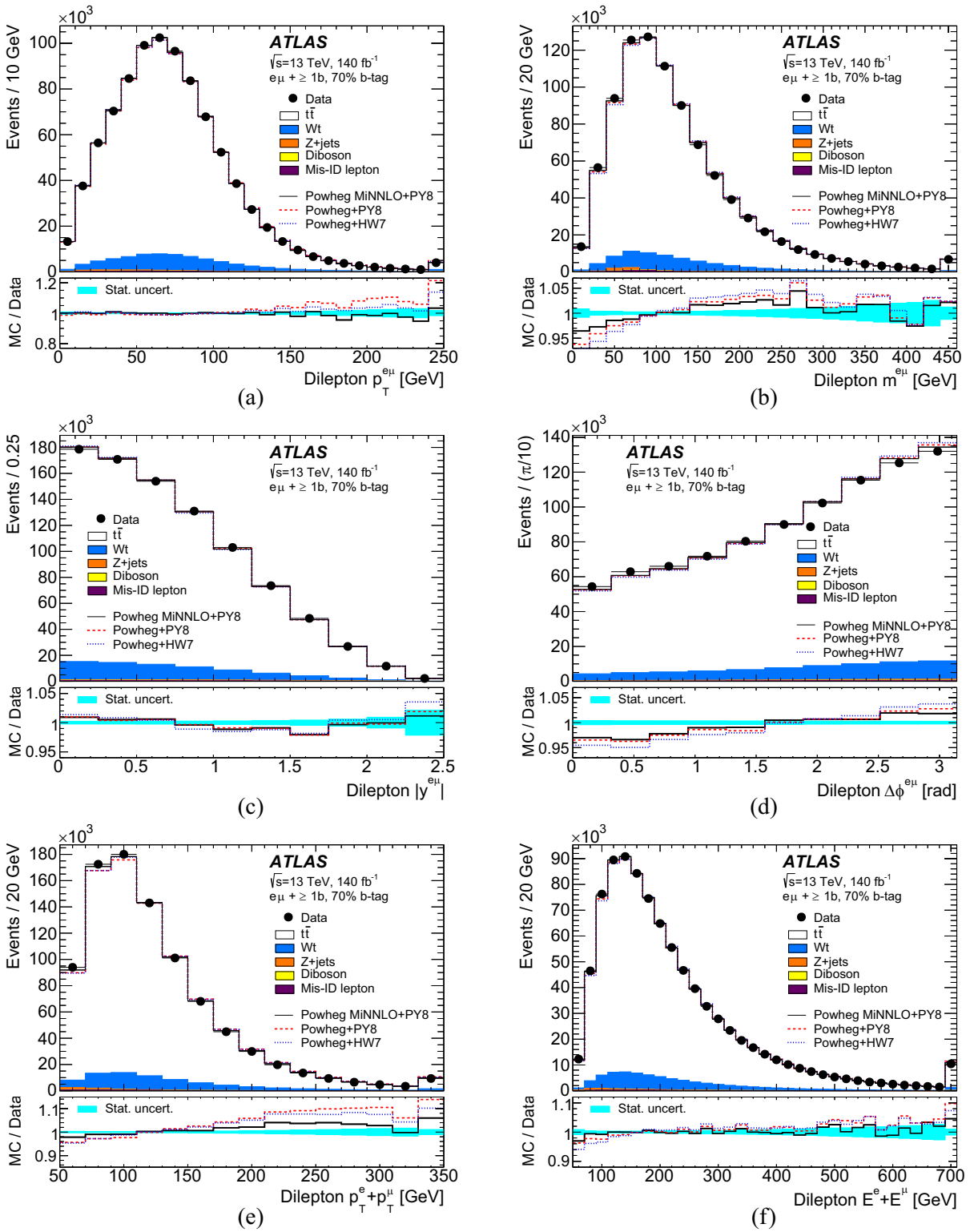

Fig. 2 Distributions of (**a**) the dilepton $p_{\mathrm{T}}^{e\mu}$, (**b**) invariant mass $m^{e\mu}$, (**c**) rapidity $|y^{e\mu}|$, (**d**) azimuthal angle difference $\Delta\phi^{e\mu}$, (**e**) lepton p_{T} sum $p_{\mathrm{T}}^{e} + p_{\mathrm{T}}^{\mu}$ and (**f**) lepton energy sum $E^{e} + E^{\mu}$, in events with an opposite-charge $e\mu$ pair and at least one b-tagged jet. The reconstruction-level data are compared with the expectation from simulation, broken down into contributions from $t\bar{t}$ (modelled with POWHEG MiNNLO+PYTHIA8), Wt, Z+jets, dibosons, and events with misidentified electrons or muons, normalised to the same number of entries as the data. The lower panels show the ratios of simulation to data, using various $t\bar{t}$ signal samples and with the cyan shaded band indicating the statistical uncertainty. The last bin includes the overflow in panels (**a**), (**b**), (**e**) and (**f**)

uncertainties and reduces the uncertainties in the absolute differential cross-sections $\sigma^{i}_{e\mu b\bar{b}}$. As the S_{tag} correction is the same for all bins of all differential cross-sections, it has no effect on the normalised $e\mu b\bar{b}$ differential cross-sections, which were calculated from the $\sigma^{i}_{e\mu b\bar{b}}$ values in the same way as for the $t\bar{t} \to e\mu$ measurement. These cross-sections include the contributions from leptonic decays of τ-leptons, and a second set of results with the τ contributions removed analogously to Eq. (3) was also derived, using the POWHEG MiNNLO+PYTHIA8 $t\bar{t}$ and POWHEG+PYTHIA8 Wt (with the diagram removal scheme) samples to calculate the corrections.

A total of 378,266 opposite-charge $e\mu$ events with two b-tagged jets were selected in data, with an estimated background from processes other than $t\bar{t}$ and Wt of 0.4%. The contribution from non-resonant $WWb\bar{b}$ events to the fiducial $e\mu b\bar{b}$ cross-section is negligible. A further 564,501 one b-tag events were used in the determination of S_{tag}. Figure 3(a) shows the b-tagged jet multiplicity using the 77% working point, and Fig. 3(b)–(f) show kinematic distributions for events with two b-tagged jets, with data compared with the baseline simulation with POWHEG MiNNLO+PYTHIA8 $t\bar{t}$ events and POWHEG+PYTHIA8 Wt events with the diagram removal scheme, and alternative predictions using diagram subtraction Wt events [38,80], and the POWHEG $bb4l$+PYTHIA8 sample that covers both $t\bar{t}$ and Wt final states. All samples were reweighted to enhance the number of events with at least three particle-level b-jets by 50%. The modelling of the data lepton p_{T} and $|\eta|$ distributions by all three predictions in Fig. 3 is similar, although the sample using diagram subtraction Wt events has a slightly softer lepton p_{T} distribution than that using diagram removal Wt events, and the POWHEG $bb4l$+PYTHIA8 sample has a slightly more central lepton $|\eta|$ distribution.

4.4 Background estimates

The dominant background in the inclusive $\sigma_{t\bar{t}}$ and $t\bar{t} \to e\mu$ differential cross-section analyses comes from Wt production, and was evaluated from simulation as discussed in Sect. 2. In the $e\mu b\bar{b}$ analysis, this process is part of the signal. The small diboson contribution (dominated by WW production with additional b-tagged jets) is treated as background in all analyses and was evaluated using simulation. The production of a Z boson accompanied by heavy-flavour jets is subject to large theoretical uncertainties, so the $Z(\to \tau\tau \to e\mu)$+b-tagged jets background predictions from SHERPA 2.2 were scaled using the corresponding yield ratios of $Z(\to ee/\mu\mu)$+b-tagged jets events in data and simulation. These yields were extracted from template fits to the ee and $\mu\mu$ invariant mass distributions, giving yield ratios of 0.91 ± 0.04 (one b-tagged jet) and 1.10 ± 0.04 (two b-tagged jets). The uncertainties include the effect of the harder Z-boson p_{T} spectrum in selected $Z \to \tau\tau$ vs. $Z \to ee/\mu\mu$ events and residual differences between the ratios measured in ee and $\mu\mu$ events.

The background from events with misidentified leptons was estimated using the same charge-sign (SS) $e\mu$ sample. Following the method used in Ref. [35], the SS sample was selected as described in Sect. 3, but additionally requiring the electron to be accepted by a charge misidentification boosted decision tree (BDT) [57]. This requirement reduces the rate of electron charge misreconstruction by up to an order of magnitude and suppresses the contribution of dilepton $t\bar{t}$ events with a misreconstructed electron charge to the SS sample. The misidentified-lepton background $N_j^{i,\text{mis-id}}$ in lepton kinematic bin i with j b-tagged jets was estimated from the number of SS events in data, $N_j^{i,\text{d,SS}}$, after subtracting the number of SS events with two prompt leptons $N_j^{i,\text{prompt,SS}}$ estimated using simulation, and then scaling by the ratio R_j^i of misidentified-lepton events in the opposite charge-sign (OS) and SS samples in simulation:

$$N_j^{i,\text{mis-id}} = R_j^i (N_j^{i,\text{d,SS}} - N_j^{i,\text{prompt,SS}})$$
$$R_j^i = \frac{N_j^{i,\text{mis-id,OS,sim}}}{N_j^{i,\text{mis-id,SS,sim}}}. \quad (5)$$

This method relies on simulation to predict the ratio of OS to SS misidentified-lepton events, and the prompt SS contribution, but not the absolute number of misidentified-lepton events $N_j^{i,\text{mis-id}}$, which is calculated using the SS event counts in data. The same formalism was used with a single bin i for the inclusive cross-section measurement.

The electron and muon p_{T} and $|\eta|$ distributions in the SS samples with at least one b-tagged jet are shown in Fig. 4, and compared with the simulation prediction broken down into various sources of prompt and misidentified leptons. The simulation models the overall numbers of events in the one b-tagged sample to better than 5% and the two b-tagged sample to 10%, and also reproduces the shapes of the kinematic distributions. The values of R_j for the inclusive cross-section and their total uncertainties are $R_1 = 1.9 \pm 0.4$ and $R_2 = 3.9 \pm 1.6$, with variations of R_1^i in the range 1.5–3 and R_2^i in the range 3–5 for both the $t\bar{t} \to e\mu$ and $e\mu b\bar{b}$ differential analyses. Deviations of R_j^i from unity are caused by the charge misidentification BDT, which has an inefficiency of up to 50% for misidentified electrons and is applied to the SS sample only, and differences in the composition of misidentified leptons between the OS and SS samples. The uncertainties in R_j^i were assessed by removing the photon conversion, misidentified hadron and muon decay-in-flight contributions in turn, and recalculating R_j^i. A 25% uncertainty in the prompt SS contribution with correctly reconstructed electron charge sign was assumed, covering the uncertainties

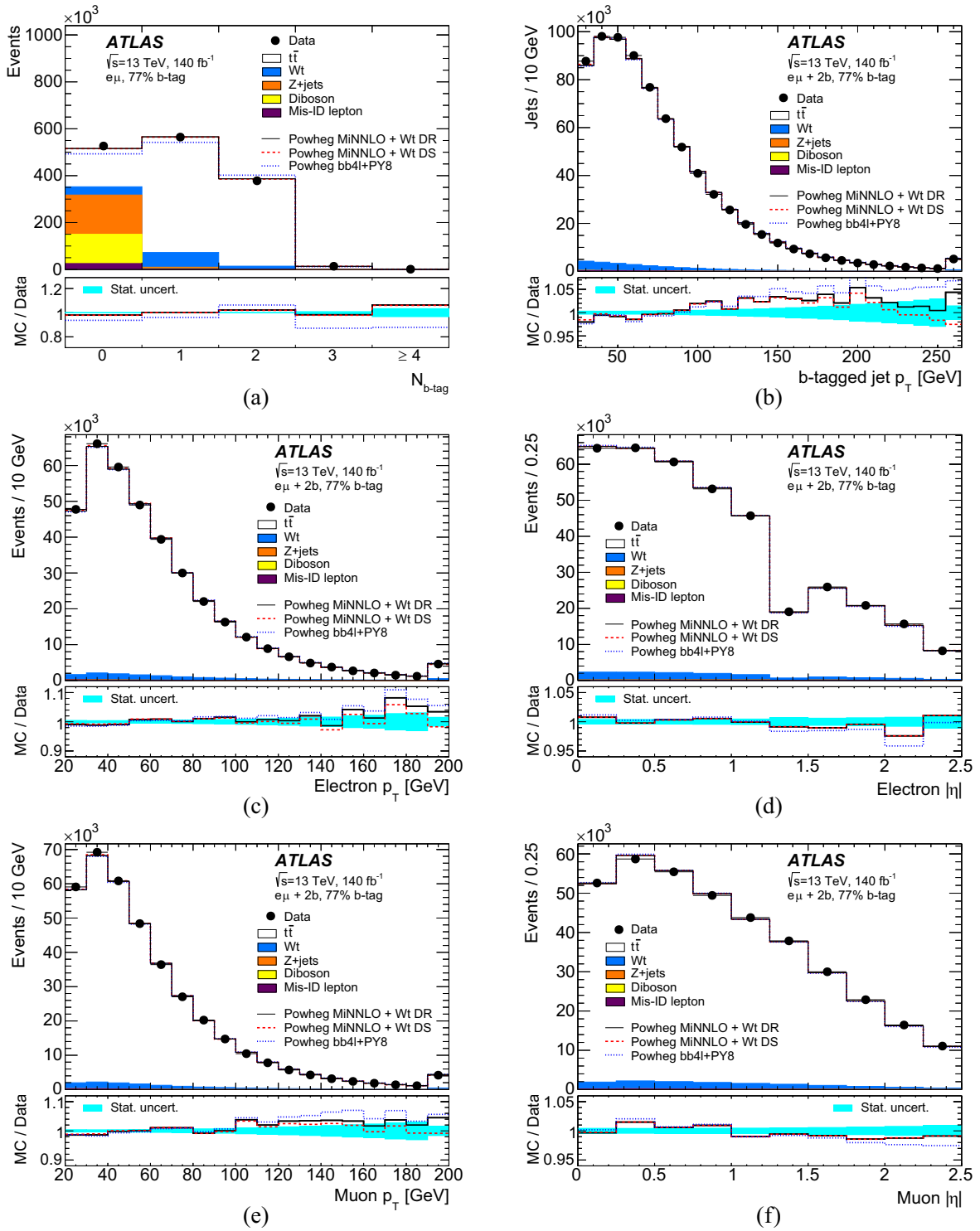

Fig. 3 Distributions of (**a**) the number of b-tagged jets in selected opposite-sign $e\mu$ events; and (**b**) the p_{T} of b-tagged jets, (**c**) the p_{T} of the electron, (**d**) the $|\eta|$ of the electron, (**e**) the p_{T} of the muon and (**f**) the $|\eta|$ of the muon, in events with an opposite-sign $e\mu$ pair and exactly two b-tagged jets with the 77% efficiency working point. The reconstruction-level data are compared with the expectation from simulation, broken down into contributions from $t\bar{t}$ (modelled with POWHEG MiNNLO+PYTHIA8), Wt, Z+jets, dibosons, and events with misidentified electrons or muons. The simulation prediction is normalised to the same integrated luminosity as the data in (**a**) and to the same number of entries as the data in (**b**–**f**). The lower panels show the ratios of simulation to data, using various simulation samples and with the cyan shaded band indicating the statistical uncertainty. The last bin includes the overflows in panels (**b**), (**c**) and (**e**)

in modelling the major contributing processes ($t\bar{t}+W$, $t\bar{t}+Z$ and $t\bar{t}+H$, and WZ). The modelling of the charge misidentification BDT was validated using $Z \to ee$ events, leading to a 10% uncertainty in the prompt SS component where the electron charge is misreconstructed. Overall, the misidentified lepton background contributes about $0.6 \pm 0.2\%$ of the OS sample with one b-tagged jet and $0.4 \pm 0.2\%$ of the two b-tagged jet sample (see Table 1), concentrated at low lepton p_{T}. Further studies were performed with SS control samples where the lepton isolation cuts were inverted to increase the misidentified lepton contributions. The simulation also gives a good description of these samples, with absolute rates within 15% of those observed in data.

4.5 Validation of the differential measurements

Tests using pseudo-experiment datasets generated from simulation were used to validate the analysis procedures for the differential measurements, as discussed in Refs. [34,37]. These tests demonstrated that the method is unbiased and correctly estimates the statistical uncertainties in each bin of each distribution. Figure 5 shows examples for the p_{T}^{ℓ}, $p_{\mathrm{T}}^{e\mu}$, $|\eta^{\ell}|$ and $|y^{e\mu}|$ distributions in the $t\bar{t} \to e\mu$ analysis. The filled black points show the relative differences between the mean of the normalised differential cross-sections obtained from 1000 pseudo-experiments and the true cross-sections in each bin, divided by the true cross-sections to give fractional differences. The pseudo-experiments were generated from a reference sample with POWHEG + PYTHIA8 $t\bar{t}$ events plus backgrounds, which was also used to determine the values of $G_{e\mu}^{i}$ and C_{b}^{i}. The compatibility of the filled black points with zero confirms that the method is unbiased for these samples. For the alternative samples with different underlying distributions, the open red points show the mean pseudo-experiment results and the dotted red lines the true values, again expressed as fractional deviations from the true cross-sections in the reference sample, and obtained using $G_{e\mu}^{i}$ and C_{b}^{i} values calculated from the reference sample. An independent POWHEG + PYTHIA8 $t\bar{t}$ sample with $m_t = 176\,\mathrm{GeV}$ was used as the alternative sample in Fig. 5(a) and (b), and the POWHEG + PYTHIA8 sample generated with NNPDF3.0 was reweighted to the predictions of the CT14 PDF set [99] for Fig. 5(c) and (d). In general, the results obtained from the pseudo-experiments with alternative samples are consistent with the true values within statistical uncertainties for all distributions and a variety of alternative samples. These tests demonstrate that the simple bin-by-bin correction procedure using $G_{e\mu}^{i}$ correctly recovers the alternative distributions, without the need for iteration or a matrix-based unfolding procedure. The two-dimensional differential cross-sections were validated using similar procedures and no significant biases were observed.

Pseudo-experiment tests were also performed for the $e\mu b\bar{b}$ differential cross-section analysis, using POWHEG + PYTHIA8 $t\bar{t}$ and diagram-removal scheme Wt events for the reference sample, and either $t\bar{t}$ plus diagram-subtraction Wt events, or the POWHEG $bb4l$+PYTHIA8 sample, for the alternative sample. Figure 6 shows the corresponding results for the p_{T}^{ℓ} and $p_{\mathrm{T}}^{e\mu}$ distributions, two of the distributions that are most sensitive to the modelling of $t\bar{t}/Wt$ interference. The largest discrepancy in any of these tests occurs for the last bin of the $p_{\mathrm{T}}^{e\mu}$ distribution when using POWHEG $bb4l$+ PYTHIA8 for the alternative sample (Fig. 6(d)). This discrepancy has a statistical significance of 3.5 standard deviations, which is comparable to the data statistical uncertainty but less than half the total uncertainty in this bin when systematic uncertainties are included. Other pseudo-experiment tests using alternative values of m_t or diagram subtraction Wt events produced larger changes in the differential cross-section in this bin but showed smaller discrepancies, so no additional uncertainties were included.

5 Systematic uncertainties

Systematic uncertainties in the measured cross-sections arise from uncertainties in the input quantities appearing in Eq. (1), namely the $e\mu$ selection efficiency $\epsilon_{e\mu}$, the tagging correlation coefficient C_b, the non-$t\bar{t}$ background estimates N_1^{bkg} and N_2^{bkg}, and the integrated luminosity L, and from the corresponding quantities in Eqs. (2) and (4) for the $t\bar{t} \to e\mu$ and $e\mu b\bar{b}$ differential cross-sections. Each uncertainty was evaluated by changing all relevant input quantities coherently and re-solving the tagging equations, thus taking into account correlations between the different inputs, and between different bins in the differential analyses. Partial correlations of systematic effects between bins in the differential analyses (e.g. for PDF and lepton efficiency uncertainties) were propagated to the final results. The sources of systematic uncertainty are divided into the five groups discussed below, and are shown for the inclusive and fiducial $t\bar{t}$ cross-sections in Table 2. The uncertainties for the normalised single-differential $t\bar{t} \to e\mu$ cross-sections are shown graphically in Fig. 7, and those for the $e\mu b\bar{b}$ cross-sections in Fig. 8.

5.1 $t\bar{t}$ modelling

The $t\bar{t}$ modelling uncertainties in $\epsilon_{e\mu}$, $G_{e\mu}$, $G_{e\mu}^{i}$, $G_{e\mu b\bar{b}}^{i}$, C_b and C_b^i (and $f_{\mathrm{no}-\tau}^{i}$ for the τ-corrected cross-sections) were evaluated by reweighting the baseline POWHEG MiNNLO + PYTHIA8 $t\bar{t}$ sample and by using the various alternative samples described in Section 2. Specifically, the $t\bar{t}$ matrix element matching uncertainty was evaluated by comparing the POWHEG + PYTHIA8 sample generated with the setting

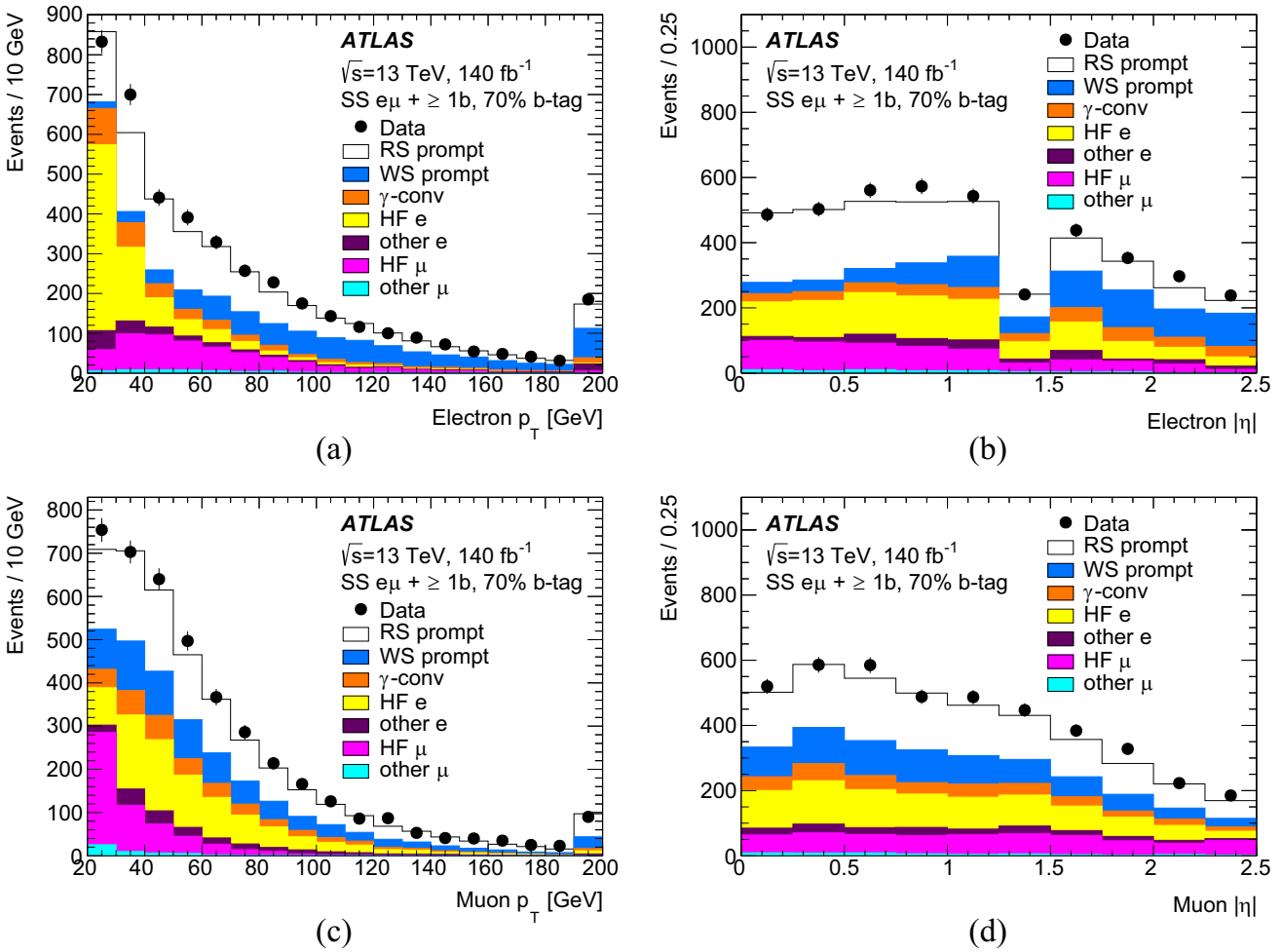

Fig. 4 Distributions of (**a**) the electron p_{T}, (**b**) the electron $|\eta|$, (**c**) the muon p_{T} and (**d**) the muon $|\eta|$, in events with a same-charge $e\mu$ pair and at least one b-tagged jet, also requiring the electron to pass the charge misidentification BDT. The simulation prediction is normalised to the same integrated luminosity as the data, and broken down into contributions where both leptons are prompt and reconstructed with correct charge signs (RS), both leptons are prompt but one has a misreconstructed charge sign (WS), or one is a misidentified lepton from a photon conversion, a heavy-flavour (HF) hadron decay to an electron, a heavy-flavour hadron decay to a muon, or other sources of misidentified electrons (such as misidentified hadrons) and muons (such as decays in flight of pions and kaons). In the p_{T} distributions, the last bin includes the overflows

$p_{\mathrm{T,hard}} = 1$, which changes the definition of the shower veto region, with the nominal $p_{\mathrm{T,hard}} = 0$ POWHEG + PYTHIA8 sample.[5] The uncertainties due to unknown higher-order corrections in the matrix element were assessed by changing the QCD renormalisation and factorisation scales through event weights in the baseline POWHEG MiNNLO + PYTHIA8 sample, taking half the difference between $(\mu_R, \mu_F) = (0.5, 1)$ and $(2, 1)$ variations and half the difference between $(\mu_R, \mu_F) = (1, 0.5)$ and $(1, 2)$ variations. These changes were treated as being independent and added in quadrature. The uncertainty due to the choice of hadronisation, underlying event and parton shower model was assessed from the difference between POWHEG $t\bar{t}$ samples interfaced to HERWIG7.1.3 instead of PYTHIA8. The initial/final-state radiation uncertainty was evaluated by reweighting the POWHEG MiNNLO + PYTHIA8 sample according to the `var3c` A14 tune variations [69] and by variations of the parameter $\mu_{\mathrm{R,FSR}}$ controlling the amount of final-state radiation in the PYTHIA8 shower by factors of 2 and 0.625 with respect to its default value [100]. All these uncertainties were evaluated without applying the lepton isolation requirements, to avoid double-counting efficiency differences absorbed in the lepton isolation efficiency scale factors described in Section 5.2 below.

[5] Since only the baseline sample with nominal settings was available for POWHEG MiNNLO, uncertainty estimates requiring comparison to alternative samples were assessed by evaluating variations with respect to the POWHEG + PYTHIA8 sample with nominal settings, and applying the same relative variation to the efficiencies and tagging correlations obtained from the POWHEG MiNNLO + PYTHIA8 sample.

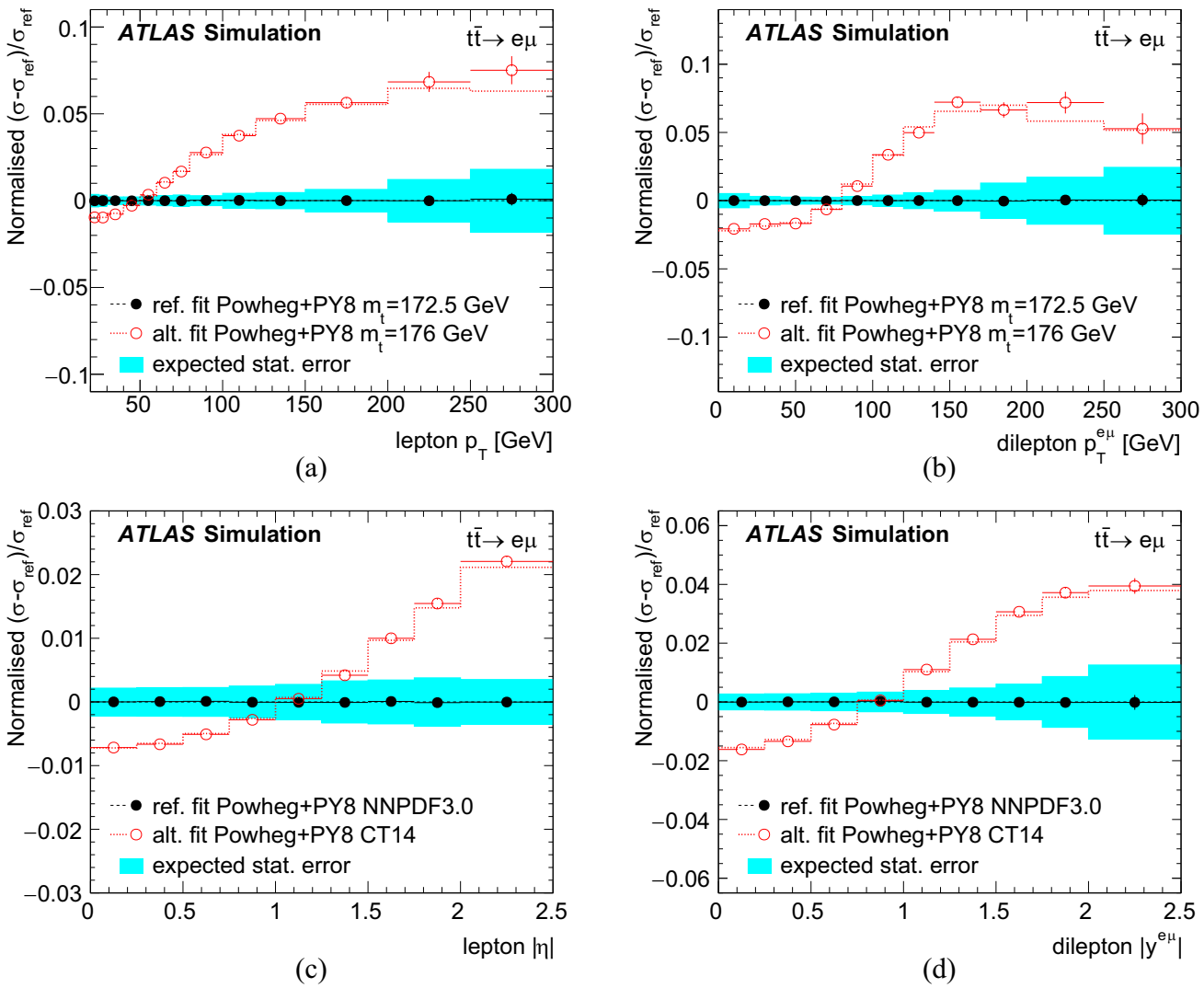

Fig. 5 Results of pseudo-experiment studies on simulated events for the extraction of the normalised $t\bar{t} \to e\mu$ differential cross-section distributions. The upper two plots show (**a**) p_{T}^{ℓ} and (**b**) $p_{\mathrm{T}}^{e\mu}$ using POWHEG + PYTHIA8 $t\bar{t}$ events with $m_t = 172.5\,\mathrm{GeV}$ for the reference sample and $t\bar{t}$ events with $m_t = 176\,\mathrm{GeV}$ for the alternative sample. The lower two plots show (**c**) $|\eta^{\ell}|$ and (**d**) $|y^{e\mu}|$ using $t\bar{t}$ events reweighted to the CT14 PDF set instead of NNPDF3.0 for the alternative sample. The black filled points show the mean deviations from the reference values of the results from pseudo-data samples generated with the reference simulation sample, with error bars indicating the uncertainties due to the limited number of simulated events. The cyan shaded bands indicate the expected statistical uncertainties for a single sample corresponding to the data integrated luminosity. The open red points show the mean deviations from the reference values obtained from pseudo-experiments generated from the alternative simulation sample. The red error bars represent the uncertainty due to the limited size of these alternative samples, and the red dotted lines show the true deviations from the reference in the alternative samples

The values of C_b and C_b^i are sensitive to the fraction of $t\bar{t}$ events with extra $b\bar{b}$ pairs, which increase the probability of b-tagging at least two jets in the event, and also contribute to the rate of events with three or more b-tagged jets. As can be seen from the purple dot-dashed line in Figure 1(a), POWHEG MiNNLO + PYTHIA8 underestimates this rate, as also seen for POWHEG + PYTHIA8 in dedicated analyses [100,101]. The discrepancy was quantified through the ratio of event counts $R_{32} = N(N_{\mathrm{b-tag}} \geq 3)/N(N_{\mathrm{b-tag}} \geq 2)$, measured to be $2.63 \pm 0.03\,\%$ in data compared with $2.02 \pm 0.01\,\%$ in simulation, where the uncertainties are statistical only. The fraction of simulated $t\bar{t}$ events with at least three particle-level b-jets was varied by reweighting, defining such b-jets as particle level jets reconstructed as discussed in Section 4.3 with $p_{\mathrm{T}} > 10\,\mathrm{GeV}$ and matched within $\Delta R < 0.3$ to a weakly decaying b-hadron with $p_{\mathrm{T}} > 5\,\mathrm{GeV}$. These studies showed a linear relationship between R_{32} and C_b, and that increasing the fraction of events with at least three particle-level b-jets by 50% brings R_{32} into agreement with data. The reweighted simulation models the kinematics of the third-highest p_{T} b-

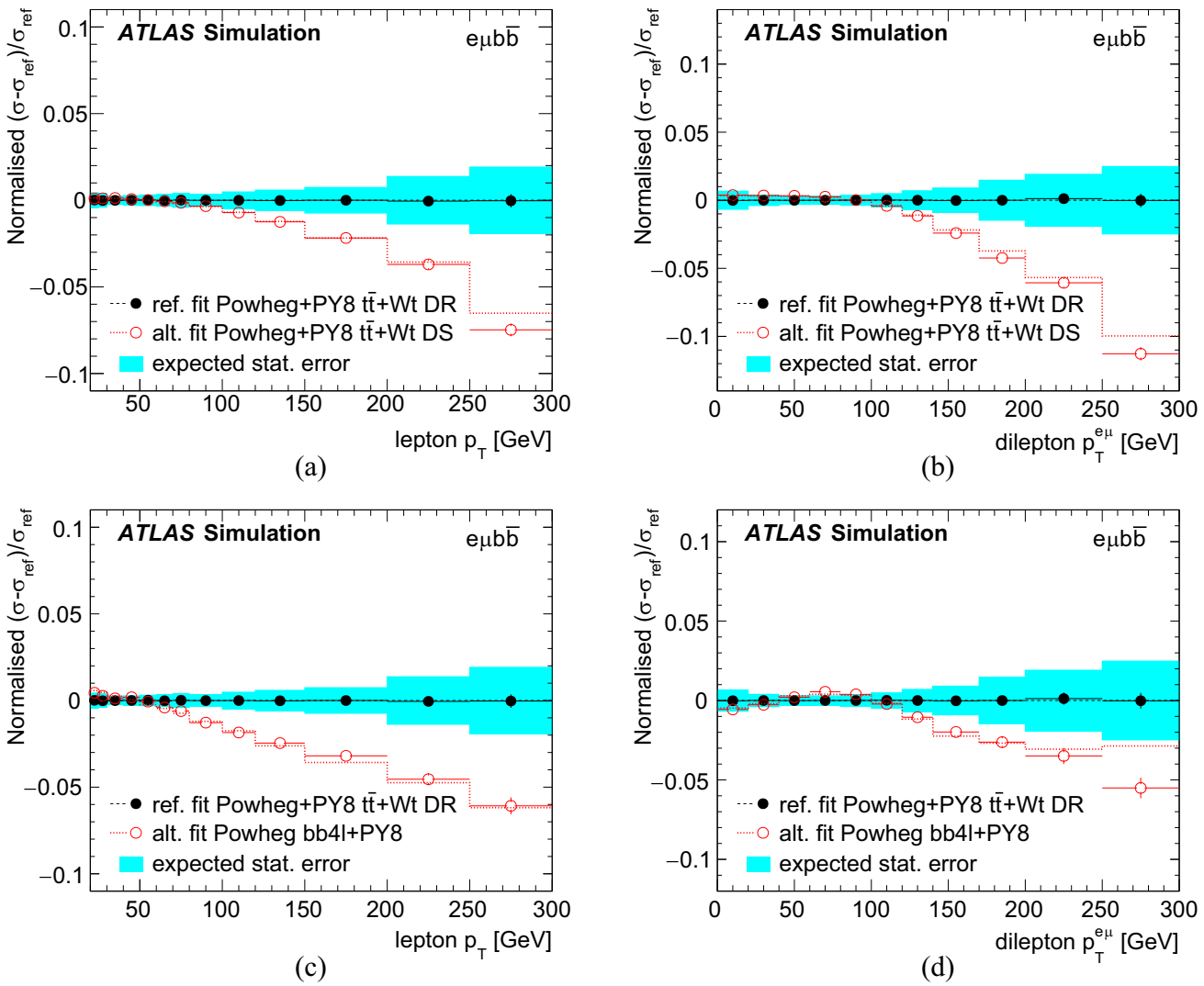

Fig. 6 Results of pseudo-experiment studies on simulated events for the extraction of the normalised $e\mu b\bar{b}$ differential cross-section distributions, showing (**a**, **c**) p_{T}^{ℓ} and (**b**, **d**) $p_{\mathrm{T}}^{e\mu}$. Plots (**a**) and (**b**) use POWHEG + PYTHIA8 $t\bar{t}$ and Wt events, with the diagram removal (DR) scheme used for the reference sample and the diagram subtraction (DS) scheme for the alternative sample. Plots (**c**) and (**d**) use the same reference sample, but POWHEG $bb4l$ + PYTHIA8 for the alternative sample. The interpretation of the points and lines is the same as in Fig. 5

tagged jet well, and increases the value of C_b for the inclusive cross-section analysis by 0.35%. Half the size of this correction was taken as the corresponding uncertainty (shown as '$t\bar{t}$ heavy-flavour production' in Table 2), based on the modelling of the kinematics of the third- and forth-highest p_{T} b-tagged jets. The shifts in C_b from all the $t\bar{t}$ modelling variations discussed above were also included, but are small in comparison.

Parton distribution function uncertainties were evaluated by reweighting the POWHEG MiNNLO + PYTHIA8 $t\bar{t}$ sample to the 100 variations (replicas) of NNPDF3.0 [68] and calculating the RMS of the changes induced in $\epsilon_{e\mu}$, $G_{e\mu}$ $G^{i}_{e\mu}$ and $G^{i}_{e\mu b\bar{b}}$. The resulting uncertainty is 0.47% in $\epsilon_{e\mu}$, but less than 0.1% in $G_{e\mu}$ as PDF variations mainly affect the acceptance rather than the reconstruction efficiency. The central values from the CT18 [23], MSHT20 [24] and NNPDF3.1 [25] PDF sets lie within the NNPDF3.0 uncertainty.

The lepton kinematics, and hence the prediction for $\epsilon_{e\mu}$, also depend slightly on the assumed value of m_t. This effect was evaluated using five POWHEG + PYTHIA8 $t\bar{t}$ samples with different m_t values in the range 169–176 GeV, and gives a relative change of $\pm 0.4\%$ in $\epsilon_{e\mu}$ for a ± 1 GeV change in m_t. In the $\sigma_{t\bar{t}}$ measurement, this effect is partially counterbalanced by changes in the Wt background prediction, which decreases with increasing m_t. Both effects were parameterised using second-order polynomials as functions of m_t, and their combination gives a relative change of -0.29% in $\sigma_{t\bar{t}}$ for a 1 GeV increase in m_t. By convention, the mea-

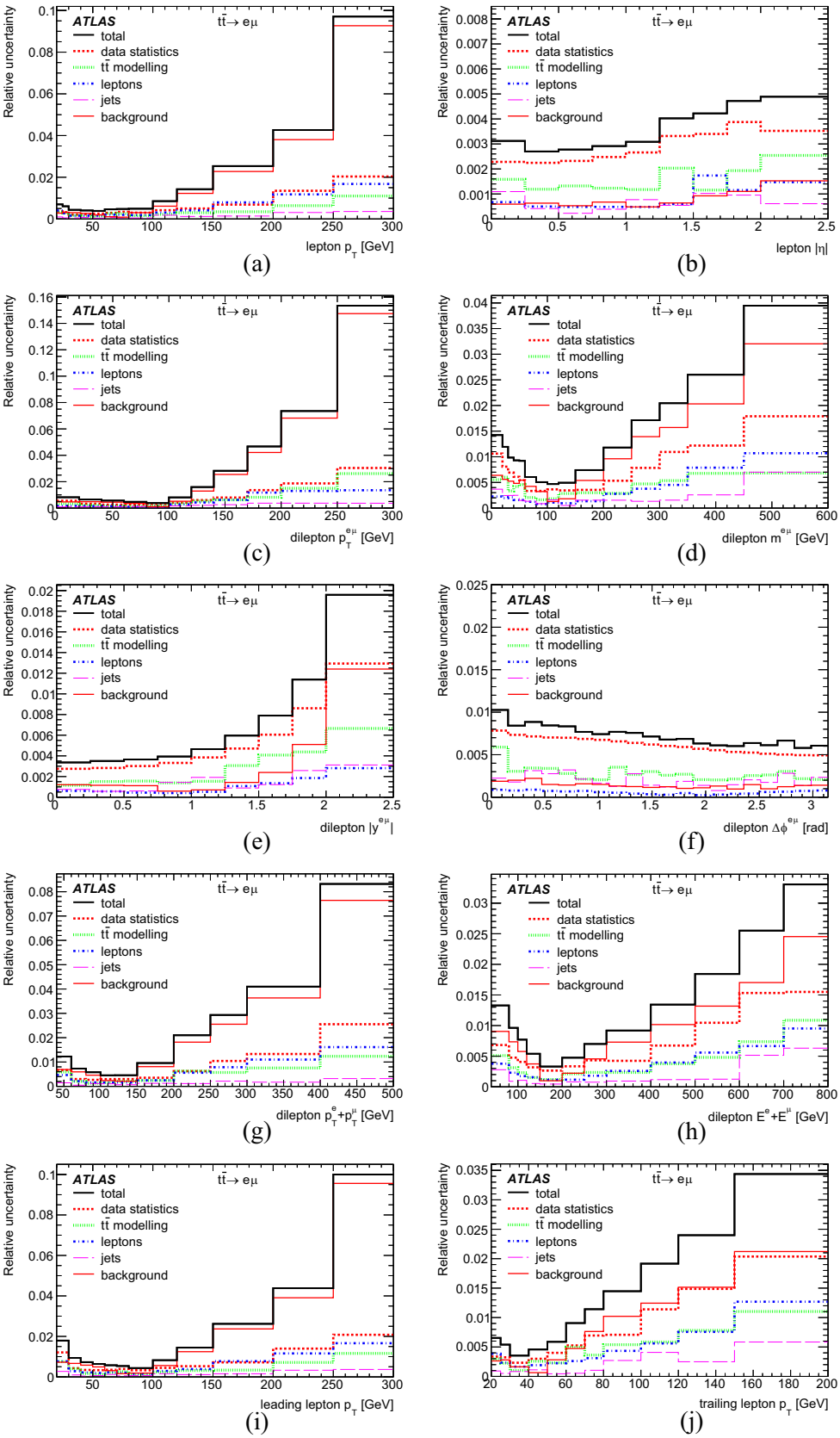

Fig. 7 Relative uncertainties in the measured one-dimensional normalised $t\bar{t} \to e\mu$ differential cross-sections coming from data statistics, $t\bar{t}$ modelling, leptons, jets and background, as a function of each lepton or dilepton differential variable. The total uncertainty is shown by the thick black lines, and also includes small contributions from the integrated luminosity and LHC beam energy uncertainties

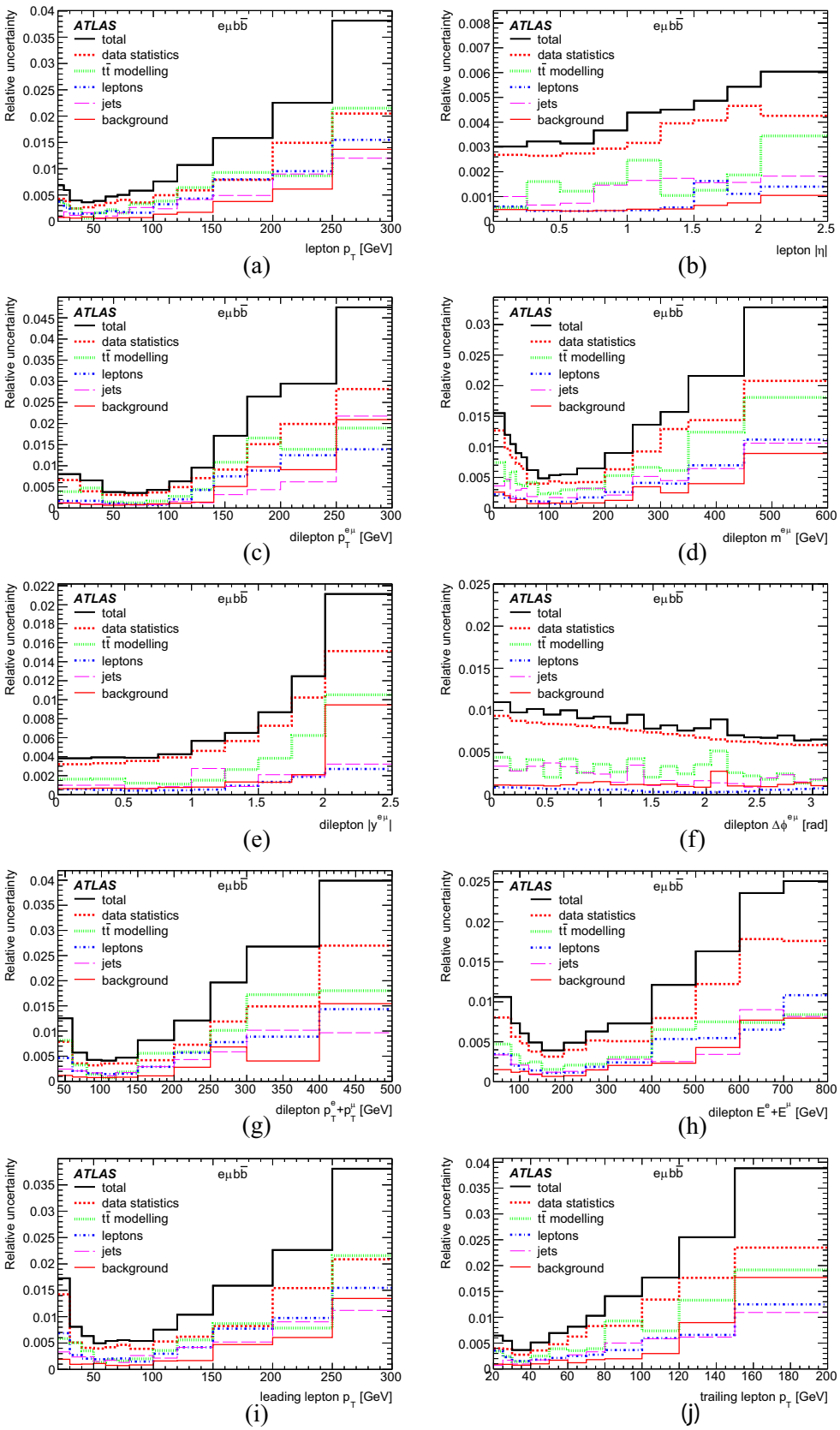

Fig. 8 Relative uncertainties in the measured one-dimensional normalised $e\mu b\bar{b}$ differential cross-sections coming from data statistics, $t\bar{t}$ modelling, leptons, jets and background, as a function of each lepton or dilepton differential variable. The total uncertainty is shown by the thick black lines, and also includes small contributions from the integrated luminosity and LHC beam energy uncertainties

Table 2 Breakdown of the relative systematic uncertainties in $\epsilon_{e\mu}$, $G_{e\mu}$ and C_b, and the statistical, systematic (excluding luminosity and beam energy) and total uncertainties in the inclusive and fiducial $t\bar{t}$ cross-section measurements. The five groups of systematic uncertainties corresponding to the discussion in Sections 5.1 to 5.5 are indicated in the leftmost column

Group	Uncertainty source	$\Delta\epsilon_{e\mu}/\epsilon_{e\mu}$ (%)	$\Delta G_{e\mu}/G_{e\mu}$ (%)	$\Delta C_b/C_b$ (%)	$\Delta\sigma_{t\bar{t}}/\sigma_{t\bar{t}}$ (%)	$\Delta\sigma_{t\bar{t}}^{\text{fid}}/\sigma_{t\bar{t}}^{\text{fid}}$ (%)
	Data statistics				0.16	0.16
$t\bar{t}$ mod.	$t\bar{t}$ matrix element matching	0.01	0.02	0.02	0.01	0.00
	QCD scale variation	0.29	0.07	0.02	0.31	0.09
	$t\bar{t}$ hadronisation	0.23	0.06	0.06	0.29	0.00
	Initial/final state radiation	0.04	0.03	0.09	0.16	0.17
	$t\bar{t}$ heavy-flavour production	0.00	0.00	0.17	0.17	0.17
	Parton distribution functions	0.47	0.05	–	0.47	0.08
	Simulation statistics	0.07	0.04	0.05	0.05	0.04
Lept.	Electron identification	0.12	0.12	–	0.14	0.14
	Muon identification	0.13	0.13	–	0.14	0.14
	Electron charge mis-id	0.05	0.05	–	0.06	0.06
	Lepton trigger	0.10	0.10	0.00	0.11	0.11
	Electron energy scale	0.04	0.04	0.00	0.05	0.05
	Electron energy resolution	0.01	0.01	0.00	0.01	0.01
	Muon momentum scale	0.01	0.01	0.00	0.02	0.02
	Muon momentum resolution	0.00	0.00	0.00	0.00	0.00
	Electron isolation	0.10	0.10	–	0.11	0.11
	Muon isolation	0.12	0.12	–	0.13	0.13
Jet/b	Jet energy scale	–	–	0.05	0.02	0.02
	Jet energy resolution	–	–	0.03	0.06	0.06
	Pileup jet veto	–	–	0.00	0.02	0.02
	b-tagging efficiency	–	–	0.01	0.13	0.13
	b-tag mistagging	–	–	0.02	0.02	0.02
Bkg.	Single-top cross-section	–	–	–	0.40	0.40
	Single-top/$t\bar{t}$ interference	–	–	–	0.28	0.28
	Single-top modelling	–	–	–	0.30	0.30
	Z+jets extrapolation	–	–	–	0.02	0.02
	Diboson cross-sections	–	–	–	0.01	0.01
	Diboson modelling	–	–	–	0.05	0.05
	Misidentified leptons	–	–	–	0.18	0.18
	Analysis systematics	0.66	0.29	0.22	0.97	0.74
L/E_{b}	Integrated luminosity	–	–	–	0.89	0.89
	Beam energy	–	–	–	0.23	0.23
	Total uncertainty	0.66	0.29	0.22	1.34	1.19

sured $\sigma_{t\bar{t}}$ is quoted at a fixed value of $m_t = 172.5\,\text{GeV}$, but a $\pm 1\,\text{GeV}$ m_t variation is included in the differential cross-section uncertainties.

The total $t\bar{t}$ modelling uncertainties also include the small contributions due to the limited size of the POWHEG MiNNLO+PYTHIA8 $t\bar{t}$ sample ('Simulation statistics' in Table 2) and are shown for the differential distributions by the green hatched lines in Figures 7 and 8.

5.2 Lepton identification and measurement

The lepton identification efficiencies were measured using tag-and-probe techniques applied to $Z \to ee$ and $Z \to \mu\mu$ events [60,61], as functions of lepton p_{T} and η for electrons, and η and ϕ for muons. The corresponding uncertainties are only partially correlated across p_{T}, η and ϕ, and this information was propagated to the final results by generating multiple sets of scale factors whose variations represent

the full uncertainty model. The uncertainties due to electron charge misidentification were studied using $Z \to ee$ events and taken into account using the same technique. The lepton trigger efficiencies were also measured in $Z \to ee$ and $Z \to \mu\mu$ events using tag-and-probe techniques [49,50], giving per-lepton uncertainties of 0.2–1% for electrons and 0.5–3% for muons. Since a large fraction of dilepton events are triggered redundantly by both leptons, the corresponding uncertainty in $\sigma_{t\bar{t}}$ is only 0.11%. The electron energy scale, muon momentum scale and corresponding resolution were determined using $Z \to ee$ and $Z \to \mu\mu$ events [57,58], and varied according to the corresponding uncertainties.

The lepton isolation efficiencies were measured directly in $t\bar{t}$-dominated $e\mu$ plus b-tagged jet samples by determining the fraction of events where either the electron or muon fails the isolation cut. After correcting for background contamination [35], the results as a function of lepton p_{T} for $|\eta| < 1.5$ and $|\eta| > 1.5$ are shown in Figure 9, for data and simulation with POWHEG MiNNLO + PYTHIA8 $t\bar{t}$ events. At low p_{T}, the simulation underestimates the electron efficiency in data by about 1.5%, and overestimates the muon efficiency by 1%. The ratios of data to simulation efficiencies were used to define multiplicative efficiency corrections (scale factors) applied to simulation on a per-lepton basis. The uncertainties in these scale factors are dominated by the subtraction of the misidentified-lepton background for the samples of leptons that fail the isolation requirement [35]; such events are not used in the differential cross-section measurements. The uncertainties amount to about 0.1% per lepton, partially correlated across the differential distributions. The method was validated using various reweighted and alternative $t\bar{t}$ simulation samples that predict different isolation efficiencies, also demonstrating that the sum of the measured electron and muon efficiency shifts reproduce the isolation-related component of the shifts in $\epsilon_{e\mu}$ and $G_{e\mu}$. The total lepton-related uncertainties are shown by the blue dot-dashed lines in Figures 7 and 8, and include the effects on both $t\bar{t}$ and Wt events.

5.3 Jet measurement and b-tagging

Uncertainties in jet reconstruction and calibration affect the estimates of the background contributions from Wt and diboson events, the values of C_b and C_b^i, and the values of $G^i_{e\mu b\bar{b}}$ and ϵ_b^{MC} for the $e\mu b\bar{b}$ differential cross-section analysis. The jet energy scale was determined using a combination of simulation, test beam and in-situ measurements, and the jet energy resolution was evaluated using di-jet balance techniques [59]. The modelling of the pileup jet veto JVT requirement was studied using jets in $Z \to \mu\mu$ events [95].

The efficiency for b-tagging jets in $t\bar{t}$ events was extracted from the data via Eqs. (1), but simulation was used to predict the number of b-tagged jets in Wt and diboson background events, as well as $G^i_{e\mu b\bar{b}}$ and ϵ_b^{MC}. The corresponding scale factors and uncertainties for b, charm and light-flavour jets were determined using $t\bar{t}$ and Z+jets events [62,102,103]. As these b-tagging efficiency scale factors are used only for background determination in the $t\bar{t}$ cross-section measurements, the use of the same data sample to determine them in Ref. [62] does not result in significant correlation. The uncertainties related to jets and b-tagging are shown by the purple long-dashed lines in Figures 7 and 8.

5.4 Background modelling

The normalisation of the Wt background was varied by 3.7%, corresponding to the PDF and QCD uncertainties in the prediction discussed in Section 2. The uncertainty due to $t\bar{t}/Wt$ interference was assessed by comparing POWHEG + PYTHIA8 Wt samples with the diagram removal and diagram subtraction schemes [38,80]. Although small for the inclusive cross-section, this uncertainty is dominant at the high ends of the lepton p_{T} and dilepton $p_{\mathrm{T}}^{e\mu}$, $m^{e\mu}$, $p_{\mathrm{T}}^{e} + p_{\mathrm{T}}^{\mu}$, $E^e + E^\mu$, $p_{\mathrm{T}}^{\ell,\mathrm{max}}$ and $p_{\mathrm{T}}^{\ell,\mathrm{min}}$ distributions in the $t\bar{t} \to e\mu$ measurements. The studies of Ref. [43] suggest that data lies between the diagram removal and diagram subtraction predictions in the region where interference becomes important. Further modelling uncertainties were evaluated by comparing the baseline Wt sample with samples generated with $p_{\mathrm{T,hard}} = 1$, with $h_{\mathrm{damp}} = 3m_t$, with POWHEG + HERWIG7.1, and by reweighting to change the values of μ_R and μ_F. These uncertainties were taken to be uncorrelated with the corresponding $t\bar{t}$ modelling uncertainties. Initial/final state radiation uncertainties were also evaluated based on `var3c` A14 tune and $\mu_{\mathrm{R,FSR}}$ variations, and taken to be correlated with the corresponding $t\bar{t}$ uncertainties. The small background acceptance uncertainties from NNPDF3.0 variations were also included.

The Wt component is part of the signal in the $e\mu b\bar{b}$ differential analysis, so the Wt modelling uncertainties were evaluated as changes in $G^i_{e\mu b\bar{b}}$, and correlated with the corresponding variations in the $t\bar{t}$ signal component where appropriate. In addition, $G^i_{e\mu b\bar{b}}$ depends on the relative fractions of $t\bar{t}$ and Wt events in the signal, evaluated by separately changing the $t\bar{t}$ normalisation by 4.0% and the Wt normalisation by 3.7%, based on the predicted cross-sections given in Sections 1 and 2.

The $Z(\to \tau\tau \to e\mu)$+jets background prediction was normalised using the corresponding yield ratios in $Z(\to ee/\mu\mu)$ events as described in Section 4.4, and the corresponding uncertainties were propagated to the cross-section results. For the differential analyses, the changes in predictions as a function of lepton kinematics when performing the normalisation in bins of Z-boson p_{T} rather than inclusively were also taken into account. The inclusive diboson

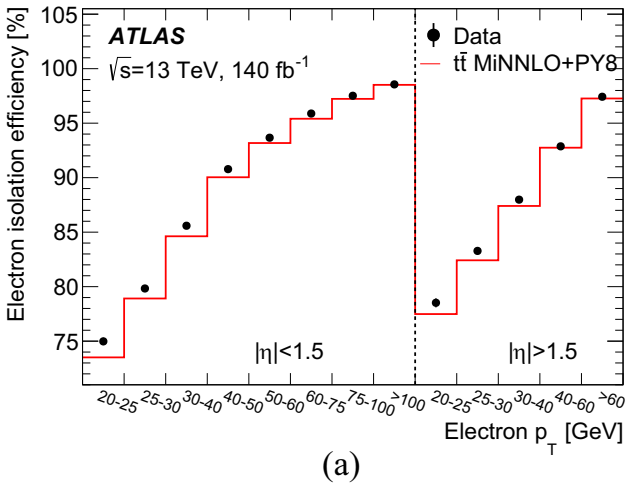

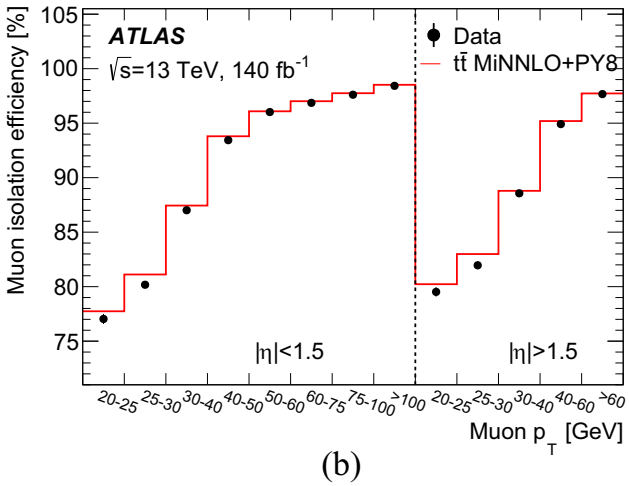

Fig. 9 Lepton isolation efficiencies measured in $t\bar{t} \to e\mu$ events for (a) electrons and (b) muons, as functions of lepton p_{T} in two bins of $|\eta|$. The data is shown by the points with error bars and compared with simulation with POWHEG MiNNLO+PYTHIA8 $t\bar{t}$ events without isolation efficiency scale factors, shown by the red histograms

cross-sections were varied by 6%, based on MCFM predictions [104], and the QCD factorisation and normalisation scales were varied by reweighting the SHERPA samples. The uncertainties in the background from events with misidentified leptons, evaluated using the same-charge $e\mu$ samples, are discussed in Section 4.4. The total background uncertainties are shown by the red solid lines in Figures 7 and 8, and are dominated by those in the Wt background.

5.5 Luminosity and beam energy

The integrated luminosity of the dataset was evaluated using the LUCID2 detector [105], complemented by measurements from the inner detector and calorimeters, and has an uncertainty of 0.83% [47]. In the inclusive cross-section analysis, an optimised combination of results from the separate 2015+16, 2017 and 2018 datasets is used as discussed in Section 6.1, slightly reducing the effective luminosity uncertainty. For both inclusive and differential analyses, the luminosity-related uncertainty in the cross-section values is around 10% larger than that in the integrated luminosity itself, as the simulation-based Wt and diboson background estimates depend on the integrated luminosity of the dataset.

The LHC beam energy is known to be within 0.1% of the nominal value at $\sqrt{s} = 13\,\mathrm{TeV}$ [106], which translates into an 0.23% uncertainty in $\sigma_{t\bar{t}}$, quoted as part of the experimental uncertainty as discussed in Ref. [34]. Similar uncertainties arise in the absolute $t\bar{t} \to e\mu$ and $e\mu b\bar{b}$ differential cross-sections, but almost completely cancel in the normalised measurements.

6 Inclusive cross-section results and interpretation

The results of the inclusive cross-section analysis are given in Section 6.1, followed by the top quark mass in Section 6.2. The analysis results were initially blinded by multiplying the $\sigma_{t\bar{t}}$ values by a randomly chosen scale factor that was only removed after finalising all systematic uncertainties and stability studies, and verifying that consistent results were obtained from the 2015+16, 2017 and 2018 datasets.

6.1 Total and fiducial cross-section results

Table 3 shows the results for $\sigma_{t\bar{t}}$ and $\sigma_{t\bar{t}}^{\mathrm{fid}}$ from the entire dataset treated as a single sample, separate results from the 2015+16, 2017 and 2018 datasets, and the combination of these three datasets using the best linear unbiased estimator technique [107,108], taking into account correlations in the systematic uncertainties. Since the largest uncertainties come from the luminosity measurement, and these uncertainties are only partially correlated between years [47], this combination gives a greater weight to the 2015+16 data despite its larger statistical uncertainty, and is used for the final results:

$$\sigma_{t\bar{t}} = 829.3 \pm 1.3 \pm 8.0 \pm 7.3 \pm 1.9\,\mathrm{pb}, \text{ and}$$
$$\sigma_{t\bar{t}}^{\mathrm{fid}} = 14.04 \pm 0.02 \pm 0.10 \pm 0.12 \pm 0.03\,\mathrm{pb},$$

where the four uncertainties are due to data statistics, experimental and theoretical systematic effects internal to the analysis, the knowledge of the integrated luminosity, and the knowledge of the LHC beam energy. The total relative uncertainties are 1.3% for $\sigma_{t\bar{t}}$ and 1.2% for $\sigma_{t\bar{t}}^{\mathrm{fid}}$. The three datasets have weights of 0.53, 0.23 and 0.24, and the combination has a χ^2 of 1.5 for two degrees of freedom, demonstrating the good compatibility of the results. The values of ϵ_b are 0.5–

1% lower in data than in simulation, well within the uncertainties in modelling the b-tagging performance [62]. The result for $\sigma_{t\bar{t}}$ is reported for a fixed top quark mass of $m_t = 172.5\,\text{GeV}$, and depends on the assumed value according to $(1/\sigma_{t\bar{t}})\,\mathrm{d}\sigma_{t\bar{t}}/\mathrm{d}m_t = -0.29\%/\text{GeV}$. The m_t dependence of the measured $\sigma_{t\bar{t}}^{\text{fid}}$ is negligible. The fiducial cross-section corrected to remove the contribution from leptonic decays of τ-leptons is $\sigma_{t\bar{t},\text{no}-\tau}^{\text{fid}} = 12.03 \pm 0.02 \pm 0.10 \pm 0.11 \pm 0.03\,\text{pb}$.

The results are stable within statistical uncertainties when increasing the jet p_{T} requirement from the nominal $p_T^{\text{jet}} > 25\,\text{GeV}$ to $p_T^{\text{jet}} > 75\,\text{GeV}$ (where the tagging correlation increases to $C_b = 1.17$), when reducing the jet acceptance to $|\eta^{\text{jet}}| < 1.5$ and when using the looser 77% b-tagging efficiency working point. The cross-section decreases slightly when increasing the lepton p_{T} requirement, e.g. $\sigma_{t\bar{t}}$ changes by $-0.77 \pm 0.11\%$ with $p_{\text{T}}^{\ell} > 35\,\text{GeV}$ instead of $p_{\text{T}}^{\ell} > 20\,\text{GeV}$, where the uncertainty represents the uncorrelated statistical component only. However, the $t\bar{t}$ modelling uncertainty from QCD scale variations, initial/final-state radiation and hadronisation also increases from 0.43% to 0.86%, suggesting this change in central value is reasonable given the 40% reduction in acceptance.

Table 2 shows the breakdown of statistical and systematic uncertainties in $\sigma_{t\bar{t}}$ and $\sigma_{t\bar{t}}^{\text{fid}}$, together with the average uncertainty contributions to $\epsilon_{e\mu}$, $G_{e\mu}$ and C_b, weighted as in the combination. The largest uncertainty comes from the calibration of the integrated luminosity, followed by $t\bar{t}$ modelling (in particular PDF uncertainties, hadronisation and QCD scale variations, which are significantly smaller in the fiducial cross-section measurement) and background uncertainties from the Wt cross-section and modelling. The result is consistent with the previous ATLAS measurement of $\sigma_{t\bar{t}}$ at $\sqrt{s} = 13\,\text{TeV}$ [12], which it supersedes. The total uncertainty has been reduced from 1.8% to 1.3%, giving the most precise measurement of $\sigma_{t\bar{t}}$ to date. The new result benefits from the better modelling of the top quark (and hence lepton) kinematics in POWHEG MiNNLO + PYTHIA8 compared with POWHEG + PYTHIA8, a more inclusive lepton selection requiring $p_{\text{T}} > 20\,\text{GeV}$ rather than $p_{\text{T}} > 25\,\text{GeV}$, a more precise understanding of lepton identification and isolation efficiencies, refined modelling of the Wt background and an optimal treatment of the data given the luminosity uncertainties.

The inclusive cross-section result, together with other ATLAS measurements in dilepton and lepton+jets final states at $\sqrt{s} = 5.02\,\text{TeV}$ [8], $\sqrt{s} = 7\,\text{TeV}$ [9,10], $\sqrt{s} = 8\,\text{TeV}$ [9,11], $\sqrt{s} = 13\,\text{TeV}$ [13] and $\sqrt{s} = 13.6\,\text{TeV}$ [14], is compared in Figure 10 with the NNLO+NNLL QCD prediction described in Section 1, calculated with `Top++` [21] with the PDF4LHC21 [22] PDF combination. The result is in good agreement with the prediction, and has about one third of the uncertainty. The result also agrees with measurements at $\sqrt{s} = 13\,\text{TeV}$ from the CMS Collaboration [18,19] but again has significantly higher precision.

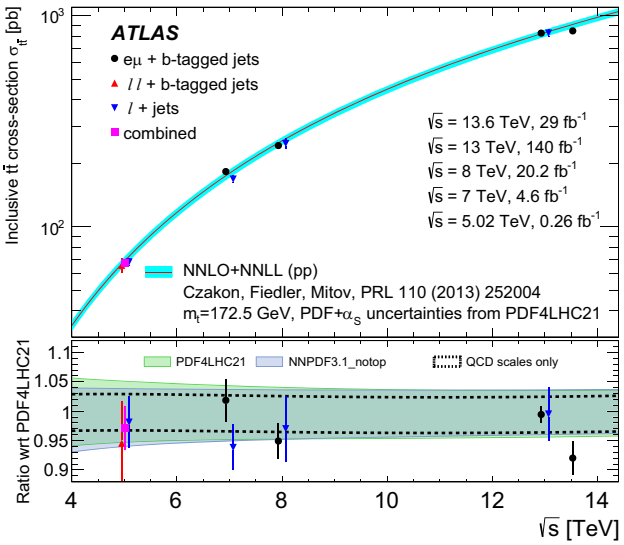

Fig. 10 The upper panel shows the inclusive $t\bar{t}$ cross-section as a function of centre-of-mass energy $\sqrt{s}$, comparing ATLAS results from the $e\mu$, dilepton ($\ell\ell$) and lepton+jets final states (and the combination of $\ell\ell$ and lepton+jets at $\sqrt{s} = 5.02\,\text{TeV}$) with NNLO+NNLL theoretical predictions [6,21] using the PDF4LHC21 PDF set [22]. The lower panel shows the ratios of measurements and predictions to the central value of the prediction with PDF4LHC21. The total uncertainties when using the PDF4LHC21 and NNPDF3.1_notop PDF sets are shown as the overlapping coloured bands, and the dotted lines show the QCD scale uncertainties alone

6.2 Extraction of the top quark pole mass

The strong dependence of the prediction for $\sigma_{t\bar{t}}$ on the top quark pole mass m_t^{pole} can be exploited to interpret the precise measurement of $\sigma_{t\bar{t}}$ as a measurement of m_t^{pole}. This interpretation was performed for two recent PDF sets that do not use any LHC $t\bar{t}$ differential cross-section data as input, as the use of such data in PDF fits can introduce a dependence on the assumed value of m_t. The baseline result is based on the NNPDF3.1_notop NNLO PDF set [25] with $\alpha_{\text{s}} = 0.1180 \pm 0.0010$, as used in Ref. [109]. This prediction is shown in the lower panel of Figure 10. The CT14 [99] NNLO PDF set was also considered, assuming $\alpha_{\text{s}} = 0.1180 \pm 0.0012$ and scaling the uncertainties to correspond to 68% confidence levels.

Figure 11 shows the dependence of the predicted $\sigma_{t\bar{t}}$ on m_t^{pole} for the NNPDF3.1_notop PDF set, calculated using `Top++` [6,21]. It also shows the experimental measurement from Section 6.1 with its dependence on the top quark mass in simulation m_t^{MC} obtained from the polynomial parameterisation described in Section 5.1, assuming $m_t^{\text{MC}} \approx m_t^{\text{pole}}$. The value of m_t^{pole} maximising the compatibility with the

Table 3 Measurements of the inclusive total ($\sigma_{t\bar{t}}$) and fiducial ($\sigma_{t\bar{t}}^{\text{fid}}$) $t\bar{t}$ production cross-sections at $\sqrt{s} = 13\,\text{TeV}$ using the full dataset, the 2015+16, 2017 and 2018 datasets separately, and the combination of the three separate measurements. The four uncertainties for each measurement correspond to the statistical, experimental and theoretical systematic, integrated luminosity, and beam energy uncertainties. The total uncertainties are given in parentheses. The integrated luminosity L of each dataset is also shown

Dataset	L [fb^{-1}]	$\sigma_{t\bar{t}}$ [pb]	$\sigma_{t\bar{t}}^{\text{fid}}$ [pb]
All data	140.1	$827.5 \pm 1.1 \pm 8.0 \pm 7.6 \pm 1.9$ (11.3)	$14.01 \pm 0.02 \pm 0.10 \pm 0.13 \pm 0.03$ (0.17)
2015+16 data	36.6	$831.5 \pm 2.2 \pm 8.1 \pm 8.0 \pm 1.9$ (11.7)	$14.08 \pm 0.04 \pm 0.10 \pm 0.14 \pm 0.03$ (0.18)
2017 data	44.6	$833.1 \pm 2.0 \pm 8.1 \pm 10.5 \pm 1.9$ (13.5)	$14.11 \pm 0.03 \pm 0.10 \pm 0.18 \pm 0.03$ (0.21)
2018 data	58.8	$820.8 \pm 1.7 \pm 8.0 \pm 10.0 \pm 1.9$ (13.1)	$13.90 \pm 0.03 \pm 0.10 \pm 0.17 \pm 0.03$ (0.21)
Combination	140.1	$829.3 \pm 1.3 \pm 8.0 \pm 7.3 \pm 1.9$ (11.1)	$14.04 \pm 0.02 \pm 0.10 \pm 0.12 \pm 0.03$ (0.17)

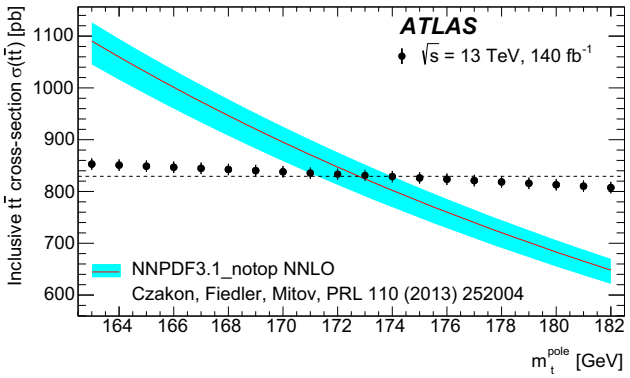

Fig. 11 The red line shows the predicted inclusive $t\bar{t}$ cross-section at $\sqrt{s} = 13\,\text{TeV}$ as a function of m_t^{pole} for the NNPDF3.1_notop PDF set, with the cyan band indicating the total uncertainty in the prediction from PDF+α_s and QCD scale uncertainties. The black points show the experimental measurement with its uncertainty and dependence on the assumed value of m_t through acceptance and background corrections. The dotted line shows the experimental central value at a fixed top quark mass of 172.5 GeV

measured $\sigma_{t\bar{t}}$ was extracted using the Bayesian likelihood formulation detailed in Ref. [34], giving a result of:

$$m_t^{\text{pole}} = 172.8^{+1.5}_{-1.7}\,\text{GeV} .$$

The breakdown of uncertainties is shown in Table 4. The high precision of the experimental measurement of $\sigma_{t\bar{t}}$ results in the uncertainty being dominated by those on the theoretical prediction. The result for the CT14 PDF set is also given; this PDF set gives a slightly higher central value for m_t and a larger uncertainty. Compared with these uncertainties, the assumption that the top quark mass used in simulation for the $\sigma_{t\bar{t}}$ measurement is close to m_t^{pole} has a very small effect, corresponding e.g. to a 0.12 GeV shift for a 1 GeV difference between m_t^{MC} and m_t^{pole}.

The result is compatible with the value of $172.9 \pm 1.7\,\text{GeV}$ derived from the ATLAS measurement of $\sigma_{t\bar{t}}$ with $36\,\text{fb}^{-1}$ of $\sqrt{s} = 13\,\text{TeV}$ data [34], and with the value of $173.4^{+1.8}_{-2.0}\,\text{GeV}$ obtained from the combination of ATLAS and CMS $\sigma_{t\bar{t}}$ measurements at $\sqrt{s} = 7$–$8\,\text{TeV}$ [109], both using NNPDF3.1_notop, as well as with measurements from CMS at $\sqrt{s} = 13\,\text{TeV}$ [19] and from D0 at the Tevatron pp collider [110]. It is also compatible with the average of direct measurements of the top quark mass from its decay products, $m_t = 172.57 \pm 0.29\,\text{GeV}$ [32], which has much higher precision but makes stronger assumptions on the interpretation of the mass parameter in $t\bar{t}$ event generators.

Table 4 Extraction of the top quark pole mass from the $t\bar{t}$ production cross-section measurement at $\sqrt{s} = 13\,\text{TeV}$ using the NNPDF3.1_notop and CT14 PDF sets. The first row gives the result with the total uncertainty, and the subsequent rows show the individual uncertainty components

PDF set	NNPDF3.1_notop	CT14
Result [GeV]	$172.79^{+1.52}_{-1.70}$	$173.00^{+1.84}_{-2.04}$
Experimental	0.55	0.55
PDF+α_s	$^{+1.00}_{-0.89}$	$^{+1.50}_{-1.48}$
QCD scales	$^{+1.00}_{-1.48}$	$^{+1.01}_{-1.49}$

7 Differential cross-section results

The single-lepton and dilepton $t\bar{t} \to e\mu$ differential cross-sections were obtained from the full dataset by solving the tagging equations Eqs. (2) for each bin i of each distribution. The results were found to be stable when varying the jet p_{T}, $|\eta|$ and b-tagging requirements. The single-lepton p_{T}^{ℓ} and $|\eta^{\ell}|$ distributions were also measured separately for electrons and muons, instead of combining them into lepton distributions with two entries per event, and found to be compatible. The distributions of bin-by-bin differences between the electron and muon differential cross-sections have χ^2 per degree of freedom of 8/12 for p_{T}^{ℓ} and 10/8 for $|\eta^{\ell}|$, taking statistical and uncorrelated systematic uncertainties into account. The normalised distributions were also found to be consistent with the measurements from the $36\,\text{fb}^{-1}$ data sample [34], in most cases within the uncorrelated statistical uncertainties.

Table 5 Breakdown of uncertainties in the measured $e\mu b\bar{b}$ fiducial cross-section in broad categories

Uncertainty	$\Delta\sigma^{\text{fid}}_{e\mu b\bar{b}}/\sigma^{\text{fid}}_{e\mu b\bar{b}}$ (%)
Data statistics	0.16
$t\bar{t}+Wt$ modelling	1.34
Leptons	0.29
Jets/b-tagging	0.26
Backgrounds	0.36
Luminosity/E_{beam}	0.92
Total uncertainty	1.72

The $e\mu b\bar{b}$ differential cross-sections were obtained from Eq. (4). The value of ϵ_b obtained from solving Eq. (1) with the inclusive data event counts corresponding to the 77% b-tagging efficiency working point is slightly lower than that in simulation, leading to a correction factor $S_{\text{tag}} = 1.0086 \pm 0.0007$, where the uncertainty is statistical only. The correction S^2_{tag} was applied to all bins of all absolute $e\mu b\bar{b}$ differential cross-sections. The integrals of the ten one-dimensional differential distributions each give the integrated fiducial cross-section $\sigma^{\text{fid}}_{e\mu b\bar{b}}$, and agree at the 0.1% level.[6] The cross-section for the complete $e\mu b\bar{b}$ fiducial region was calculated from the unweighted average of the individual distribution integrals, giving:

$$\sigma^{\text{fid}}_{e\mu b\bar{b}} = 9.56 \pm 0.02 \pm 0.16 \text{ pb},$$

where the first uncertainty is statistical, and the second systematic (including the luminosity and beam energy uncertainties), giving a relative uncertainty of 1.7%. A breakdown of the uncertainties in broad categories is given in Table 5, This fiducial cross-section is more inclusive than that measured in Ref. [43], which requires $p^{\ell}_{\text{T}} > 28\,\text{GeV}$ rather than $p^{\ell}_{\text{T}} > 20\,\text{GeV}$, with overlap removal requirements between the b-jets and leptons, and has a relative precision of 4.8%. The better precision of the present result is due primarily to the in situ measurement of the b-tagging and jet reconstruction efficiency via S_{tag}.

7.1 Results for $t\bar{t} \to e\mu$ and $e\mu b\bar{b}$ differential cross-sections

The measured absolute one-dimensional $t\bar{t} \to e\mu$ and $e\mu b\bar{b}$ differential cross-sections are shown in the upper panels of Figures 12, 13, 14, 15, 16, and the two-dimensional cross-sections are shown in Figures 17, 18, 19. The latter Figures show 'unrolled' distributions with the four groups of $|\eta^{\ell}|$, $|y^{e\mu}|$ or $\Delta\phi^{e\mu}$ bins corresponding to each $m^{e\mu}$ bin shown consecutively on the x-axis. Numerical values for both the absolute and normalised differential cross-sections, including a set of results corrected to remove the contributions from $W \to \tau \to e/\mu$ decays, can be found at Ref. [97], and are available in the HEPData repository [111].

The uncertainties in the one-dimensional normalised $t\bar{t} \to e\mu$ cross-sections are shown in Fig. 7, and range from 0.3% to around 10% at the upper ends of the p_{T}-related distributions. For the $|\eta^{\ell}|$, $|y^{e\mu}|$ and $\Delta\phi^{e\mu}$ distributions, the largest uncertainties are typically statistical, whereas $t\bar{t}$ modelling also plays an important role at the lower ends of the p_{T}-related distributions. At the upper ends of those distributions, the background modelling, in particular the $t\bar{t}/Wt$ interference uncertainty, becomes dominant. The normalised differential cross-sections benefit from substantial cancellations in the systematic uncertainties across bins, which are absent in the absolute differential cross-section measurements; the latter also suffer from the integrated luminosity uncertainty, which contributes 0.9–1.1% in most bins. The corresponding uncertainties in the one-dimensional $e\mu b\bar{b}$ cross-sections are shown in Fig. 8, and exhibit many similar features. However, the background uncertainties in the p_{T}-related distributions do not suffer as much from the $t\bar{t}/Wt$ interference uncertainty, being e.g. 2.3% and 3.8% in the $200 < p^{\ell}_{\text{T}} < 250\,\text{GeV}$ and $p^{\ell}_{\text{T}} > 250\,\text{GeV}$ bins in the $e\mu b\bar{b}$ measurement compared with 4.3% and 9.7% in the $t\bar{t} \to e\mu$ measurement.

As an additional validation of the analysis procedure, the measured $t\bar{t} \to e\mu$ and $e\mu b\bar{b}$ differential cross-sections were used to reweight the POWHEG + PYTHIA8 simulation at particle level. This sample was then used in pseudo-experiment studies as described in Sect. 4.5, taking unweighted simulation as the reference for the calculation of $G^i_{e\mu}$, C^i_b and $G^i_{e\mu b\bar{b}}$. The mean values of the differential cross-sections obtained from the pseudo-experiments were found to be consistent with the values extracted from data, and no significant biases were observed.

7.2 Comparison with event generator predictions

The measured normalised $t\bar{t} \to e\mu$ and $e\mu b\bar{b}$ differential cross-sections are compared with a set of particle-level predictions from different Monte Carlo event generators in the ratio panels of Figures 12, 13, 14, 15, 16, 17, 18, 19. For each distribution, the first three ratio panels show comparisons of the $t\bar{t} \to e\mu$ cross-sections to $t\bar{t}$ event generators, and the last ratio panel shows comparisons of the $e\mu b\bar{b}$ distributions to combined samples of $t\bar{t}$ and Wt events, or the POWHEG $bb4l$ + PYTHIA8 sample. The samples considered are summarised in Table 6. They include $t\bar{t}$ event generator configurations discussed in Sect. 2, as well as a sample generated with AMC@NLO + PYTHIA8.

[6] These integrals do not agree exactly because of statistical fluctuations and the variation of $G^i_{e\mu b\bar{b}}$ with each differential variable.

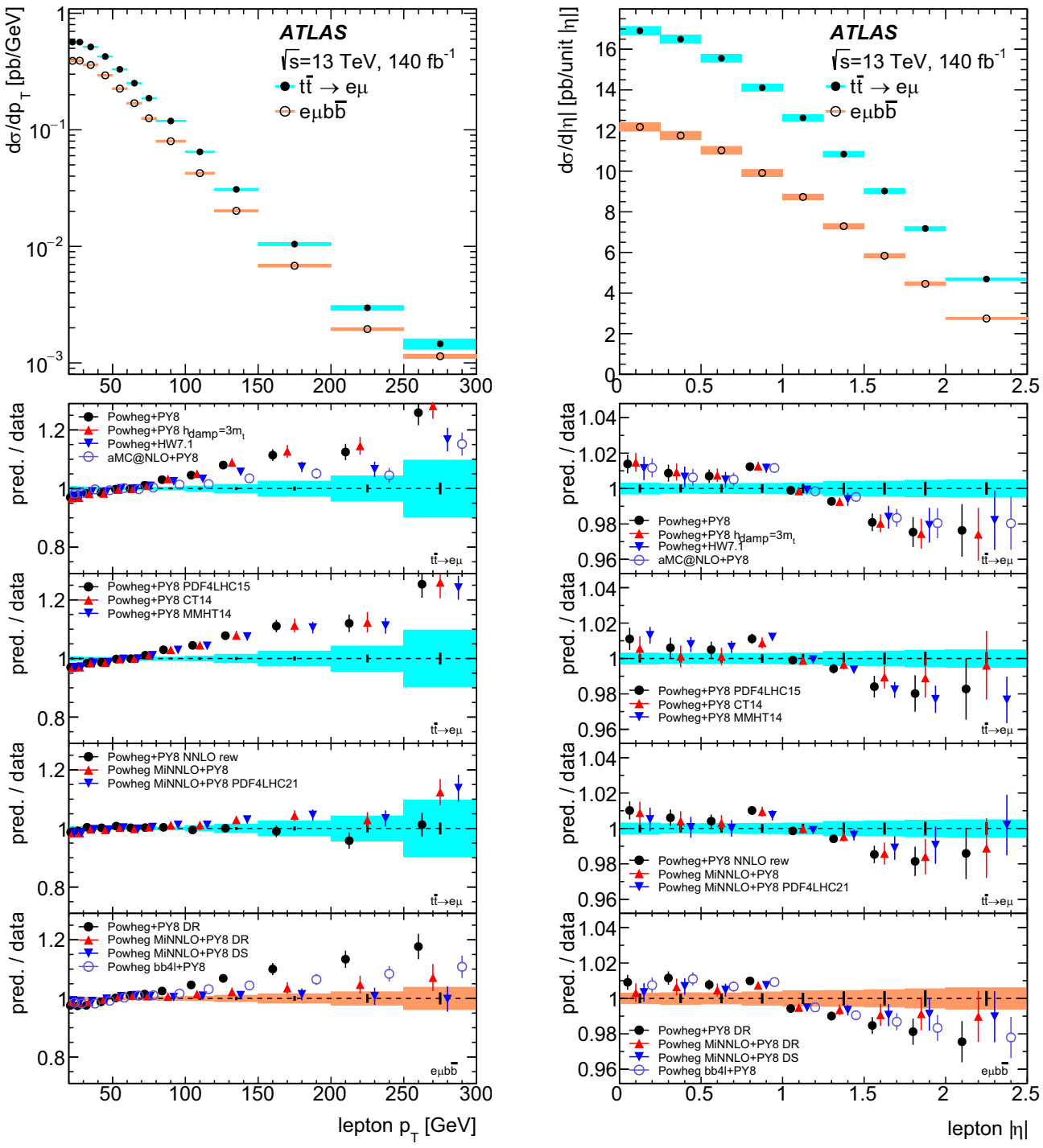

Fig. 12 Differential cross-sections as functions of (**a**) p_{T}^{ℓ} and (**b**) $|\eta^{\ell}|$. The upper panels show the measured absolute $t\bar{t} \to e\mu$ (filled points) and $e\mu b\bar{b}$ (open points) cross-sections, including the contributions from $W \to \tau \to e/\mu$ decays, with the total uncertainties shown by the shaded bands. The other panels show ratios of various predictions to the measured normalised differential cross-sections, for $t\bar{t} \to e\mu$ (middle three panels) and $e\mu b\bar{b}$ (lower panels). The markers showing the ratios for each prediction are offset from the bin centres for better visibility, and the total uncertainty in the prediction is shown by the error bar. The data statistical uncertainty is shown by the black error bars and the total uncertainty by the cyan ($t\bar{t} \to e\mu$) or orange ($e\mu b\bar{b}$) band around unity

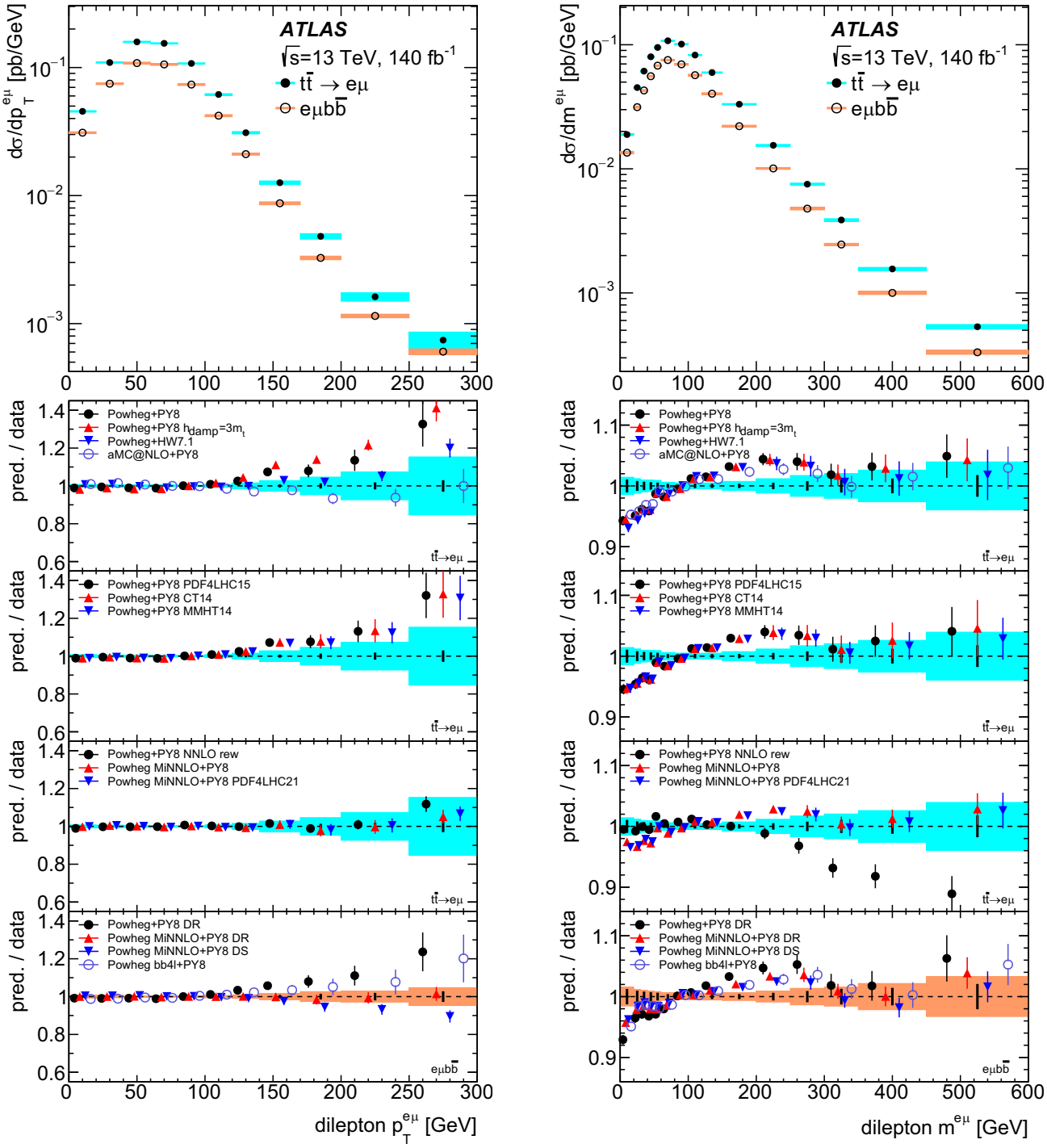

Fig. 13 Differential cross-sections as functions of (**a**) $p_{\mathrm{T}}^{e\mu}$ and (**b**) $m^{e\mu}$. The upper panels show the measured absolute $t\bar{t} \to e\mu$ (filled points) and $e\mu b\bar{b}$ (open points) cross-sections, including the contributions from $W \to \tau \to e/\mu$ decays, with the total uncertainties shown by the shaded bands. The other panels show ratios of various predictions to the measured normalised differential cross-sections, for $t\bar{t} \to e\mu$ (middle three panels) and $e\mu b\bar{b}$ (lower panels). The markers showing the ratios for each prediction are offset from the bin centres for better visibility, and the total uncertainty in the prediction is shown by the error bar. The data statistical uncertainty is shown by the black error bars and the total uncertainty by the cyan ($t\bar{t} \to e\mu$) or orange ($e\mu b\bar{b}$) band around unity

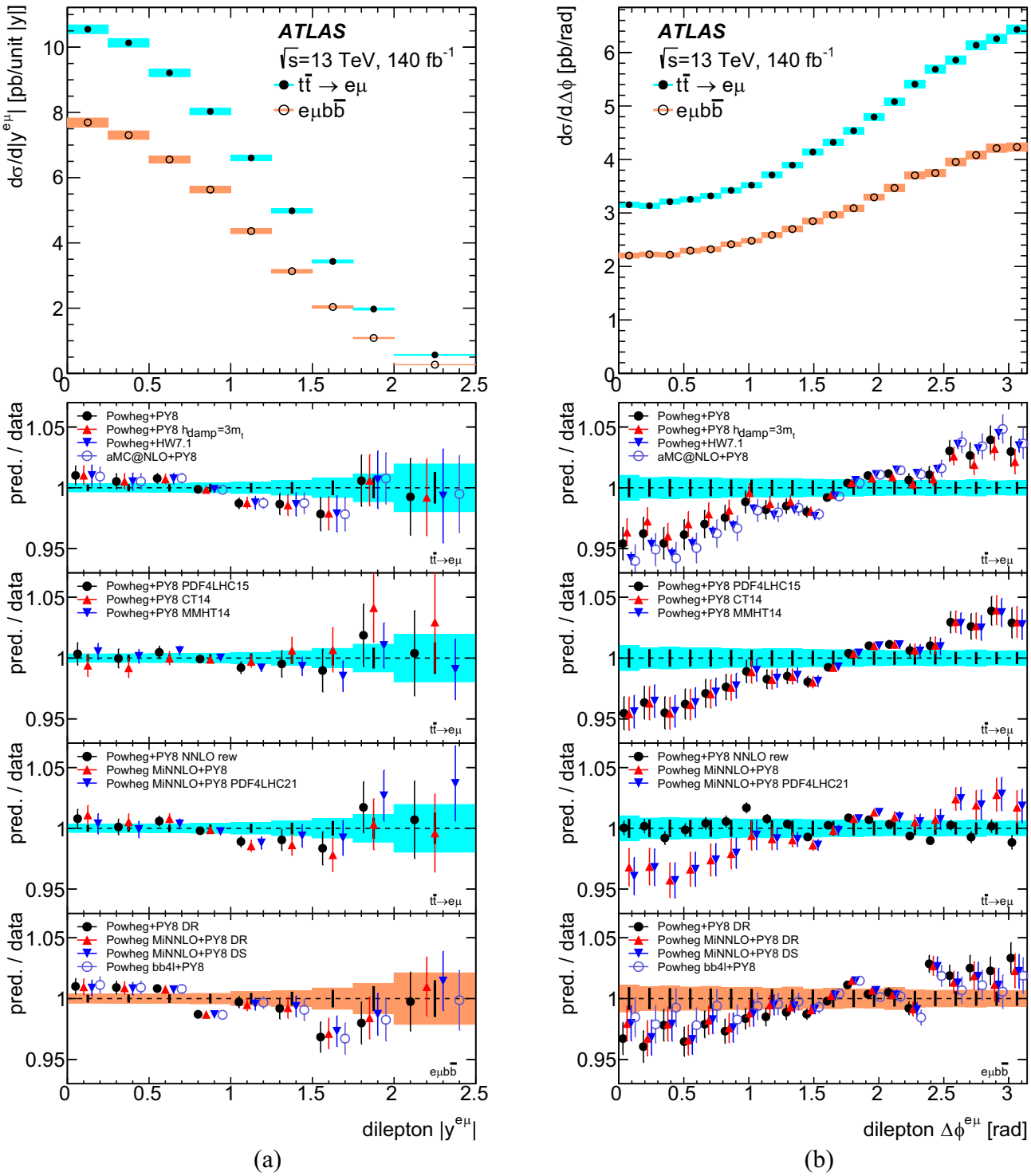

Fig. 14 Differential cross-sections as functions of (**a**) $|y^{e\mu}|$ and (**b**) $\Delta\phi^{e\mu}$. The upper panels show the measured absolute $t\bar{t} \to e\mu$ (filled points) and $e\mu b\bar{b}$ (open points) cross-sections, including the contributions from $W \to \tau \to e/\mu$ decays, with the total uncertainties shown by the shaded bands. The other panels show ratios of various predictions to the measured normalized differential cross-sections, for $t\bar{t} \to e\mu$ (middle three panels) and $e\mu b\bar{b}$ (lower panels). The markers showing the ratios for each prediction are offset from the bin centers for better visibility, and the total uncertainty in the prediction is shown by the error bar. The data statistical uncertainty is shown by the black error bars and the total uncertainty by the cyan ($t\bar{t} \to e\mu$) or orange ($e\mu b\bar{b}$) band around unity

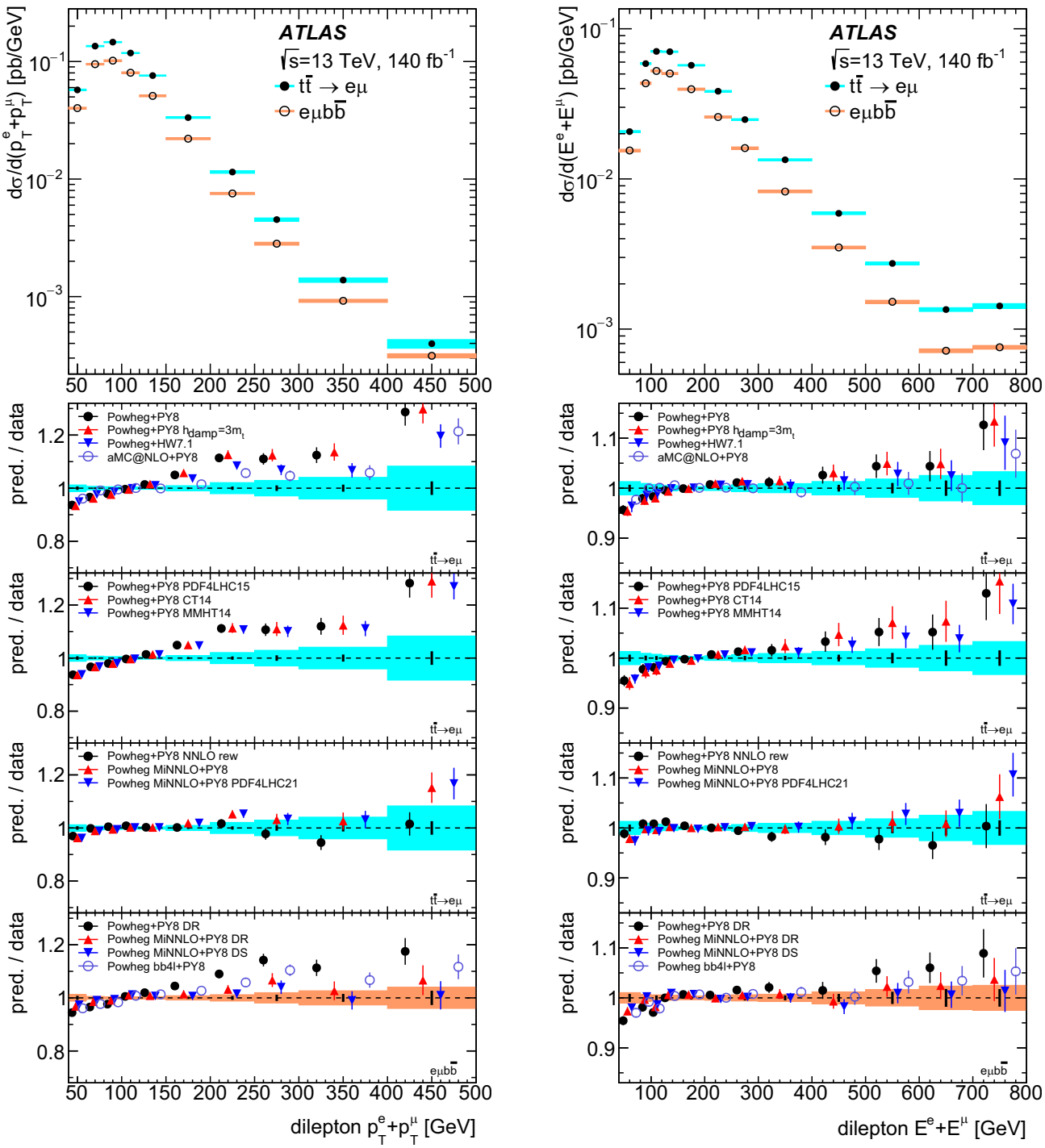

Fig. 15 Differential cross-sections as functions of (**a**) $p_{\mathrm{T}}^{e} + p_{\mathrm{T}}^{\mu}$ and (**b**) $E^{e} + E^{\mu}$. The upper panels show the measured absolute $t\bar{t} \to e\mu$ (filled points) and $e\mu b\bar{b}$ (open points) cross-sections, including the contributions from $W \to \tau \to e/\mu$ decays, with the total uncertainties shown by the shaded bands. The other panels show ratios of various predictions to the measured normalised differential cross-sections, for $t\bar{t} \to e\mu$ (middle three panels) and $e\mu b\bar{b}$ (lower panels). The markers showing the ratios for each prediction are offset from the bin centres for better visibility, and the total uncertainty in the prediction is shown by the error bar. The data statistical uncertainty is shown by the black error bars and the total uncertainty by the cyan ($t\bar{t} \to e\mu$) or orange ($e\mu b\bar{b}$) band around unity

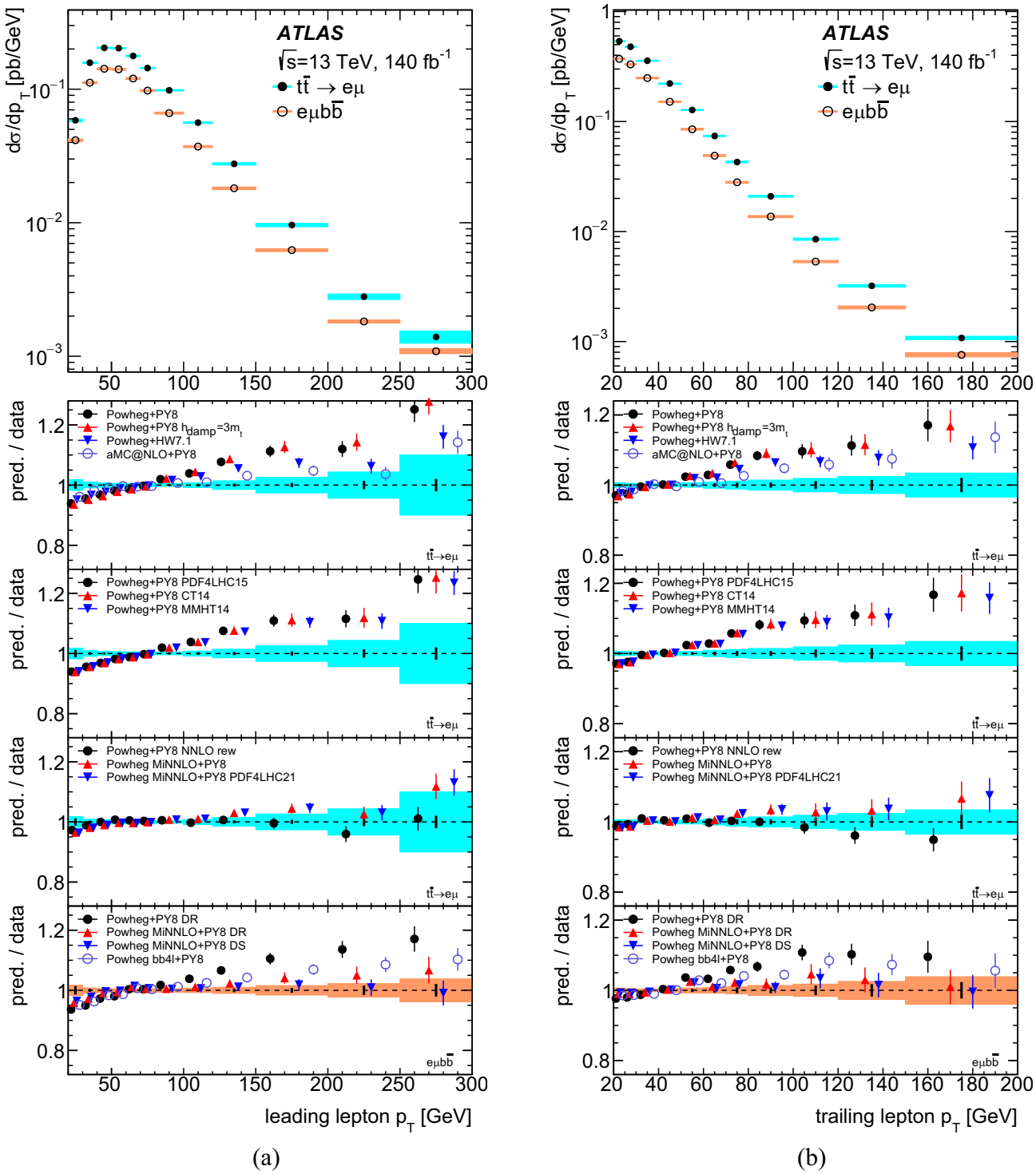

Fig. 16 Differential cross-sections as functions of (**a**) $p_{\mathrm{T}}^{\ell,\mathrm{max}}$ and (**b**) $p_{\mathrm{T}}^{\ell,\mathrm{min}}$. The upper panels show the measured absolute $t\bar{t} \to e\mu$ (filled points) and $e\mu b\bar{b}$ (open points) cross-sections, including the contributions from $W \to \tau \to e/\mu$ decays, with the total uncertainties shown by the shaded bands. The other panels show ratios of various predictions to the measured normalised differential cross-sections, for $t\bar{t} \to e\mu$ (middle three panels) and $e\mu b\bar{b}$ (lower panels). The markers showing the ratios for each prediction are offset from the bin centres for better visibility, and the total uncertainty in the prediction is shown by the error bar. The data statistical uncertainty is shown by the black error bars and the total uncertainty by the cyan ($t\bar{t} \to e\mu$) or orange ($e\mu b\bar{b}$) band around unity

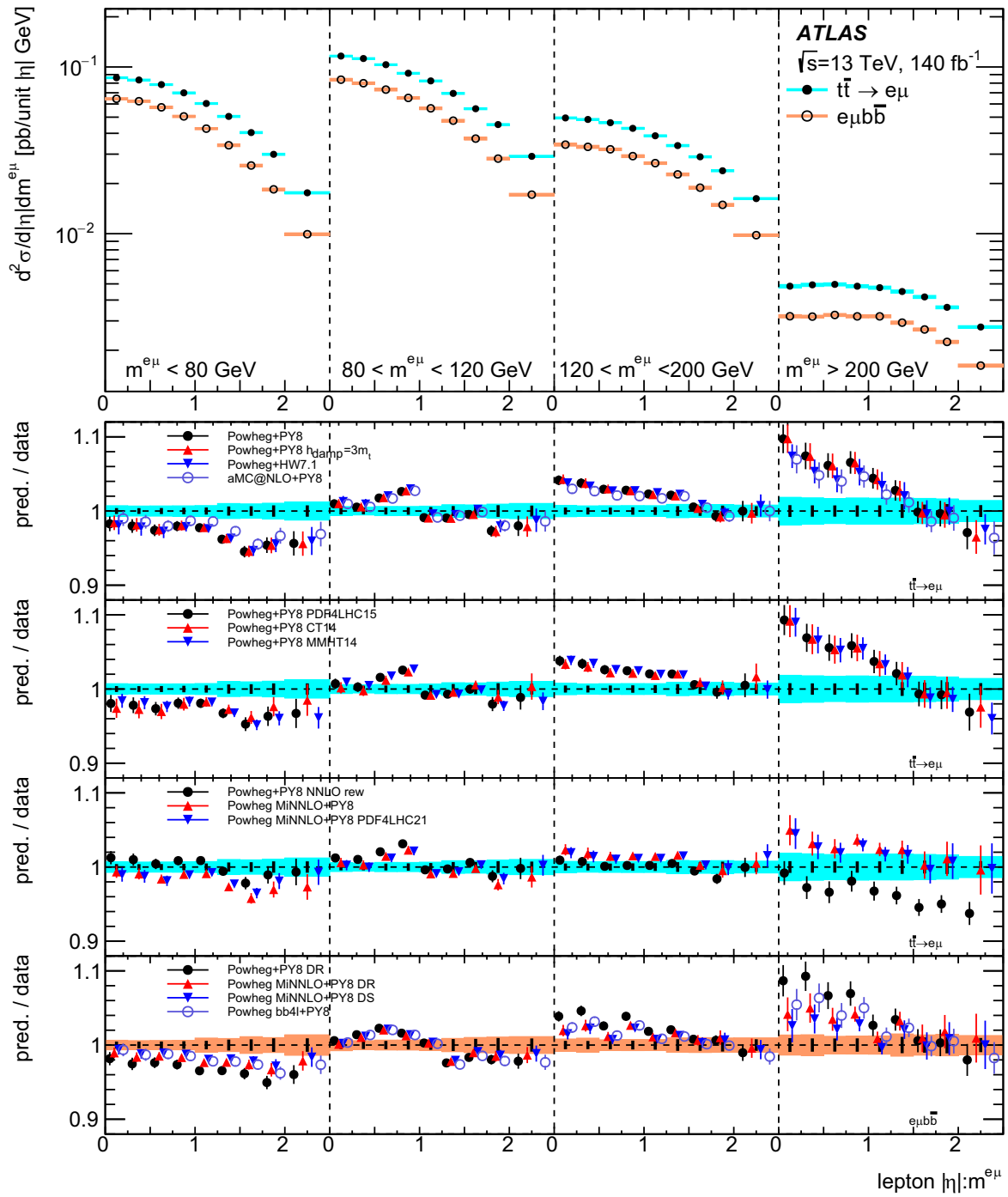

Fig. 17 Double-differential cross-section as a function of $|\eta^{\ell}|$ and $m^{e\mu}$, showing the unrolled cross-sections as a function of $|\eta^{\ell}|$ in four bins of $m^{e\mu}$. The upper panel shows the measured absolute $t\bar{t} \to e\mu$ (filled points) and $e\mu b\bar{b}$ (open points) cross-sections, including the contributions from $W \to \tau \to e/\mu$ decays, with the total uncertainties shown by the shaded bands. The other panels show ratios of various predictions to the measured normalised differential cross-sections, for $t\bar{t} \to e\mu$ (middle three panels) and $e\mu b\bar{b}$ (lower panel). The markers showing the ratios for each prediction are offset from the bin centres for better visibility, and the total uncertainty in the prediction is shown by the error bar. The data statistical uncertainty is shown by the black error bars and the total uncertainty by the cyan ($t\bar{t} \to e\mu$) or orange ($e\mu b\bar{b}$) band around unity

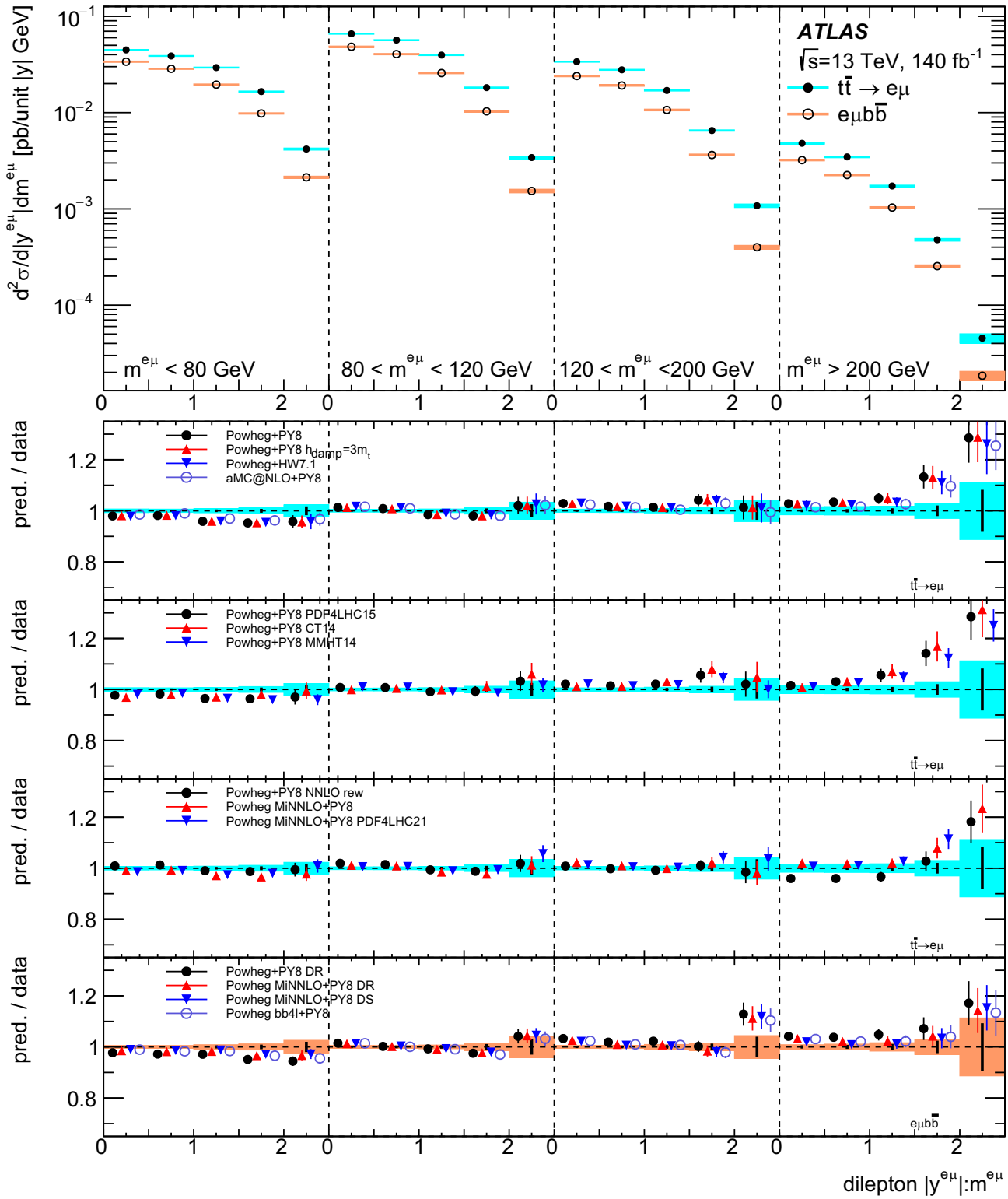

Fig. 18 Double-differential cross-section as a function of $|y^{e\mu}|$ and $m^{e\mu}$, showing the unrolled cross-sections as a function of $|y^{e\mu}|$ in four bins of $m^{e\mu}$. The upper panel shows the measured absolute $t\bar{t} \to e\mu$ (filled points) and $e\mu b\bar{b}$ (open points) cross-sections, including the contributions from $W \to \tau \to e/\mu$ decays, with the total uncertainties shown by the shaded bands. The other panels show ratios of various predictions to the measured normalised differential cross-sections, for $t\bar{t} \to e\mu$ (middle three panels) and $e\mu b\bar{b}$ (lower panel). The markers showing the ratios for each prediction are offset from the bin centres for better visibility, and the total uncertainty in the prediction is shown by the error bar. The data statistical uncertainty is shown by the black error bars and the total uncertainty by the cyan ($t\bar{t} \to e\mu$) or orange ($e\mu b\bar{b}$) band around unity

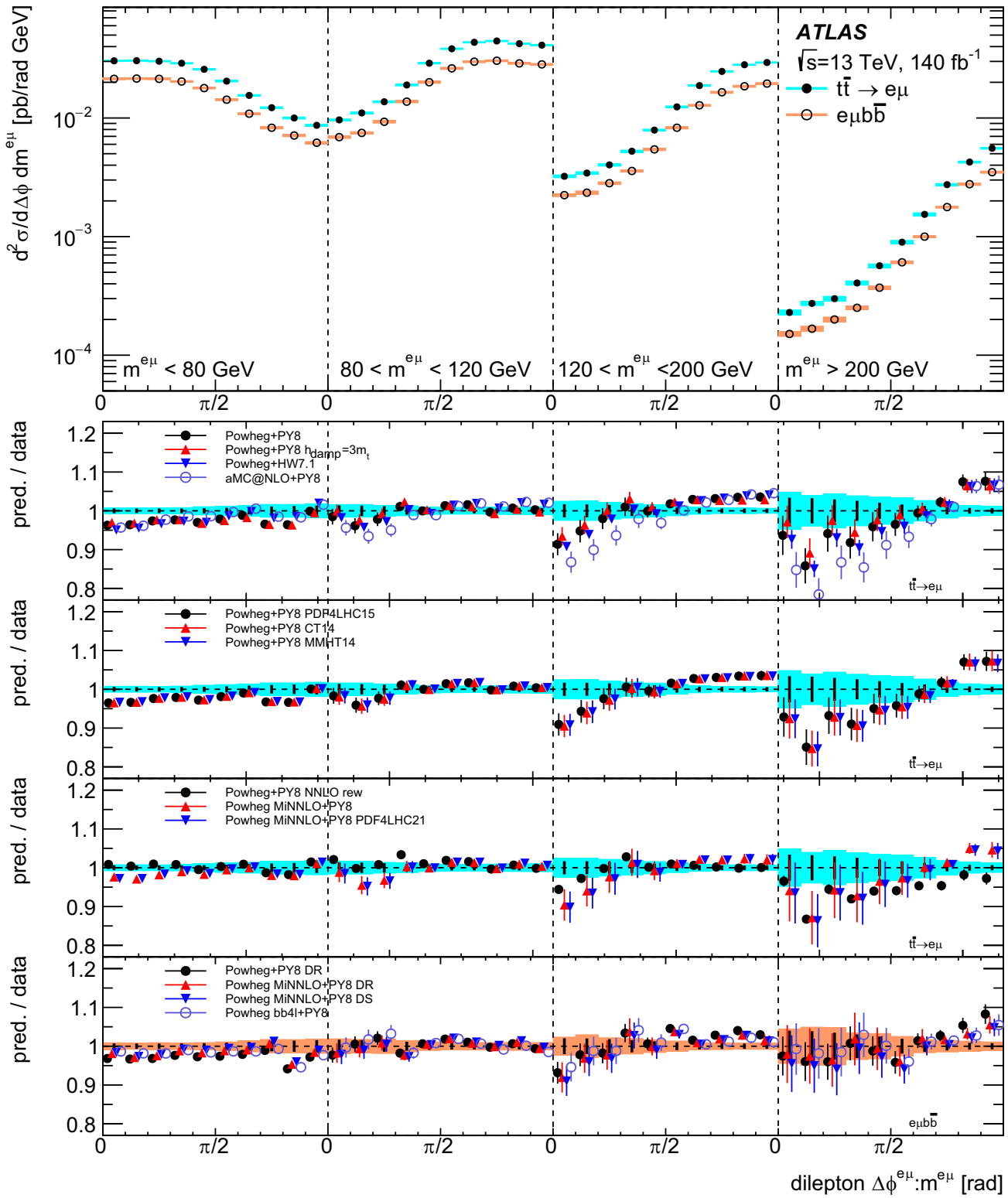

Fig. 19 Double-differential cross-section as a function of $\Delta\phi^{e\mu}$ and $m^{e\mu}$, showing the unrolled cross-sections as a function of $\Delta\phi^{e\mu}$ in four bins of $m^{e\mu}$. The upper panel shows the measured absolute $t\bar{t} \to e\mu$ (filled points) and $e\mu b\bar{b}$ (open points) cross-sections, including the contributions from $W \to \tau \to e/\mu$ decays, with the total uncertainties shown by the shaded bands. The other panels show ratios of various predictions to the measured normalised differential cross-sections, for $t\bar{t} \to e\mu$ (middle three panels) and $e\mu b\bar{b}$ (lower panel). The markers showing the ratios for each prediction are offset from the bin centres for better visibility, and the total uncertainty in the prediction is shown by the error bar. The data statistical uncertainty is shown by the black error bars and the total uncertainty by the cyan ($t\bar{t} \to e\mu$) or orange ($e\mu b\bar{b}$) band around unity

The POWHEG MiNNLO + PYTHIA8 and POWHEG + PYTHIA8 samples generated with NNPDF3.0 were also reweighted to the predictions of the PDF4LHC15 [112], CT14 [99], MMHT14 [113] and PDF4LHC21 [22] NLO PDF sets. The $t\bar{t}$ NNLO reweighting procedure described in Ref. [43] was also applied to the POWHEG + PYTHIA8 $t\bar{t}$ sample, in order to bring the top quark kinematics into agreement with the predictions of the NNLO QCD + NLO electroweak calculation of Ref. [114]. In these studies, no reweighting of the fraction of events with three or more b-jets was applied to any of the samples.

In previous comparisons of ATLAS $t\bar{t}$ lepton differential distributions with predictions [12,34,37], the predictions were treated without uncertainties due to e.g. QCD scale or PDF variations, making the comparisons harder to interpret. In this analysis, such prediction uncertainties have been explicitly considered, including separate variations of the QCD renormalisation and factorisation scales by factors of two up and down about their default values, and PDF variations according to the eigenvector or replica variations provided with each PDF set. These variations were calculated using event weights in each sample. In addition, the effects of the `var3c` A14 tune variations, changes in the $\mu_{\mathrm{R,FSR}}$ parameter by factors of 2 and 0.625, and variations of the top quark mass by $\pm 0.5\,\mathrm{GeV}$ around the default value of $m_t = 172.5\,\mathrm{GeV}$ were evaluated using POWHEG + PYTHIA8 and applied to all samples. The PDF eigenvectors or replicas were used to calculate the correlations between bins of each distribution, whilst other variations were taken to be fully correlated between bins. The resulting uncertainties are shown as error bars on the predictions in Figures 12, 13, 14, 15, 16, 17, 18, 19, and are typically dominated by PDF uncertainties for $|\eta^{\ell}|$ and $|y^{e\mu}|$, and QCD scale uncertainties for the other distributions.

The compatibility of each prediction with each measured normalised distribution was tested using a χ^2 calculated as

$$\chi^2 = \Delta^T_{(n-1)} \mathbf{S}^{-1}_{(n-1)} \Delta_{(n-1)}, \tag{6}$$

where $\Delta_{(n-1)}$ is the vector of differences between the measured and predicted normalised differential cross-section in each of the n bins, excluding the last one, and $\mathbf{S}^{-1}_{(n-1)}$ is the inverse of the corresponding covariance matrix, including both the experimental uncertainties in the measurement and the uncertainties in the predictions, and their bin-to-bin correlations through off-diagonal terms. The last bin of each distribution was excluded to account for the normalisation condition. The resulting χ^2 and associated p values (for $n-1$ degrees of freedom) are shown for the single-differential distributions in Table 7, and for the double-differential distributions in Table 8.

The measurements are precise and discriminating, and many of the predictions disagree strongly with the data, even after taking the prediction uncertainties into account. Predictions based on the POWHEG `hvq` process with the PYTHIA8 or HERWIG7 parton shower generally model distributions sensitive to the top quark p_{T} distribution poorly, but this can be improved by reweighting the top quark kinematics to the NNLO prediction of Ref. [114]. The POWHEG MiNNLO + PYTHIA8 and POWHEG *bb4l* + PYTHIA8 samples provide a much better description of the data, and AMC@NLO + PYTHIA8 is also better than POWHEG + PYTHIA8. For $e\mu b\bar{b}$, some distributions e.g. p_{T}^{ℓ} and $p_{\mathrm{T}}^{e\mu}$ offer potential discrimination between the diagram removal and diagram subtraction models of Wt events (as suggested by Fig. 6), but the uncertainties in both measurements and predictions mean that definite conclusions cannot be drawn. Here, more discrimination can be achieved by dedicated measurements in the interference region [43].

In more detail, the p_{T}^{ℓ}, $p_{\mathrm{T}}^{\ell,\mathrm{max}}$ and $p_{\mathrm{T}}^{\ell,\mathrm{min}}$ $t\bar{t} \to e\mu$ distributions (Figs. 12(a) and 16) predicted by POWHEG + PYTHIA8 and its $h_{\mathrm{damp}} = 3m_t$ variation are significantly harder than the data. POWHEG + HERWIG7 and AMC@NLO + PYTHIA8 are closer but still harder than the data, whereas POWHEG MiNNLO + PYTHIA8 and POWHEG *bb4l* + PYTHIA8 are compatible with the data. In the $p_{\mathrm{T}}^{\ell,\mathrm{min}}$ distribution, which is most relevant for modelling the acceptance in the inclusive $\sigma_{t\bar{t}}$ analysis, POWHEG MiNNLO + PYTHIA8 is still slightly harder than the data (which is the origin of the dependence of $\sigma_{t\bar{t}}$ on the lepton p_{T} requirement discussed in Sect. 6.1), but is still compatible within uncertainties. The best modelling of the corresponding $e\mu b\bar{b}$ distributions is provided by POWHEG MiNNLO + PYTHIA8 combined with POWHEG + PYTHIA8 diagram subtraction Wt events. The diagram removal Wt sample predicts a harder p_{T} spectrum, as does POWHEG *bb4l* + PYTHIA8 but these are still consistent with the data within uncertainties.

The data are more forward than all the predictions for the $t\bar{t} \to e\mu$ $|\eta^{\ell}|$ distribution (Fig. 12(b)) and to a lesser extent for $|y^{e\mu}|$ (Fig. 14(a)). For POWHEG + PYTHIA8, the PDF sets PDF4LHC15 and CT14 give a better description than NNPDF3.0 or MMHT14, demonstrating the sensitivity to PDFs. For POWHEG MiNNLO + PYTHIA8, both NNPDF3.0 and PDF4LHC21 give similar predictions. Similar features are seen in the corresponding $e\mu b\bar{b}$ distributions.

All the predictions model the $t\bar{t} \to e\mu$ and $e\mu b\bar{b}$ $p_{\mathrm{T}}^{e\mu}$ distributions well at low $p_{\mathrm{T}}^{e\mu}$ (Fig. 13(a)), but the POWHEG + PYTHIA8 samples give a too-hard distribution at high $p_{\mathrm{T}}^{e\mu}$. No prediction models the $m^{e\mu}$ distributions (Fig. 13(b)) at low $m^{e\mu}$, where there is a clear data excess. POWHEG MiNNLO + PYTHIA8 provides the best modelling of the intermediate $100 < p_{\mathrm{T}}^{e\mu} < 200\,\mathrm{GeV}$ range, whilst the NNLO-reweighted POWHEG + PYTHIA8 sample undershoots the data at high $m^{e\mu}$. The poor modelling of $m^{e\mu}$ is also seen in the double-differential cross-sections shown in Figs. 17, 18, 19, where all predictions except POWHEG MiNNLO + PYTHIA8 have very poor χ^2 values in Table 8.

Table 6 Summary of particle-level simulation samples used in the comparison with measured $t\bar{t} \to e\mu$ and $e\mu b\bar{b}$ differential cross-sections, giving the matrix-element generator, PDF set, parton shower and other relevant settings. The top quark mass was set to $m_t = 172.5\,\text{GeV}$ in all samples. The four groups shown correspond to the four ratio panels on Figures 12–19

Group	Matrix element	PDF set	Parton shower	Comments
$t\bar{t}$-1	POWHEG	NNPDF3.0	PYTHIA8	
	POWHEG	NNPDF3.0	PYTHIA8	$h_{\text{damp}} = 3m_t$
	POWHEG	NNPDF3.0	HERWIG7.1.3	
	aMC@NLO	NNPDF3.0	PYTHIA8	
$t\bar{t}$-2	POWHEG	PDF4LHC15	PYTHIA8	
	POWHEG	CT14	PYTHIA8	
	POWHEG	MMHT14	PYTHIA8	
$t\bar{t}$-3	POWHEG	NNPDF3.0	PYTHIA8	NNLO reweighting ($p_{\text{T}}(t)$, $p_{\text{T}}(t\bar{t})$, $m(t\bar{t})$)
	POWHEG MiNNLO	NNPDF3.0	PYTHIA8	Baseline
	POWHEG MiNNLO	PDF4LHC21	PYTHIA8	
$e\mu b\bar{b}$	POWHEG	NNPDF3.0	PYTHIA8	Wt diagram removal
	POWHEG MiNNLO	NNPDF3.0	PYTHIA8	Wt diagram removal, baseline
	POWHEG MiNNLO	NNPDF3.0	PYTHIA8	Wt diagram subtraction
	POWHEG *bb4l*	NNPDF3.0	PYTHIA8	Complete $e\mu\nu\bar{\nu}b\bar{b}$

Most of the predictions show a clear slope with respect to the data for $\Delta\phi^{e\mu}$ (Fig. 14(b)), but bin-to-bin correlations in the uncertainties in the predictions (in particular from QCD renormalisation scale variations) result in the χ^2 values still being acceptable, with the exception of POWHEG + HERWIG7. The double-differential cross-section of $\Delta\phi^{e\mu}$ in bins of $m^{e\mu}$ (Fig. 19) suggests that the slope between data and predictions increases with $m^{e\mu}$. The NNLO-reweighted POWHEG + PYTHIA8 sample models this distribution well, without a significant slope except for $m^{e\mu} > 200\,\text{GeV}$. However, the POWHEG MiNNLO + PYTHIA8 sample does not model this distribution significantly better than POWHEG + PYTHIA8.

The $t\bar{t} \to e\mu$ data is softer than all predictions for $p_{\text{T}}^e + p_{\text{T}}^\mu$ (Fig. 15(a)), with POWHEG MiNNLO + PYTHIA8 coming closest, but still with a χ^2 probability of only around 1%. These predictions are in better agreement with the $e\mu b\bar{b}$ $p_{\text{T}}^e + p_{\text{T}}^\mu$ data distribution, where POWHEG *bb4l* + PYTHIA8 shows some tension. For $E^e + E^\mu$ (Fig. 15(b)), all the predictions except POWHEG MiNNLO + PYTHIA8 and NNLO-reweighted POWHEG + PYTHIA8 are harder than the data at low $E^e + E^\mu$, but the χ^2 values are still acceptable, except for the $e\mu b\bar{b}$ prediction from POWHEG + PYTHIA8 with the diagram removal scheme for Wt events.

8 Conclusions

The inclusive $t\bar{t}$ production cross-section $\sigma_{t\bar{t}}$ has been measured in pp collisions at $\sqrt{s} = 13\,\text{TeV}$ using the $140\,\text{fb}^{-1}$ ATLAS dataset recorded at the LHC in 2015–18. Using events with an opposite-charge $e\mu$ pair and b-tagged jets, the result is:

$$\sigma_{t\bar{t}} = 829.3 \pm 1.3 \pm 8.0 \pm 7.3 \pm 1.9\,\text{pb},$$

where the four uncertainties reflect the limited size of the data sample, experimental and theoretical systematic effects, uncertainty in the integrated luminosity and the knowledge of the LHC beam energy, giving a total uncertainty of 1.3%. The result is the most precise achieved to date, and is consistent with NNLO+NNLL QCD predictions. Fiducial cross-sections corresponding to the lepton acceptance have also been measured, with or without the contribution from leptonic decays of tau leptons. The dependence of predictions for $\sigma_{t\bar{t}}$ on the top quark pole mass has been exploited to determine

$$m_t^{\text{pole}} = 172.8^{+1.5}_{-1.7}\,\text{GeV},$$

using the NNPDF3.1_notop PDF set. This result is consistent with other determinations of m_t using a variety of techniques.

The same dataset has been used to measure ten single-differential and three double-differential cross-sections as functions of lepton and dilepton kinematic variables, for both the $t\bar{t} \to e\mu$ process and the $e\mu b\bar{b}$ final state including contributions from both $t\bar{t}$ and Wt processes. Uncertainties as small as 0.3% have been achieved for normalised distributions in some parts of the fiducial regions. Comparisons with event generator predictions show that state-of-the-art generators such as POWHEG MiNNLO or POWHEG *bb4l* better model the lepton kinematics than the POWHEG `hvq` process traditionally used for LHC physics analyses. These precise

Table 7 χ^2 values (top block) and associated probabilities (bottom block) for comparison of normalised measured single-differential fiducial cross-sections with various simulation samples. Within each block, the last four rows correspond to comparisons of the $e\mu b\bar{b}$ cross-sections with combined $t\bar{t}+Wt$ samples, and the other rows to $t\bar{t} \to e\mu$ cross-sections compared with $t\bar{t}$ samples. Probabilities smaller than 10^{-10} are shown as zero

Generator N_{dof}	p_{T}^{ℓ} 12	$\lvert\eta^{\ell}\rvert$ 8	$p_{\text{T}}^{e\mu}$ 10	$m^{e\mu}$ 14	$\lvert y^{e\mu}\rvert$ 8	$\Delta\phi^{e\mu}$ 19	$p_{\text{T}}^{e}+p_{\text{T}}^{\mu}$ 9	$E^{e}+E^{\mu}$ 11	$p_{\text{T}}^{\ell,\text{max}}$ 11	$p_{\text{T}}^{\ell,\text{min}}$ 10
χ^2 values										
POWHEG + PY8	35.2	19.7	12.5	49.8	11.6	22.7	34.9	14.7	32.0	27.4
POWHEG + PY8 $h_{\text{damp}} = 3m_t$	38.9	20.1	20.2	50.1	11.0	24.0	41.0	15.3	36.3	30.6
POWHEG + HW7.1	32.5	15.9	20.4	92.9	10.2	71.3	27.6	12.2	26.6	20.9
aMC@NLO + PY8	16.2	16.7	15.4	35.2	12.0	30.5	27.5	13.5	12.5	17.4
POWHEG + PY8 PDF4LHC15	33.7	15.2	12.0	47.3	8.7	22.3	33.8	13.3	30.3	26.0
POWHEG + PY8 CT14	32.8	12.6	11.8	44.6	8.0	22.4	33.0	12.7	29.4	25.3
POWHEG + PY8 MMHT14	33.0	19.0	11.5	48.2	9.5	22.0	33.1	13.5	29.6	25.5
POWHEG + PY8 NNLO rew	16.4	14.9	11.7	33.6	12.8	16.5	24.6	11.3	14.3	14.6
POWHEG MiNNLO + PY8	15.4	12.3	7.2	25.9	11.7	23.6	20.9	7.5	12.1	12.5
POWHEG MiNNLO + PY8 PDF4LHC21	15.6	12.8	7.5	25.6	12.6	25.2	21.3	10.2	11.8	13.1
POWHEG + PY8 DR	26.9	12.0	10.1	48.6	14.7	23.8	34.5	28.0	32.5	35.3
POWHEG MiNNLO + PY8 DR	12.4	6.4	1.4	31.4	14.4	26.7	15.3	17.9	16.4	14.9
POWHEG MiNNLO + PY8 DS	10.8	6.6	6.0	25.8	14.4	26.1	14.0	17.1	14.3	13.1
POWHEG *bb4l* + PY8	15.5	11.2	3.1	20.5	14.7	21.4	20.5	18.6	19.2	21.8
χ^2 probabilities										
POWHEG + PY8	$4\ 10^{-4}$	0.011	0.25	$7\ 10^{-6}$	0.17	0.25	$6\ 10^{-5}$	0.20	$8\ 10^{-4}$	$2\ 10^{-3}$
POWHEG + PY8 $h_{\text{damp}} = 3m_t$	$1\ 10^{-4}$	0.010	0.027	$6\ 10^{-6}$	0.20	0.20	$5\ 10^{-6}$	0.17	$1\ 10^{-4}$	$7\ 10^{-4}$
POWHEG + HW7.1	$1\ 10^{-3}$	0.044	0.026	0	0.25	$6\ 10^{-8}$	$1\ 10^{-3}$	0.35	$5\ 10^{-3}$	0.022
aMC@NLO + PY8	0.18	0.033	0.12	$1\ 10^{-3}$	0.15	0.046	$1\ 10^{-3}$	0.26	0.33	0.065
POWHEG + PY8 PDF4LHC15	$8\ 10^{-4}$	0.056	0.29	$2\ 10^{-5}$	0.37	0.27	$1\ 10^{-4}$	0.27	$1\ 10^{-3}$	$4\ 10^{-3}$
POWHEG + PY8 CT14	$1\ 10^{-3}$	0.13	0.30	$5\ 10^{-5}$	0.44	0.27	$1\ 10^{-4}$	0.32	$2\ 10^{-3}$	$5\ 10^{-3}$
POWHEG + PY8 MMHT14	$1\ 10^{-3}$	0.015	0.32	$1\ 10^{-5}$	0.30	0.28	$1\ 10^{-4}$	0.26	$2\ 10^{-3}$	$4\ 10^{-3}$
POWHEG + PY8 NNLO rew	0.18	0.061	0.31	$2\ 10^{-3}$	0.12	0.62	$3\ 10^{-3}$	0.41	0.22	0.15
POWHEG MiNNLO + PY8	0.22	0.14	0.71	0.026	0.16	0.21	0.013	0.76	0.35	0.25
POWHEG MiNNLO + PY8 PDF4LHC21	0.21	0.12	0.68	0.029	0.13	0.15	0.012	0.51	0.38	0.22
POWHEG + PY8 DR	$8\ 10^{-3}$	0.15	0.44	$1\ 10^{-5}$	0.065	0.20	$7\ 10^{-5}$	$3\ 10^{-3}$	$6\ 10^{-4}$	$1\ 10^{-4}$
POWHEG MiNNLO + PY8 DR	0.41	0.60	1.00	$5\ 10^{-3}$	0.071	0.11	0.084	0.083	0.13	0.13
POWHEG MiNNLO + PY8 DS	0.54	0.58	0.82	0.027	0.072	0.13	0.12	0.11	0.22	0.22
POWHEG *bb4l* + PY8	0.22	0.19	0.98	0.11	0.064	0.32	0.015	0.069	0.057	0.016

Table 8 χ^2 values (top block) and associated probabilities (bottom block) for comparison of normalised measured double-differential fiducial cross-sections with various simulation samples. Within each block, the last four rows correspond to comparisons of the $e\mu b\bar{b}$ cross-sections with combined $t\bar{t}+Wt$ samples, and the other rows to $t\bar{t} \to e\mu$ cross-sections compared with $t\bar{t}$ samples. Probabilities smaller than 10^{-10} are shown as zero

Generator N_{dof}	$\lvert\eta^{\ell}\rvert \times m^{e\mu}$ 35	$\lvert y^{e\mu}\rvert \times m^{e\mu}$ 19	$\lvert\Delta\phi^{\ell}\rvert \times m^{e\mu}$ 39
χ^2 values			
POWHEG + PY8	72.7	46.0	79.9
POWHEG + PY8 $h_{\text{damp}} = 3m_t$	74.2	44.9	78.3
POWHEG + HW7.1	122.2	67.4	150.8
aMC@NLO + PY8	63.0	34.2	63.2
POWHEG + PY8 PDF4LHC15	69.9	43.7	77.2
POWHEG + PY8 CT14	68.8	42.2	74.9
POWHEG + PY8 MMHT14	71.6	47.3	78.5
POWHEG + PY8 NNLO rew	71.0	33.8	71.0
POWHEG MiNNLO + PY8	44.8	26.7	50.2
POWHEG MiNNLO + PY8 PDF4LHC21	44.3	27.0	49.7
POWHEG + PY8 DR	63.7	37.0	75.3
POWHEG MiNNLO + PY8 DR	49.1	29.3	60.9
POWHEG MiNNLO + PY8 DS	41.9	24.5	54.5
POWHEG *bb4l* + PY8	47.8	23.7	66.0
χ^2 probabilities			
POWHEG + PY8	$2\ 10^{-4}$	$5\ 10^{-4}$	$1\ 10^{-4}$
POWHEG + PY8 $h_{\text{damp}} = 3m_t$	$1\ 10^{-4}$	$7\ 10^{-4}$	$2\ 10^{-4}$
POWHEG + HW7.1	0	$2\ 10^{-7}$	0
aMC@NLO + PY8	$3\ 10^{-3}$	0.018	$8\ 10^{-3}$
POWHEG + PY8 PDF4LHC15	$4\ 10^{-4}$	$1\ 10^{-3}$	$3\ 10^{-4}$
POWHEG + PY8 CT14	$6\ 10^{-4}$	$2\ 10^{-3}$	$5\ 10^{-4}$
POWHEG + PY8 MMHT14	$3\ 10^{-4}$	$3\ 10^{-4}$	$2\ 10^{-4}$
POWHEG + PY8 NNLO rew	$3\ 10^{-4}$	0.020	$1\ 10^{-3}$
POWHEG MiNNLO + PY8	0.12	0.11	0.11
POWHEG MiNNLO + PY8 PDF4LHC21	0.13	0.10	0.12
POWHEG + PY8 DR	$2\ 10^{-3}$	$8\ 10^{-3}$	$4\ 10^{-4}$
POWHEG MiNNLO + PY8 DR	0.057	0.062	0.014
POWHEG MiNNLO + PY8 DS	0.20	0.18	0.050
POWHEG *bb4l* + PY8	0.073	0.21	$4\ 10^{-3}$

measurements provide input that can be used to further refine the modelling of top quark production at hadron colliders.

Acknowledgements We thank CERN for the very successful operation of the LHC and its injectors, as well as the support staff at CERN and at our institutions worldwide without whom ATLAS could not be operated efficiently. The crucial computing support from all WLCG partners is acknowledged gratefully, in particular from CERN, the ATLAS Tier-1 facilities at TRIUMF/SFU (Canada), NDGF (Denmark, Norway, Sweden), CC-IN2P3 (France), KIT/GridKA (Germany), INFN-CNAF (Italy), NL-T1 (Netherlands), PIC (Spain), RAL (UK) and BNL (USA), the Tier-2 facilities worldwide and large non-WLCG resource providers. Major contributors of computing resources are listed in Ref. [115]. We gratefully acknowledge the support of ANPCyT, Argentina; YerPhI, Armenia; ARC, Australia; BMWFW and FWF, Austria; ANAS, Azerbaijan; CNPq and FAPESP, Brazil; NSERC, NRC and CFI, Canada; CERN; ANID, Chile; CAS, MOST and NSFC, China; Minciencias, Colombia; MEYS CR, Czech Republic; DNRF and DNSRC, Denmark; IN2P3-CNRS and CEA-DRF/IRFU, France; SRNSFG, Georgia; BMFTR, HGF and MPG, Germany; GSRI, Greece; RGC and Hong Kong SAR, China; ICHEP and Academy of Sciences and Humanities, Israel; INFN, Italy; MEXT and JSPS, Japan; CNRST, Morocco; NWO, Netherlands; RCN, Norway; MNiSW, Poland; FCT, Portugal; MNE/IFA, Romania; MSTDI, Serbia; MSSR, Slovakia; ARIS and MVZI, Slovenia; DSI/NRF, South Africa; MICIU/AEI, Spain; SRC and Wallenberg Foundation, Sweden; SERI, SNSF and Cantons of Bern and Geneva, Switzerland; NSTC, Taipei; TENMAK, Türkiye; STFC/UKRI, United Kingdom; DOE and NSF, United States of America. Individual groups and members have received support from BCKDF, CANARIE, CRC and DRAC, Canada; CERN-CZ, FORTE and PRIMUS, Czech Republic; COST, ERC, ERDF, Horizon 2020, ICSC-NextGenerationEU and Marie Skłodowska-Curie Actions, European Union; Investissements d'Avenir Labex, Investissements d'Avenir Idex and ANR, France; DFG and AvH Foundation, Germany; Herakleitos, Thales and Aristeia programmes co-financed by EU-ESF and the Greek NSRF, Greece; BSF-NSF and MINERVA, Israel; NCN and NAWA, Poland; La Caixa Banking Foundation, CERCA Programme Generalitat de Catalunya and PROMETEO and GenT Programmes Generalitat Valenciana, Spain; Göran Gustafssons Stiftelse, Sweden; The Royal Society and Lev-

erhulme Trust, United Kingdom. In addition, individual members wish to acknowledge support from CERN: European Organization for Nuclear Research (CERN DOCT); Chile: Agencia Nacional de Investigación y Desarrollo (ANID FONDECYT reg. 1230987, FONDECYT 1230812, FONDECYT 1240864, Fondecyt 3240661, Fondecyt Regular 1240721); China: Chinese Ministry of Science and Technology (MOST-2023YFA1605700, MOST-2023YFA1609300), National Natural Science Foundation of China (NSFC - 12175119, NSFC 12275265); Czech Republic: Czech Science Foundation (GACR - 24-11373S), Ministry of Education Youth and Sports (ERC-CZ-LL2327, FORTE CZ.02.01.01/00/22_008/0004632), PRIMUS Research Programme (PRIMUS/21/SCI/017); EU: H2020 European Research Council (ERC - 101002463); European Union: European Research Council (BARD No. 101116429, ERC - 948254, ERC 101089007), European Regional Development Fund (HE COFUND GA No.101081355, ERDF), European Union, Future Artificial Intelligence Research (FAIR-NextGenerationEU PE00000013), Italian Center for High Performance Computing, Big Data and Quantum Computing (ICSC, NextGenerationEU), Marie Sklodowska-Curie Actions (GAP-101168829); France: Agence Nationale de la Recherche (ANR-21-CE31-0013, ANR-21-CE31-0022, ANR-22-EDIR-0002, ANR-24-CE31-0504-01); Germany: Deutsche Forschungsgemeinschaft (DFG - 469666862, DFG - CR 312/5-2); China: Research Grants Council (GRF); Italy: Istituto Nazionale di Fisica Nucleare (ICSC, NextGenerationEU), Ministero dell'Università e della Ricerca (NextGenEU 153D23001490006 M4C2.1.1, NextGenEU I53D23000820006 M4C2.1.1, NextGenEU I53D23001490006 M4C2.1.1, SOE2024_0000023); Japan: Japan Society for the Promotion of Science (JSPS KAKENHI JP22H01227, JSPS KAKENHI JP22H04944, JSPS KAKENHI JP22KK0227, JSPS KAKENHI JP24K23939, JSPS KAKENHI JP24KK0251, JSPS KAKENHI JP25H00650, JSPS KAKENHI JP25H01291, JSPS KAKENHI JP25K01023); Norway: Research Council of Norway (RCN-314472); Poland: Ministry of Science and Higher Education (IDUB AGH, POB8, D4 no 9722), Polish National Science Centre (NCN 2021/42/E/ST2/00350, NCN OPUS 2023/51/B/ST2/02507, OPUS nr 2022/47/B/ST2/03059, NCN NCN UMO-2019/34/E/ST2/00393, UMO-2022/47/O/ST2/00148, UMO-2023/49/B/ST2/04085, UMO-2023/51/B/ST2/00920, UMO-2024/53/N/ST2/00869); Portugal: Foundation for Science and Technology (FCT); Spain: Agencia de Gestión de Ayudas Universitarias y de Investigación (AGAUR - 2023 BP 00141), Generalitat Valenciana (ASFAE/2022/008), Ministry of Science and Innovation (MCIN & NextGenEU PCI2022-135018-2, MICIN & FEDER PID2021-125273NB, RYC2019-028510-I, RYC2020-030254-I, RYC2021-031273-I, RYC2022-038164-I), Ministerio de Ciencia, Innovación y Universidades/Agencia Estatal de Investigación (PID2022-142604OB-C22); Sweden: Carl Trygger Foundation (Carl Trygger Foundation CTS 22:2312), Swedish Research Council (Swedish Research Council 2023-04654, VR 2021-03651, VR 2022-03845, VR 2022-04683, VR 2023-03403, VR 2024-05451), Knut and Alice Wallenberg Foundation (KAW 2018.0458, KAW 2022.0358, KAW 2023.0366); Switzerland: Swiss National Science Foundation (SNSF - PCEFP2_194658); United Kingdom: Royal Society (NIF-R1-231091); United States of America: U.S. Department of Energy (ECA DE-AC02-76SF00515), Neubauer Family Foundation.

Data Availability Statement This manuscript has associated data. [Authors' comment: "All ATLAS scientific output is published in journals, and preliminary results are made available in Conference Notes. All are openly available, without restriction on use by external parties beyond copyright law and the standard conditions agreed by CERN. Data associated with journal publications are also made available: tables and data from plots (e.g. cross section values, likelihood profiles, selection efficiencies, cross section limits, ...) are stored in appropriate repositories such as HEPDATA (http://hepdata.cedar.ac.uk/). ATLAS also strives to make additional material related to the paper available that allows a reinterpretation of the data in the context of new theoretical models. For example, an extended encapsulation of the analysis is often provided for measurements in the framework of RIVET (http://rivet.hepforge.org/)." This information is taken from the ATLAS Data Access Policy, which is a public document that can be downloaded from http://opendata.cern.ch/record/413 [opendata.cern.ch].]

Code Availability Statement This manuscript has associated code/software. [Authors' comment: ATLAS collaboration software is open source, and all code necessary to recreate an analysis is publicly available. The Athena (http://gitlab.cern.ch/atlas/athena) software repository provides all code needed for calibration and uncertainty application, with configuration files that are also publicly available via Docker containers and cvmfs. The specific code and configurations written in support of this analysis are not public; however, these are internally preserved.]

Funded by SCOAP[3].

References

1. ATLAS Collaboration, *Climbing to the Top of the ATLAS 13 TeV data*, Phys. Rept. **1116** (2025) 127, https://doi.org/10.1016/j.physrep.2024.12.004 arXiv:2404.10674 [hep-ex]
2. M. Cacciari, M. Czakon, M. Mangano, A. Mitov, P. Nason, Top-pair production at hadron colliders with next-to-next-to-leading logarithmic soft-gluon resummation. Phys. Lett. B **710**, 612 (2012). https://doi.org/10.1016/j.physletb.2012.03.013. arXiv:1111.5869 [hep-ph]
3. P. Bärnreuther, M. Czakon, A. Mitov, Percent-Level-Precision Physics at the Tevatron: Next-to-Next-to-Leading Order QCD Corrections to $q\bar{q} \to t\bar{t} + X$. Phys. Rev. Lett. **109**, 132001 (2012). https://doi.org/10.1103/PhysRevLett.109.132001. arXiv:1204.5201 [hep-ph]
4. M. Czakon, A. Mitov, NNLO corrections to top-pair production at hadron colliders: the all-fermionic scattering channels. JHEP **12**, 054 (2012). https://doi.org/10.1007/JHEP12(2012)054. arXiv:1207.0236 [hep-ph]
5. M. Czakon, A. Mitov, NNLO corrections to top pair production at hadron colliders: the quark-gluon reaction. JHEP **01**, 080 (2013). https://doi.org/10.1007/JHEP01(2013)080. arXiv:1210.6832 [hep-ph]
6. M. Czakon, P. Fiedler, A. Mitov, Total Top-Quark Pair-Production Cross Section at Hadron Colliders Through $\mathcal{O}(\alpha_s^4)$. Phys. Rev. Lett. **110**, 252004 (2013). https://doi.org/10.1103/PhysRevLett.110.252004. arXiv:1303.6254 [hep-ph]
7. S. Catani et al., Top-quark pair hadroproduction at next-to-next-to-leading order in QCD. Phys. Rev. D **99**, 051501 (2019). https://doi.org/10.1103/PhysRevD.99.051501. arXiv:1901.04005 [hep-ph]
8. ATLAS Collaboration, Measurement of the $t\bar{t}$ production cross-section in pp collisions at $\sqrt{s} = 5.02$ TeV with the

ATLAS detector, JHEP **06** (2023) 138, https://doi.org/10.1007/JHEP06(2023)138 arXiv:2207.01354 [hep-ex]
9. ATLAS Collaboration, Measurement of the $t\bar{t}$ production cross-section using $e\mu$ events with b-tagged jets in pp collisions at $\sqrt{s} = 7$ and 8 TeV with the ATLAS detector, Eur. Phys. J. C **74** (2014) 3109, https://doi.org/10.1140/epjc/s10052-014-3109-7 arXiv:1406.5375 [hep-ex], Addendum: Eur. Phys. J. C **76** (2016) 642
10. ATLAS Collaboration, Measurement of the inclusive $t\bar{t}$ production cross section in the lepton + jets channel in pp collisions at $\sqrt{s} = 7$ TeV with the ATLAS detector using support vector machines, Phys. Rev. D **108** (2023) 032014, https://doi.org/10.1103/PhysRevD.108.032014 arXiv:2212.00571 [hep-ex]
11. ATLAS Collaboration, Measurement of the inclusive and fiducial $t\bar{t}$ production cross-sections in the lepton+jets channel in pp collisions at $\sqrt{s} = 8$ TeV with the ATLAS detector, Eur. Phys. J. C **78** (2018) 487, https://doi.org/10.1140/epjc/s10052-018-5904-z arXiv:1712.06857 [hep-ex]
12. ATLAS Collaboration, Inclusive and differential cross-sections for dilepton $t\bar{t}$ production measured in $\sqrt{s} = 13$ TeV pp collisions with the ATLAS detector, JHEP **07** (2023) 141, https://doi.org/10.1007/JHEP07(2023)141 arXiv:2303.15340 [hep-ex]
13. ATLAS Collaboration, Measurement of the $t\bar{t}$ production cross-section in the lepton+jets channel at $\sqrt{s} = 13$ TeV with the ATLAS experiment, Phys. Lett. B **810** (2020) 135797, https://doi.org/10.1016/j.physletb.2020.135797 arXiv:2006.13076 [hep-ex]
14. ATLAS Collaboration, Measurement of the $t\bar{t}$ cross section and its ratio to the Z production cross section using pp collisions at $\sqrt{s} = 13.6$ TeV with the ATLAS detector, Phys. Lett. B **848** (2024) 138376, https://doi.org/10.1016/j.physletb.2023.138376 arXiv:2308.09529 [hep-ex]
15. CMS Collaboration, Measurement of the inclusive $t\bar{t}$ cross section in final states with at least one lepton and additional jets with 302 pb^{-1} of pp collisions at $\sqrt{s} = 5.02$ TeV, JHEP **04** (2025) 099, https://doi.org/10.1007/JHEP04(2025)099 arXiv:2410.21631 [hep-ex]
16. CMS Collaboration, Measurement of the $t\bar{t}$ production cross section in the $e\mu$ channel in proton–proton collisions at $\sqrt{s} = 7$ and 8 TeV. JHEP **08**, 029 (2016). https://doi.org/10.1007/JHEP08(2016)029. arXiv:1603.02303 [hep-ex]
17. CMS Collaboration, Measurements of the $t\bar{t}$ production cross section in lepton+jets final states in pp collisions at 8 TeV and ratio of 8 to 7 TeV cross sections. Eur. Phys. J. C **77**, 15 (2017). https://doi.org/10.1140/epjc/s10052-016-4504-z. arXiv:1602.09024 [hep-ex]
18. CMS Collaboration, Measurement of the $t\bar{t}$ production cross section using events with one lepton and at least one jet in pp collisions at $\sqrt{s} = 13$ TeV. JHEP **09**, 051 (2017). https://doi.org/10.1007/JHEP09(2017)051. arXiv:1701.06228 [hep-ex]
19. CMS Collaboration, Measurement of the $t\bar{t}$ production cross section, the top quark mass, and the strong coupling constant using dilepton events in pp collisions at $\sqrt{s} = 13$ TeV. Eur. Phys. J. C **79**, 368 (2019). https://doi.org/10.1140/epjc/s10052-019-6863-8. arXiv:1812.10505 [hep-ex]
20. CMS Collaboration, First measurement of the top quark pair production cross section in proton–proton collisions at $\sqrt{s} = 13.6$ TeV, JHEP **08** (2023) 204, https://doi.org/10.1007/JHEP08(2023)204 arXiv:2303.10680 [hep-ex]
21. M. Czakon, A. Mitov, Top++: A program for the calculation of the top-pair cross-section at hadron colliders. Comput. Phys. Commun. **185**, 2930 (2014). https://doi.org/10.1016/j.cpc.2014.06.021. arXiv:1112.5675 [hep-ph]
22. R.D. Ball et al., The PDF4LHC21 combination of global PDF fits for the LHC Run III. J. Phys. G **49**, 080501 (2022). https://doi.org/10.1088/1361-6471/ac7216. arXiv:2203.05506 [hep-ph]
23. T.-J. Hou et al., New CTEQ global analysis of quantum chromodynamics with high-precision data from the LHC. Phys. Rev. D **103**, 014013 (2021). https://doi.org/10.1103/PhysRevD.103.014013. arXiv:1912.10053 [hep-ph]
24. S. Bailey, T. Cridge, L.A. Harland-Lang, A.D. Martin, R.S. Thorne, Parton distributions from LHC, HERA, Tevatron and fixed target data: MSHT20 PDFs. Eur. Phys. J. C **81**, 341 (2021). https://doi.org/10.1140/epjc/s10052-021-09057-0. arXiv:2012.04684 [hep-ph]
25. R.D. Ball et al., Parton distributions from high-precision collider data. Eur. Phys. J. C **77**, 663 (2017). https://doi.org/10.1140/epjc/s10052-017-5199-5. arXiv:1706.00428 [hep-ph]
26. M. Cacciari, S. Frixione, M.L. Mangano, P. Nason, G. Ridolfi, The $t\bar{t}$ cross-section at 1.8 and 1.96 TeV: a study of the systematics due to parton densities and scale dependence. JHEP **04**, 068 (2004). https://doi.org/10.1088/1126-6708/2004/04/068. arXiv:hep-ph/0303085
27. S. Catani, D. de Florian, M. Grazzini, P. Nason, Soft-gluon resummation for Higgs boson production at hadron colliders. JHEP **07**, 028 (2003). https://doi.org/10.1088/1126-6708/2003/07/028. arXiv:hep-ph/0306211
28. A. Buckley et al., General-purpose event generators for LHC physics. Phys. Rept. **504**, 145 (2011). https://doi.org/10.1016/j.physrep.2011.03.005. arXiv:1101.2599 [hep-ph]
29. S. Moch et al., *High precision fundamental constants at the TeV scale*, (2014), arXiv:1405.4781 [hep-ph]
30. M. Butenschoen et al., Top Quark Mass Calibration for Monte Carlo Event Generators. Phys. Rev. Lett. **117**, 232001 (2016). https://doi.org/10.1103/PhysRevLett.117.232001. arXiv:1608.01318 [hep-ph]
31. S. Ferrario Ravasio, T. Ježo, P. Nason, C. Oleari, A theoretical study of top-mass measurements at the LHC using NLO+PS generators of increasing accuracy. Eur. Phys. J. C **78**, 458 (2018). https://doi.org/10.1140/epjc/s10052-018-5909-7. arXiv:1801.03944 [hep-ph]
32. Particle Data Group Collaboration, Review of Particle Physics. Phys. Rev. D **110**, 030001 (2024). https://doi.org/10.1103/PhysRevD.110.030001
33. ATLAS Collaboration, Measurement of the $t\bar{t}$ production cross-section using $e\mu$ events with b-tagged jets in pp collisions at $\sqrt{s} = 13$ TeV with the ATLAS detector, Phys. Lett. B **761** (2016) 136, arXiv:1606.02699 [hep-ex], Erratum: Phys. Lett. B **772** (2017) 879. https://doi.org/10.1016/j.physletb.2016.08.019
34. ATLAS Collaboration, Measurement of the $t\bar{t}$ production cross-section and lepton differential distributions in $e\mu$ dilepton events from pp collisions at $\sqrt{s} = 13$ TeV with the ATLAS detector, Eur. Phys. J. C **80** (2020) 528, https://doi.org/10.1140/epjc/s10052-020-7907-9 arXiv:1910.08819 [hep-ex]
35. ATLAS Collaboration, Precise test of lepton flavour universality in W-boson decays into muons and electrons in pp collisions at $\sqrt{s} = 13$ TeV with the ATLAS detector, Eur. Phys. J. C **84** (2024) 993, https://doi.org/10.1140/epjc/s10052-024-13070-4 arXiv:2403.02133 [hep-ex]
36. J. Mazzitelli et al., Next-to-Next-to-Leading Order Event Generation for Top-Quark Pair Production. Phys. Rev. Lett. **127**, 062001 (2021). https://doi.org/10.1103/PhysRevLett.127.062001. arXiv:2012.14267 [hep-ph]
37. ATLAS Collaboration, Measurement of lepton differential distributions and the top quark mass in $t\bar{t}$ production in pp collisions at $\sqrt{s} = 8$ TeV with the ATLAS detector, Eur. Phys. J. C **77** (2017) 804, https://doi.org/10.1140/epjc/s10052-017-5349-9 arXiv:1709.09407 [hep-ex]
38. C.D. White, S. Frixione, E. Laenen, F. Maltoni, Isolating Wt production at the LHC. JHEP **11**, 074 (2009). https://doi.org/10.1088/1126-6708/2009/11/074. arXiv:0908.0631 [hep-ph]

39. S. Frixione, E. Laenen, P. Motylinski, C. White, B.R. Webber, Single-top hadroproduction in association with a W boson. JHEP **07**, 029 (2008). https://doi.org/10.1088/1126-6708/2008/07/029. arXiv:0805.3067 [hep-ph]
40. F. Demartin, B. Maier, F. Maltoni, K. Mawatari, M. Zaro, tWH associated production at the LHC. Eur. Phys. J. C **77**, 34 (2017). https://doi.org/10.1140/epjc/s10052-017-4601-7. arXiv:1607.05862 [hep-ph]
41. ATLAS Collaboration, Studies on top-quark Monte Carlo modelling for Top2016, ATL-PHYS-PUB-2016-020, 2016, url: `https://cds.cern.ch/record/2216168`
42. T. Ježo, J.M. Lindert, P. Nason, C. Oleari, S. Pozzorini, An NLO+PS generator for $t\bar{t}$ and Wt production and decay including non-resonant and interference effects. Eur. Phys. J. C **76**, 691 (2016). https://doi.org/10.1140/epjc/s10052-016-4538-2. arXiv:1607.04538 [hep-ph]
43. ATLAS Collaboration, Measurements of differential cross-sections of $WbWb$ production in the dilepton channel in pp collisions at $\sqrt{s} = 13$ TeV using the ATLAS detector, (2025), arXiv:2506.14700 [hep-ex]
44. ATLAS Collaboration, The ATLAS Experiment at the CERN Large Hadron Collider, JINST **3** (2008) S08003. https://doi.org/10.1088/1748-0221/3/08/S08003
45. B. Abbott et al., Production and integration of the ATLAS Insertable B-Layer. JINST **13**, T05008 (2018). https://doi.org/10.1088/1748-0221/13/05/T05008. arXiv:1803.00844 [physics.ins-det]
46. ATLAS Collaboration, ATLAS Insertable B-Layer: Technical Design Report, ATLAS-TDR-19; CERN-LHCC-2010-013, 2010, https://cds.cern.ch/record/1291633, Addendum: ATLAS-TDR-19-ADD-1; CERN-LHCC-2012-009, 2012, https://cds.cern.ch/record/1451888
47. ATLAS Collaboration, Luminosity determination in pp collisions at $\sqrt{s} = 13$ TeV using the ATLAS detector at the LHC, Eur. Phys. J. C **83** (2023) 982, https://doi.org/10.1140/epjc/s10052-023-11747-w arXiv:2212.09379 [hep-ex]
48. ATLAS Collaboration, ATLAS data quality operations and performance for 2015–2018 data-taking, JINST **15** (2020) P04003, https://doi.org/10.1088/1748-0221/15/04/P04003 arXiv:1911.04632 [physics.ins-det]
49. ATLAS Collaboration, Performance of electron and photon triggers in ATLAS during LHC Run 2, Eur. Phys. J. C **80** (2020) 47, https://doi.org/10.1140/epjc/s10052-019-7500-2 arXiv:1909.00761 [hep-ex]
50. ATLAS Collaboration, Performance of the ATLAS muon triggers in Run 2, JINST **15** (2020) P09015, https://doi.org/10.1088/1748-0221/15/09/p09015 arXiv:2004.13447 [physics.ins-det]
51. ATLAS Collaboration, The ATLAS Simulation Infrastructure, Eur. Phys. J. C **70** (2010) 823, https://doi.org/10.1140/epjc/s10052-010-1429-9 arXiv:1005.4568 [physics.ins-det]
52. S. Agostinelli et al., GEANT4–A simulation toolkit. Nucl. Instrum. Meth. A **506**, 250 (2003). https://doi.org/10.1016/S0168-9002(03)01368-8
53. ATLAS Collaboration, The simulation principle and performance of the ATLAS fast calorimeter simulation FastCaloSim, ATL-PHYS-PUB-2010-013, 2010, url: https://cds.cern.ch/record/1300517
54. T. Sjöstrand, S. Mrenna, P. Skands, A brief introduction to PYTHIA 8.1. Comput. Phys. Commun. **178**, 852 (2008). https://doi.org/10.1016/j.cpc.2008.01.036. arXiv:0710.3820 [hep-ph]
55. ATLAS Collaboration, The Pythia 8A3 tune description of ATLAS minimum bias and inelastic measurements incorporating the Donnachie–Landshoff diffractive model, ATL-PHYS-PUB-2016-017, 2016, https://cds.cern.ch/record/2206965
56. ATLAS Collaboration, *The ATLAS Collaboration Software and Firmware*, ATL-SOFT-PUB-2021-001, 2021, https://cds.cern.ch/record/2767187
57. ATLAS Collaboration, Electron and photon performance measurements with the ATLAS detector using the 2015–2017 LHC proton–proton collision data, JINST **14** (2019) P12006, https://doi.org/10.1088/1748-0221/14/12/P12006 arXiv:1908.00005 [hep-ex]
58. ATLAS Collaboration, Studies of the muon momentum calibration and performance of the ATLAS detector with pp collisions at $\sqrt{s} = 13$ TeV, Eur. Phys. J. C **83** (2023) 686, https://doi.org/10.1140/epjc/s10052-023-11584-x arXiv:2212.07338 [hep-ex]
59. ATLAS Collaboration, Jet energy scale and resolution measured in proton–proton collisions at $\sqrt{s} = 13$ TeV with the ATLAS detector, Eur. Phys. J. C **81** (2021) 689, https://doi.org/10.1140/epjc/s10052-021-09402-3 arXiv:2007.02645 [hep-ex]
60. ATLAS Collaboration, Electron and photon efficiencies in LHC Run 2 with the ATLAS experiment, JHEP **05** (2024) 162, https://doi.org/10.1007/JHEP05(2024)162 arXiv:2308.13362 [hep-ex]
61. ATLAS Collaboration, Muon reconstruction and identification efficiency in ATLAS using the full Run 2 pp collision data set at $\sqrt{s} = 13$ TeV, Eur. Phys. J. C **81** (2021) 578, https://doi.org/10.1140/epjc/s10052-021-09233-2 arXiv:2012.00578 [hep-ex]
62. ATLAS Collaboration, ATLAS b-jet identification performance and efficiency measurement with $t\bar{t}$ events in pp collisions at $\sqrt{s} = 13$ TeV, Eur. Phys. J. C **79** (2019) 970, https://doi.org/10.1140/epjc/s10052-019-7450-8 arXiv:1907.05120 [hep-ex]
63. P. Nason, A new method for combining NLO QCD with shower Monte Carlo algorithms. JHEP **11**, 040 (2004). https://doi.org/10.1088/1126-6708/2004/11/040. arXiv:hep-ph/0409146
64. S. Frixione, P. Nason, C. Oleari, Matching NLO QCD computations with parton shower simulations: the POWHEG method. JHEP **11**, 070 (2007). https://doi.org/10.1088/1126-6708/2007/11/070. arXiv:0709.2092 [hep-ph]
65. S. Alioli, P. Nason, C. Oleari, E. Re, A general framework for implementing NLO calculations in shower Monte Carlo programs: the POWHEG BOX. JHEP **06**, 043 (2010). https://doi.org/10.1007/JHEP06(2010)043. arXiv:1002.2581 [hep-ph]
66. S. Höche, S. Mrenna, S. Payne, C.T. Preuss, P. Skands, (2022) *A Study of QCD Radiation in VBF Higgs Production with Vincia and Pythia*, SciPost Phys. **12** 010, https://doi.org/10.21468/SciPostPhys.12.1.010 arXiv:2106.10987 [hep-ph]
67. C. Bierlich et al., A comprehensive guide to the physics and usage of PYTHIA 8.3. SciPost Phys. Codebases **2022**, 8 (2022). https://doi.org/10.21468/SciPostPhysCodeb.8. arXiv:2203.11601 [hep-ph]
68. NNPDF Collaboration, *Parton distributions for the LHC Run II*, JHEP **04** (2015) 040, https://doi.org/10.1007/JHEP04(2015)040 arXiv:1410.8849 [hep-ph]
69. ATLAS Collaboration, *ATLAS Pythia 8 tunes to 7 TeV data*, ATL-PHYS-PUB-2014-021, 2014, URL: `https://cds.cern.ch/record/1966419`
70. NNPDF Collaboration, Parton distributions with LHC data, Nucl. Phys. B **867** (2013) 244, https://doi.org/10.1016/j.nuclphysb.2012.10.003 arXiv:1207.1303 [hep-ph]
71. S. Frixione, G. Ridolfi, P. Nason, A Positive-weight next-to-leading-order Monte Carlo for heavy flavour hadroproduction. JHEP **09**, 126 (2007). https://doi.org/10.1088/1126-6708/2007/09/126. arXiv:0707.3088 [hep-ph]
72. M. Bähr et al., Herwig++ physics and manual. Eur. Phys. J. C **58**, 639 (2008). https://doi.org/10.1140/epjc/s10052-008-0798-9. arXiv:0803.0883 [hep-ph]
73. J. Bellm et al., *Herwig 7.1 Release Note*, (2017), arXiv:1705.06919 [hep-ph]

74. J. Erler, A. Freitas, Electroweak model and constraints on new physics, in Review of Particle Physics, PTEP **2022** 083C01 (2022). https://doi.org/10.1093/ptep/ptac097
75. D.J. Lange, The EvtGen particle decay simulation package. Nucl. Instrum. Meth. A **462**, 152 (2001). https://doi.org/10.1016/S0168-9002(01)00089-4
76. T. Ježo, J.M. Lindert, N. Moretti, S. Pozzorini, New NLOPS predictions for $t\bar{t}+b$-jet production at the LHC. Eur. Phys. J. C **78**, 502 (2018). https://doi.org/10.1140/epjc/s10052-018-5956-0. arXiv:1802.00426 [hep-ph]
77. T. Ježo, P. Nason, On the Treatment of Resonances in Next-to-Leading Order Calculations Matched to a Parton Shower. JHEP **12**, 065 (2015). https://doi.org/10.1007/JHEP12(2015)065. arXiv:1509.09071 [hep-ph]
78. T. Ježo, J.M. Lindert, S. Pozzorini, Resonance-aware NLOPS matching for off-shell $t\bar{t}+tW$ production with semileptonic decays. JHEP **10**, 008 (2023). https://doi.org/10.1007/JHEP10(2023)008. arXiv:2307.15653 [hep-ph]
79. ATLAS Collaboration, Studies of $t\bar{t}/tW$ interference effects in $b\bar{b}\ell^+\ell^{-\prime}\nu\bar{\nu}'$ final states with POWHEG *and* MADGRAPH5_AMC@NLO *setups*, ATL-PHYS-PUB-2021-042, 2021, url: https://cds.cern.ch/record/2792254
80. E. Re, Single-top Wt-channel production matched with parton showers using the POWHEG method. Eur. Phys. J. C **71**, 1547 (2011). https://doi.org/10.1140/epjc/s10052-011-1547-z. arXiv:1009.2450 [hep-ph]
81. N. Kidonakis, N. Yamanaka, Higher-order corrections for tW production at high-energy hadron colliders. JHEP **05**, 278 (2021). https://doi.org/10.1007/JHEP05(2021)278. arXiv:2102.11300 [hep-ph]
82. E. Bothmann et al., Event generation with Sherpa 2.2, SciPost Phys. **7** 034, (2019) https://doi.org/10.21468/SciPostPhys.7.3.034 arXiv:1905.09127 [hep-ph]
83. T. Gleisberg, S. Höche, Comix, a new matrix element generator. JHEP **12**, 039 (2008). https://doi.org/10.1088/1126-6708/2008/12/039. arXiv:0808.3674 [hep-ph]
84. F. Buccioni et al., OpenLoops 2. Eur. Phys. J. C **79**, 866 (2019). https://doi.org/10.1140/epjc/s10052-019-7306-2. arXiv:1907.13071 [hep-ph]
85. S. Schumann, F. Krauss, A parton shower algorithm based on Catani-Seymour dipole factorisation. JHEP **03**, 038 (2008). https://doi.org/10.1088/1126-6708/2008/03/038. arXiv:0709.1027 [hep-ph]
86. S. Höche, F. Krauss, M. Schönherr, F. Siegert, A critical appraisal of NLO+PS matching methods. JHEP **09**, 049 (2012). https://doi.org/10.1007/JHEP09(2012)049. arXiv:1111.1220 [hep-ph]
87. S. Catani, F. Krauss, B.R. Webber, R. Kuhn, QCD Matrix Elements + Parton Showers. JHEP **11**, 063 (2001). https://doi.org/10.1088/1126-6708/2001/11/063. arXiv:hep-ph/0109231
88. S. Höche, F. Krauss, M. Schönherr, F. Siegert, QCD matrix elements + parton showers. The NLO case, JHEP **04**, 027 (2013). https://doi.org/10.1007/JHEP04(2013)027. arXiv:1207.5030 [hep-ph]
89. S. Höche, F. Krauss, S. Schumann, F. Siegert, QCD matrix elements and truncated showers. JHEP **05**, 053 (2009). https://doi.org/10.1088/1126-6708/2009/05/053. arXiv:0903.1219 [hep-ph]
90. C. Anastasiou, L. Dixon, K. Melnikov, F. Petriello, High-precision QCD at hadron colliders: Electroweak gauge boson rapidity distributions at next-to-next-to leading order. Phys. Rev. D **69**, 094008 (2004). https://doi.org/10.1103/PhysRevD.69.094008. arXiv:hep-ph/0312266
91. J. Alwall et al., The automated computation of tree-level and next-to-leading order differential cross sections, and their matching to parton shower simulations. JHEP **07**, 079 (2014). https://doi.org/10.1007/JHEP07(2014)079. arXiv:1405.0301 [hep-ph]
92. M. Cacciari, G.P. Salam, G. Soyez, The anti-k_t jet clustering algorithm. JHEP **04**, 063 (2008). https://doi.org/10.1088/1126-6708/2008/04/063. arXiv:0802.1189 [hep-ph]
93. M. Cacciari, G.P. Salam, G. Soyez, FastJet user manual. Eur. Phys. J. C **72**, 1896 (2012). https://doi.org/10.1140/epjc/s10052-012-1896-2. arXiv:1111.6097 [hep-ph]
94. ATLAS Collaboration, Jet reconstruction and performance using particle flow with the ATLAS Detector, Eur. Phys. J. C **77** (2017) 466, https://doi.org/10.1140/epjc/s10052-017-5031-2 arXiv:1703.10485 [hep-ex]
95. ATLAS Collaboration, Performance of pile-up mitigation techniques for jets in pp collisions at $\sqrt{s}=8$ TeV using the ATLAS detector, Eur. Phys. J. C **76** (2016) 581, https://doi.org/10.1140/epjc/s10052-016-4395-z arXiv:1510.03823 [hep-ex]
96. ATLAS Collaboration, ATLAS flavour-tagging algorithms for the LHC Run 2 pp collision dataset, Eur. Phys. J. C **83** (2023) 681, https://doi.org/10.1140/epjc/s10052-023-11699-1 arXiv:2211.16345 [physics.data-an]
97. Auxiliary material for this analysis, URL: https://atlas.web.cern.ch/Atlas/GROUPS/PHYSICS/PAPERS/TOPQ-2024-12/
98. M. Cacciari, G.P. Salam, G. Soyez, The Catchment Area of Jets. JHEP **04**, 005 (2008). https://doi.org/10.1088/1126-6708/2008/04/005. arXiv:0802.1188 [hep-ph]
99. S. Dulat et al., New parton distribution functions from a global analysis of quantum chromodynamics. Phys. Rev. D **93**, 033006 (2016). https://doi.org/10.1103/PhysRevD.93.033006. arXiv:1506.07443 [hep-ph]
100. ATLAS Collaboration, Measurement of $t\bar{t}$ production in association with additional b-jets in the $e\mu$ final state in proton–proton collisions at $\sqrt{s}=13$ TeV with the ATLAS detector, JHEP **01** (2025) 068, https://doi.org/10.1007/JHEP01(2025)068 arXiv:2407.13473 [hep-ex]
101. ATLAS Collaboration, Measurements of inclusive and differential fiducial cross-sections of $t\bar{t}$ production with additional heavy-flavour jets in proton–proton collisions at $\sqrt{s}=13$ TeV with the ATLAS detector, JHEP **04** (2019) 046, https://doi.org/10.1007/JHEP04(2019)046 arXiv:1811.12113 [hep-ex]
102. ATLAS Collaboration, Measurement of the c-jet mistagging efficiency in $t\bar{t}$ events using pp collision data at $\sqrt{s}=13$ TeV collected with the ATLAS detector, Eur. Phys. J. C **82** (2022) 95, https://doi.org/10.1140/epjc/s10052-021-09843-w arXiv:2109.10627 [hep-ex]
103. ATLAS Collaboration, Calibration of the light-flavour jet mistagging efficiency of the b-tagging algorithms with Z+jets events using 139 fb^{-1} of ATLAS proton–proton collision data at $\sqrt{s}=13$ TeV, Eur. Phys. J. C **83** (2023) 728, https://doi.org/10.1140/epjc/s10052-023-11736-zarXiv:2301.06319 [hep-ex]
104. J.M. Campbell, R.K. Ellis, MCFM for the Tevatron and the LHC. Nucl. Phys. B, Proc. Suppl. **205–206**, 10 (2010). https://doi.org/10.1016/j.nuclphysbps.2010.08.011. arXiv:1007.3492 [hep-ph]
105. G. Avoni et al., The new LUCID-2 detector for luminosity measurement and monitoring in ATLAS. JINST **13**, P07017 (2018). https://doi.org/10.1088/1748-0221/13/07/P07017
106. E. Todesco, J. Wenninger, Large Hadron Collider momentum calibration and accuracy. Phys. Rev. Accel. Beams **20**, 081003 (2017). https://doi.org/10.1103/PhysRevAccelBeams.20.081003
107. L. Lyons, D. Gibaut, P. Clifford, How to combine correlated estimates of a single physical quantity. Nucl. Instrum. Meth. A **270**, 110 (1988). https://doi.org/10.1016/0168-9002(88)90018-6
108. A. Valassi, Combining correlated measurements of several different physical quantities. Nucl. Instrum. Meth. A **500**, 391 (2003). https://doi.org/10.1016/S0168-9002(03)00329-2
109. ATLAS and CMS Collaborations, Combination of inclusive top-quark pair production cross-section measurements using ATLAS and CMS data at $\sqrt{s}=7$ and 8 TeV. JHEP **07**, 213 (2023). https://doi.org/10.1007/JHEP07(2023)213. arXiv:2205.13830 [hep-ex]

ATLAS Collaboration*

G. Aad[103], E. Aakvaag[17], B. Abbott[122], S. Abdelhameed[118a], K. Abeling[55], N. J. Abicht[49], S. H. Abidi[30], M. Aboelela[45], A. Aboulhorma[36e], H. Abramowicz[156], Y. Abulaiti[119], B. S. Acharya[69a,69b,m], A. Ackermann[63a], C. Adam Bourdarios[4], L. Adamczyk[86a], S. V. Addepalli[148], M. J. Addison[102], J. Adelman[117], A. Adiguzel[22c], T. Adye[136], A. A. Affolder[138], Y. Afik[40], M. N. Agaras[13], A. Aggarwal[101], C. Agheorghiesei[28c], F. Ahmadov[39,ad], S. Ahuja[96], S. Ahuja[168], X. Ai[142b], G. Aielli[76a,76b], A. Aikot[168], M. Ait Tamlihat[36e], B. Aitbenchikh[36a], T. P. A. Åkesson[99], A. V. Akimov[150], D. Akiyama[173], N. N. Akolkar[25], S. Aktas[171], G. L. Alberghi[24b], J. Albert[170], U. Alberti[20], P. Albicocco[53], G. L. Albouy[60], S. Alderweireldt[52], Z. L. Alegria[123], M. Aleksa[37], I. N. Aleksandrov[39], C. Alexa[28b], T. Alexopoulos[10], F. Alfonsi[24b], M. Algren[56], M. Alhroob[172], B. Ali[134], H. M. J. Ali[92,w], S. Ali[32], S. W. Alibocus[93], M. Aliev[34c], G. Alimonti[71a], W. Alkakhi[55], C. Allaire[66], B. M. M. Allbrooke[151], D. R. Allen[123], J. S. Allen[102], J. F. Allen[52], P. P. Allport[21], A. Aloisio[72a,72b], F. Alonso[91], C. Alpigiani[141], Z. M. K. Alsolami[92], A. Alvarez Fernandez[101], M. Alves Cardoso[56], M. G. Alviggi[72a,72b], M. Aly[102], Y. Amaral Coutinho[82b], A. Ambler[105], C. Amelung[37], M. Amerl[102], C. G. Ames[110], T. Amezza[129], D. Amidei[107], B. Amini[54], K. Amirie[160], A. Amirkhanov[39], S. P. Amor Dos Santos[132a], K. R. Amos[168], D. Amperiadou[157], S. An[83], C. Anastopoulos[144], T. Andeen[11], J. K. Anders[93], A. C. Anderson[59], A. Andreazza[71a,71b], S. Angelidakis[9], A. Angerami[42], A. V. Anisenkov[39], A. Annovi[74a], C. Antel[37], E. Antipov[150], M. Antonelli[53], F. Anulli[75a], M. Aoki[83], T. Aoki[158], M. A. Aparo[151], L. Aperio Bella[48], M. Apicella[31], C. Appelt[156], A. Apyan[27], M. Arampatzi[10], S. J. Arbiol Val[87], C. Arcangeletti[53], A. T. H. Arce[51], J.-F. Arguin[109], S. Argyropoulos[157], J.-H. Arling[48], O. Arnaez[4], H. Arnold[150], G. Artoni[75a,75b], H. Asada[112], K. Asai[120], S. Asatryan[178], N. A. Asbah[37], R. A. Ashby Pickering[172], A. M. Aslam[96], K. Assamagan[30], R. Astalos[29a], K. S. V. Astrand[99], S. Atashi[164], R. J. Atkin[34a], H. Atmani[36f], P. A. Atmasiddha[130], K. Augsten[134], A. D. Auriol[41], V. A. Austrup[102], A. S. Avad[95], G. Avolio[37], K. Axiotis[56], A. Azzam[13], D. Babal[29b], H. Bachacou[137], K. Bachas[157,q], A. Bachiu[35], E. Bachmann[50], M. J. Backes[63a], A. Badea[40], T. M. Baer[107], P. Bagnaia[75a,75b], M. Bahmani[19], D. Bahner[54], K. Bai[125], J. T. Baines[136], L. Baines[95], O. K. Baker[177], E. Bakos[16], D. Bakshi Gupta[8], L. E. Balabram Filho[82b], V. Balakrishnan[122], R. Balasubramanian[4], E. M. Baldin[38], P. Balek[86a], E. Ballabene[24a,24b], F. Balli[137], L. M. Baltes[63a], W. K. Balunas[33], J. Balz[101], I. Bamwidhi[118b], E. Banas[87], M. Bandieramonte[131], A. Bandyopadhyay[25], S. Bansal[25], L. Barak[156], M. Barakat[48], E. L. Barberio[106], D. Barberis[18b], M. Barbero[103], M. Z. Barel[116], T. Barillari[111], M.-S. Barisits[37], T. Barklow[148], P. Baron[135], D. A. Baron Moreno[102], A. Baroncelli[62], A. J. Barr[128], J. D. Barr[97], F. Barreiro[100], J. Barreiro Guimarães da Costa[14], M. G. Barros Teixeira[132a], S. Barsov[38], F. Bartels[63a], R. Bartoldus[148], A. E. Barton[92], P. Bartos[29a], M. Baselga[49], S. Bashiri[87], A. Bassalat[66,b], M. J. Basso[161a], S. Bataju[45], R. Bate[169], R. L. Bates[59], S. Batlamous[100], M. Battaglia[138], D. Battulga[19], M. Bauce[75a,75b], M. Bauer[79], P. Bauer[25], L. T. Bayer[48], L. T. Bazzano Hurrell[31], J. B. Beacham[111], T. Beau[129], J. Y. Beaucamp[91], P. H. Beauchemin[163], P. Bechtle[25], H. P. Beck[20,p], K. Becker[172], A. J. Beddall[81], V. A. Bednyakov[39], C. P. Bee[150], L. J. Beemster[16], M. Begalli[82d], M. Begel[30], J. K. Behr[48], J. F. Beirer[37], F. Beisiegel[25], M. Belfkir[118b], G. Bella[156], L. Bellagamba[24b], A. Bellerive[35], C. D. Bellgraph[68], P. Bellos[21], K. Beloborodov[38], I. Benaoumeur[21], D. Benchekroun[36a], F. Bendebba[36a], Y. Benhammou[156], K. C. Benkendorfer[61], L. Beresford[48], M. Beretta[53], E. Bergeaas Kuutmann[166], N. Berger[4], B. Bergmann[134], J. Beringer[18a], G. Bernardi[5], C. Bernius[148], F. U. Bernlochner[25], A. Berrocal Guardia[13], T. Berry[96], P. Berta[135], A. Berti[132a], R. Bertrand[103], S. Bethke[111], A. Betti[75a,75b], A. J. Bevan[95], L. Bezio[56], N. K. Bhalla[54], S. Bharthuar[111], S. Bhatta[150], P. Bhattarai[148], Z. M. Bhatti[119], K. D. Bhide[54], V. S. Bhopatkar[123], R. M. Bianchi[131], G. Bianco[24a,24b], O. Biebel[110], M. Biglietti[77a], C. S. Billingsley[45], Y. Bimgdi[36f], M. Bindi[55], A. Bingham[176], A. Bingul[22b], C. Bini[75a,75b], G. A. Bird[33], M. Birman[174], M. Biros[135], S. Biryukov[151], T. Bisanz[49], E. Bisceglie[24a,24b], J. P. Biswal[136], D. Biswas[146], I. Bloch[48], A. Blue[59], U. Blumenschein[95], V. S. Bobrovnikov[39], L. Boccardo[57a,57b], M. Boehler[54], B. Boehm[171], D. Bogavac[13], A. G. Bogdanchikov[38], L. S. Boggia[129], V. Boisvert[96], P. Bokan[37], T. Bold[86a], M. Bomben[5], M. Bona[95], M. Boonekamp[137], A. G. Borbély[59], I. S. Bordulev[38], G. Borissov[92], D. Bortoletto[128], D. Boscherini[24b], M. Bosman[13], K. Bouaouda[36a], N. Bouchhar[168], L. Boudet[4], J. Boudreau[131], E. V. Bouhova-Thacker[92], D. Boumediene[41], R. Bouquet[57a,57b], A. Boveia[121], J. Boyd[37], D. Boye[30], I. R. Boyko[39], L. Bozianu[56], J. Bracinik[21], N. Brahimi[4], G. Brandt[176], O. Brandt[33], B. Brau[104],

J. E. Brau[125], R. Brener[174], L. Brenner[116], R. Brenner[166], S. Bressler[174], G. Brianti[78a,78b], D. Britton[59], D. Britzger[111], I. Brock[25], R. Brock[108], G. Brooijmans[42], A. J. Brooks[68], E. M. Brooks[161b], E. Brost[30], L. M. Brown[161a,170], L. E. Bruce[61], T. L. Bruckler[128], P. A. Bruckman de Renstrom[87], B. Brüers[48], A. Bruni[24b], G. Bruni[24b], D. Brunner[47a,47b], M. Bruschi[24b], N. Bruscino[75a,75b], T. Buanes[17], Q. Buat[141], D. Buchin[111], A. G. Buckley[59], O. Bulekov[81], B. A. Bullard[148], S. Burdin[93], C. D. Burgard[49], A. M. Burger[90], B. Burghgrave[8], O. Burlayenko[54], J. Burleson[167], J. C. Burzynski[147], E. L. Busch[42], V. Büscher[101], P. J. Bussey[59], O. But[25], J. M. Butler[26], C. M. Buttar[59], J. M. Butterworth[97], P. Butti[37], W. Buttinger[136], C. J. Buxo Vazquez[108], A. R. Buzykaev[39], S. Cabrera Urbán[168], L. Cadamuro[66], H. Cai[37], Y. Cai[24a,24b,113c], Y. Cai[113a], V. M. M. Cairo[37], O. Cakir[3a], N. Calace[37], P. Calafiura[18a], G. Calderini[129], P. Calfayan[35], L. Calic[99], G. Callea[59], L. P. Caloba[82b], D. Calvet[41], S. Calvet[41], R. Camacho Toro[129], S. Camarda[37], D. Camarero Munoz[27], P. Camarri[76a,76b], C. Camincher[170], M. Campanelli[97], A. Camplani[43], V. Canale[72a,72b], A. C. Canbay[3a], E. Canonero[96], J. Cantero[168], Y. Cao[167], F. Capocasa[27], M. Capua[44a,44b], A. Carbone[71a,71b], R. Cardarelli[76a], J. C. J. Cardenas[8], M. P. Cardiff[27], G. Carducci[44a,44b], T. Carli[37], G. Carlino[72a], J. I. Carlotto[13], B. T. Carlson[131,r], E. M. Carlson[170], J. Carmignani[93], L. Carminati[71a,71b], A. Carnelli[4], M. Carnesale[37], S. Caron[115], E. Carquin[139g], I. B. Carr[106], S. Carrá[73a,73b], G. Carratta[24a,24b], C. Carrion Martinez[168], A. M. Carroll[125], M. P. Casado[13,h], P. Casolaro[72a,72b], M. Caspar[48], W. R. Castiglioni[40], F. L. Castillo[4], L. Castillo Garcia[13], V. Castillo Gimenez[168], N. F. Castro[132a,132e], A. Catinaccio[37], J. R. Catmore[127], T. Cavaliere[4], V. Cavaliere[30], L. J. Caviedes Betancourt[23b], E. Celebi[81], S. Cella[37], V. Cepaitis[56], K. Cerny[124], A. S. Cerqueira[82a], A. Cerri[74a,am], L. Cerrito[76a,76b], F. Cerutti[18a], B. Cervato[71a,71b], A. Cervelli[24b], G. Cesarini[53], S. A. Cetin[81], P. M. Chabrillat[129], R. Chakkappai[66], S. Chakraborty[172], A. Chambers[61], J. Chan[18a], W. Y. Chan[158], J. D. Chapman[33], E. Chapon[137], B. Chargeishvili[154b], D. G. Charlton[21], C. Chauhan[135], Y. Che[113a], S. Chekanov[6], G. A. Chelkov[39,a], B. Chen[156], B. Chen[170], H. Chen[30], J. Chen[143a], J. Chen[147], M. Chen[128], S. Chen[88], S. J. Chen[113a], X. Chen[143a], X. Chen[15,ah], Z. Chen[62], C. L. Cheng[175], H. C. Cheng[64a], S. Cheong[148], A. Cheplakov[39], E. Cherepanova[116], R. Cherkaoui El Moursli[36e], E. Cheu[7], K. Cheung[65], L. Chevalier[137], V. Chiarella[53], G. Chiarelli[74a], G. Chiodini[70a], A. S. Chisholm[21], A. Chitan[28b], M. Chitishvili[168], M. V. Chizhov[39,s], K. Choi[11], Y. Chou[141], E. Y. S. Chow[115], K. L. Chu[174], M. C. Chu[64a], X. Chu[14,113c], Z. Chubinidze[53], J. Chudoba[133], J. J. Chwastowski[87], D. Cieri[111], K. M. Ciesla[86a], V. Cindro[94], A. Ciocio[18a], F. Cirotto[72a,72b], Z. H. Citron[174], M. Citterio[71a], D. A. Ciubotaru[28b], A. Clark[56], P. J. Clark[52], N. Clarke Hall[97], C. Clarry[160], S. E. Clawson[48], C. Clement[47a,47b], L. Clissa[24a,24b], Y. Coadou[103], M. Cobal[69a,69c], A. Coccaro[57b], R. F. Coelho Barrue[132a], R. Coelho Lopes De Sa[104], S. Coelli[71a], M. M. Cohen[130], L. S. Colangeli[160], B. Cole[42], P. Collado Soto[100], J. Collot[60], M.R. Coluccia[70a], P. Conde Muiño[132a,132g], M. P. Connell[34c], S. H. Connell[34c], E. I. Conroy[128], M. Contreras Cossio[11], F. Conventi[72a,aj], A. M. Cooper-Sarkar[128], L. Corazzina[75a,75b], F. A. Corchia[24a,24b], A. Cordeiro Oudot Choi[141], L. D. Corpe[41], M. Corradi[75a,75b], F. Corriveau[105,ab], A. Cortes-Gonzalez[158], M. J. Costa[168], F. Costanza[4], D. Costanzo[144], J. Couthures[4], G. Cowan[96], K. Cranmer[175], L. Cremer[49], D. Cremonini[24a,24b], S. Crépé-Renaudin[60], F. Crescioli[129], T. Cresta[73a,73b], M. Cristinziani[146], M. Cristoforetti[78a,78b], E. Critelli[97], V. Croft[116], G. Crosetti[44a,44b], A. Cueto[100], H. Cui[97], Z. Cui[7], B. M. Cunnett[151], W. R. Cunningham[59], F. Curcio[168], J. R. Curran[52], M. J. Da Cunha Sargedas De Sousa[57a,57b], J. V. Da Fonseca Pinto[82b], C. Da Via[102], W. Dabrowski[86a], T. Dado[37], S. Dahbi[153], T. Dai[107], D. Dal Santo[20], C. Dallapiccola[104], M. Dam[43], G. D'amen[30], V. D'Amico[110], J. R. Dandoy[35], M. D'Andrea[57a,57b], D. Dannheim[37], G. D'anniballe[74a,74b], M. Danninger[147], V. Dao[150], G. Darbo[57b], S. J. Das[30], F. Dattola[48], S. D'Auria[71a,71b], A. D'Avanzo[72a,72b], T. Davidek[135], J. Davidson[172], I. Dawson[95], K. De[8], C. De Almeida Rossi[160], R. De Asmundis[72a], N. De Biase[48], S. De Castro[24a,24b], N. De Groot[115], P. de Jong[116], H. De la Torre[117], A. De Maria[113a], A. De Salvo[75a], U. De Sanctis[76a,76b], F. De Santis[70a,70b], A. De Santo[151], J. B. De Vivie De Regie[60], J. Debevc[94], D. V. Dedovich[39], J. Degens[93], A. M. Deiana[45], J. Del Peso[100], L. Delagrange[129], F. Deliot[137], C. M. Delitzsch[49], M. Della Pietra[72a,72b], D. Della Volpe[56], A. Dell'Acqua[37], L. Dell'Asta[71a,71b], M. Delmastro[4], C. C. Delogu[57a,57b], P. A. Delsart[60], S. Demers[177], M. Demichev[39], S. P. Denisov[38], H. Denizli[22a,l], M. G. Depala[93], L. D'Eramo[41], D. Derendarz[87], F. Derue[129], P. Dervan[93,*], A. M. Desai[1], K. Desch[25], F. A. Di Bello[74a,74b], A. Di Ciaccio[76a,76b], L. Di Ciaccio[4], A. Di Domenico[75a,75b], C. Di Donato[72a,72b], A. Di Girolamo[37], G. Di Gregorio[66], A. Di Luca[78a,78b], B. Di Micco[77a,77b], R. Di Nardo[77a,77b], K. F. Di Petrillo[40], M. Diamantopoulou[35], F. A. Dias[116], M. A. Diaz[139a,139b], A. R. Didenko[39], M. Didenko[168], S. D. Diefenbacher[18a], E. B. Diehl[107],

S. Díez Cornell[48], C. Diez Pardos[146], C. Dimitriadi[149], A. Dimitrievska[21], A. Dimri[150], Y. Ding[62], J. Dingfelder[25], T. Dingley[128], I.-M. Dinu[28b], S. J. Dittmeier[63b], F. Dittus[37], M. Divisek[135], B. Dixit[93], F. Djama[103], T. Djobava[154b], C. Doglioni[99,102], A. Dohnalova[29a], Z. Dolezal[135], K. Domijan[86a], K. M. Dona[40], M. Donadelli[82d], B. Dong[108], J. Donini[41], A. D'Onofrio[72a,72b], M. D'Onofrio[93], J. Dopke[136], A. Doria[72a], N. Dos Santos Fernandes[132a], I. A. Dos Santos Luz[82e], P. Dougan[102], M. T. Dova[91], A. T. Doyle[59], M. P. Drescher[55], E. Dreyer[174], I. Drivas-koulouris[10], M. Drnevich[119], D. Du[62], T. A. du Pree[116], Z. Duan[113a], M. Dubau[4], F. Dubinin[39], M. Dubovsky[29a], E. Duchovni[174], G. Duckeck[110], P. K. Duckett[97], O. A. Ducu[28b], D. Duda[52], A. Dudarev[37], M. M. Dudek[87], E. R. Duden[27], M. D'uffizi[102], L. Duflot[66], M. Dührssen[37], I. Duminica[28g], A. E. Dumitriu[28b], M. Dunford[63a], K. Dunne[47a,47b], A. Duperrin[103], H. Duran Yildiz[3a], A. Durglishvili[154b], G. I. Dyckes[18a], M. Dyndal[86a], B. S. Dziedzic[37], Z. O. Earnshaw[151], G. H. Eberwein[128], B. Eckerova[29a], S. Eggebrecht[55], E. Egidio Purcino De Souza[82e], G. Eigen[17], K. Einsweiler[18a], T. Ekelof[166], P. A. Ekman[99], S. El Farkh[36b], Y. El Ghazali[62], H. El Jarrari[105], A. El Moussaouy[36a], D. Elitez[37], M. Ellert[166], F. Ellinghaus[176], T. A. Elliot[96], N. Ellis[37], J. Elmsheuser[30], M. Elsawy[118a], M. Elsing[37], D. Emeliyanov[136], Y. Enari[83], S. Epari[109], D. Ernani Martins Neto[87], F. Ernst[37], M. Escalier[66], C. Escobar[168], E. Etzion[156], G. Evans[132a,132b], H. Evans[68], L. S. Evans[48], A. Ezhilov[38], S. Ezzarqtouni[36a], F. Fabbri[24a,24b], L. Fabbri[24a,24b], G. Facini[97], V. Fadeyev[138], R. M. Fakhrutdinov[38], D. Fakoudis[101], S. Falciano[75a], L. F. Falda Ulhoa Coelho[27], F. Fallavollita[111], G. Falsetti[44a,44b], J. Faltova[135], C. Fan[167], K. Y. Fan[64b], Y. Fan[14], Y. Fang[14,113c], M. Fanti[71a,71b], M. Faraj[69a,69b], Z. Farazpay[98], A. Farbin[8], A. Farilla[77a], K. Farman[153], T. Farooque[108], J. N. Farr[177], M. S. Farrington[61], S. M. Farrington[52,136], F. Fassi[36e], D. Fassouliotis[9], L. Fayard[66], P. Federic[135], P. Federicova[133], O. L. Fedin[38,a], M. Feickert[175], L. Feligioni[103], D. E. Fellers[18a], C. Feng[142a], Y. Feng[14], Z. Feng[116], M. J. Fenton[164], L. Ferencz[48], B. Fernandez Barbadillo[92], P. Fernandez Martinez[67], M. J. V. Fernoux[103], J. Ferrando[92], A. Ferrari[166], P. Ferrari[115,116], R. Ferrari[73a], D. Ferrere[56], C. Ferretti[107], M. P. Fewell[1], D. Fiacco[75a,75b], F. Fiedler[101], P. Fiedler[134], S. Filimonov[39], M. S. Filip[28b,t], A. Filipčič[94], E. K. Filmer[161a], F. Filthaut[115], M. C. N. Fiolhais[132a,132c,c], L. Fiorini[168], W. C. Fisher[108], T. Fitschen[102], P. M. Fitzhugh[137], I. Fleck[146], P. Fleischmann[107], T. Flick[176], M. Flores[34d,ag], L. R. Flores Castillo[64a], M. Foll[127], F. M. Follega[78a,78b], N. Fomin[33], J. H. Foo[160], A. Formica[137], A. C. Forti[102], E. Fortin[37], A. W. Fortman[18a], L. Foster[18a], L. Fountas[9,i], D. Fournier[66], H. Fox[92], P. Francavilla[74a,74b], S. Francescato[61], S. Franchellucci[56], M. Franchini[24a,24b], S. Franchino[63a], D. Francis[37], L. Franco[48], L. Franconi[48], M. Franklin[61], G. Frattari[27], Y. Y. Frid[156], J. Friend[59], N. Fritzsche[37], A. Froch[56], D. Froidevaux[37], J. A. Frost[136], Y. Fu[108], S. Fuenzalida Garrido[139g], M. Fujimoto[150], K. Y. Fung[64a], E. Furtado De Simas Filho[82e], M. Furukawa[158], M. Fuste Costa[48], J. Fuster[168], A. Gaa[55], A. Gabrielli[24a,24b], A. Gabrielli[160], P. Gadow[37], G. Gagliardi[57a,57b], L. G. Gagnon[18a], S. Gaid[84b], S. Galantzan[156], J. Gallagher[1], E. J. Gallas[128], A. L. Gallen[166], B. J. Gallop[136], K. K. Gan[121], S. Ganguly[158], Y. Gao[52], A. Garabaglu[141], F. M. Garay Walls[139a,139b], C. García[168], A. Garcia Alonso[116], A. G. Garcia Caffaro[177], J. E. García Navarro[168], M. A. Garcia Ruiz[23b], M. Garcia-Sciveres[18a], G. L. Gardner[130], R. W. Gardner[40], N. Garelli[163], R. B. Garg[148], J. M. Gargan[33], C. A. Garner[160], C. M. Garvey[34a], V. K. Gassmann[163], G. Gaudio[73a], V. Gautam[13], P. Gauzzi[75a,75b], J. Gavranovic[94], I. L. Gavrilenko[132a], A. Gavrilyuk[38], C. Gay[169], G. Gaycken[125], E. N. Gazis[10], A. Gekow[121], C. Gemme[57b], M. H. Genest[60], A. D. Gentry[114], S. George[96], T. Geralis[46], A. A. Gerwin[122], P. Gessinger-Befurt[37], M. Ghani[172], K. Ghorbanian[95], A. Ghosal[146], A. Ghosh[164], A. Ghosh[7], B. Giacobbe[24b], S. Giagu[75a,75b], T. Giani[116], A. Giannini[62], S. M. Gibson[96], M. Gignac[138], D. T. Gil[86b], A. K. Gilbert[86a], B. J. Gilbert[42], D. Gillberg[35], G. Gilles[116], D. M. Gingrich[2,ai], M. P. Giordani[69a,69c], P. F. Giraud[137], G. Giugliarelli[69a,69c], D. Giugni[71a], F. Giuli[76a,76b], I. Gkialas[9,i], L. K. Gladilin[38], C. Glasman[100], M. Glazewska[20], R. M. Gleason[164], G. Glemža[48], M. Glisic[125], I. Gnesi[44b], Y. Go[30], M. Goblirsch-Kolb[37], B. Gocke[49], D. Godin[109], B. Gokturk[22a], S. Goldfarb[106], T. Golling[56], M. G. D. Gololo[34c], A. Golub[141], D. Golubkov[38], J. P. Gombas[108], A. Gomes[132a,132b], G. Gomes Da Silva[146], A. J. Gomez Delegido[37], R. Gonçalo[132a], L. Gonella[21], A. Gongadze[154c], F. Gonnella[21], J. L. Gonski[148], R. Y. González Andana[52], S. González de la Hoz[168], M. V. Gonzalez Rodrigues[48], R. Gonzalez Suarez[166], S. Gonzalez-Sevilla[56], L. Goossens[37], B. Gorini[37], E. Gorini[70a,70b], A. Gorišek[94], T. C. Gosart[130], A. T. Goshaw[51], M. I. Gostkin[39], S. Goswami[123], C. A. Gottardo[37], S. A. Gotz[110], M. Gouighri[36b], A. G. Goussiou[141], N. Govender[34c], R. P. Grabarczyk[128], I. Grabowska-Bold[86a], K. Graham[35], E. Gramstad[127], S. Grancagnolo[70a,70b], C. M. Grant[1], P. M. Gravila[28f], F. G. Gravili[70a,70b], H. M. Gray[18a], M. Greco[111], M. J. Green[1], C. Grefe[25], A. S. Grefsrud[17],

I. M. Gregor[48], K. T. Greif[164], P. Grenier[148], S. G. Grewe[111], A. A. Grillo[138], K. Grimm[32], S. Grinstein[13,x], J.-F. Grivaz[66], E. Gross[174], J. Grosse-Knetter[55], L. H. Grossman[18b], L. Guan[107], G. Guerrieri[37], R. Guevara[127], R. Gugel[101], J. A. M. Guhit[107], A. Guida[19], E. Guilloton[172], S. Guindon[37], F. Guo[14,113c], J. Guo[143a], L. Guo[48], L. Guo[113b,v], Y. Guo[107], Y. Guo[42], A. Gupta[49], R. Gupta[131], S. Gupta[27], S. Gurbuz[25], S. S. Gurdasani[48], G. Gustavino[75a,75b], P. Gutierrez[122], L. F. Gutierrez Zagazeta[130], M. Gutsche[50], C. Gutschow[97], C. Gwenlan[128], C. B. Gwilliam[93], E. S. Haaland[127], A. Haas[119], M. Habedank[59], C. Haber[18a], H. K. Hadavand[8], A. Haddad[41], A. Hadef[50], A. I. Hagan[92], J. J. Hahn[146], E. H. Haines[97], M. Haleem[171], J. Haley[123], G. D. Hallewell[103], J. A. Hallford[48], K. Hamano[170], H. Hamdaoui[166], M. Hamer[25], S. E. D. Hammoud[66], E. J. Hampshire[96], J. Han[142a], L. Han[113a], L. Han[62], S. Han[14], K. Hanagaki[83], M. Hance[138], D. A. Hangal[42], H. Hanif[147], M. D. Hank[130], J. B. Hansen[43], P. H. Hansen[43], T. Harenberg[176], S. Harkusha[178], M. L. Harris[104], Y. T. Harris[25], J. Harrison[13], P. F. Harrison[172], M. L. E. Hart[97], N. M. Hartman[111], N. M. Hartmann[110], R. Z. Hasan[96,136], Y. Hasegawa[145], F. Haslbeck[128], S. Hassan[17], R. Hauser[108], M. Haviernik[135], C. M. Hawkes[21], R. J. Hawkings[37], Y. Hayashi[158], D. Hayden[108], C. Hayes[107], R. L. Hayes[116], C. P. Hays[128], J. M. Hays[95], H. S. Hayward[93], M. He[14,113c], Y. He[48], Y. He[97], N. B. Heatley[95], V. Hedberg[99], J. Heilman[35], S. Heim[48], T. Heim[18a], J. J. Heinrich[125], L. Heinrich[111], J. Hejbal[133], M. Helbig[50], A. Held[175], S. Hellesund[17], C. M. Helling[169], S. Hellman[47a,47b], A. M. Henriques Correia[37], H. Herde[99], Y. Hernández Jiménez[150], L. M. Herrmann[25], T. Herrmann[50], G. Herten[54], R. Hertenberger[110], L. Hervas[37], M. E. Hesping[101], N. P. Hessey[161a], J. Hessler[111], M. Hidaoui[36b], N. Hidic[135], E. Hill[160], T. S. Hillersoy[17], S. J. Hillier[21], J. R. Hinds[108], F. Hinterkeuser[25], M. Hirose[126], S. Hirose[162], D. Hirschbuehl[176], T. G. Hitchings[102], B. Hiti[94], J. Hobbs[150], R. Hobincu[28e], N. Hod[174], A. M. Hodges[167], M. C. Hodgkinson[144], B. H. Hodkinson[128], A. Hoecker[37], D. D. Hofer[107], J. Hofer[168], J. Hofner[101], M. Holzbock[37], L. B. A. H. Hommels[33], V. Homsak[128], J. J. Hong[68], T. M. Hong[131], B. H. Hooberman[167], W. H. Hopkins[6], M. C. Hoppesch[167], Y. Horii[112], M. E. Horstmann[111], S. Hou[153], M. R. Housenga[167], J. Howarth[59], J. Hoya[6], M. Hrabovsky[124], T. Hryn'ova[4], P. J. Hsu[65], S.-C. Hsu[141], T. Hsu[66], M. Hu[18a], Q. Hu[62], S. Huang[33], X. Huang[14,113c], Y. Huang[135], Y. Huang[113b], Y. Huang[14], Z. Huang[66], Z. Hubacek[134], F. Huegging[25], T. B. Huffman[128], M. Hufnagel Maranha De Faria[82a], C. A. Hugli[48], M. Huhtinen[37], S. K. Huiberts[127], R. Hulsken[105], C. E. Hultquist[18a], D. L. Humphreys[104], N. Huseynov[12], J. Huston[108], B. Huth[37], J. Huth[61], L. Huth[48], R. Hyneman[7], G. Iacobucci[56], G. Iakovidis[30], L. Iconomidou-Fayard[66], J. P. Iddon[37], P. Iengo[72a,72b], Y. Iiyama[158], T. Iizawa[158], Y. Ikegami[83], D. Iliadis[157], N. Ilic[160], H. Imam[36a], G. Inacio Goncalves[82d], S. A. Infante Cabanas[139c], T. Ingebretsen Carlson[47a,47b], J. M. Inglis[95], G. Introzzi[73a,73b], M. Iodice[77a], V. Ippolito[75a,75b], R. K. Irwin[93], M. Ishino[158], W. Islam[175], C. Issever[19], S. Istin[22a,ao], K. Itabashi[126], H. Ito[173], R. Iuppa[78a,78b], A. Ivina[174], S. Izumiyama[112], V. Izzo[72a], P. Jacka[134], P. Jackson[1], P. Jain[48], K. Jakobs[54], T. Jakoubek[174], J. Jamieson[59], W. Jang[158], S. Jankovych[135], M. Javurkova[104], P. Jawahar[102], L. Jeanty[125], J. Jejelava[154a,ae], P. Jenni[54,f], C. E. Jessiman[35], C. Jia[142a], H. Jia[169], J. Jia[150], X. Jia[111,113c], Z. Jia[113a], C. Jiang[52], Q. Jiang[64b], S. Jiggins[48], M. Jimenez Ortega[168], J. Jimenez Pena[13], S. Jin[113a], A. Jinaru[28b], O. Jinnouchi[140], P. Johansson[144], K. A. Johns[7], J. W. Johnson[138], F. A. Jolly[48], D. M. Jones[151], E. Jones[48], K. S. Jones[8], P. Jones[33], R. W. L. Jones[92], T. J. Jones[93], H. L. Joos[55], R. Joshi[121], J. Jovicevic[16], X. Ju[18a], J. J. Junggeburth[37], T. Junkermann[63a], A. Juste Rozas[13,x], M. K. Juzek[87], S. Kabana[139f], A. Kaczmarska[87], S. A. Kadir[148], M. Kado[111], H. Kagan[121], M. Kagan[148], A. Kahn[130], C. Kahra[101], T. Kaji[158], E. Kajomovitz[155], N. Kakati[174], N. Kakoty[13], I. Kalaitzidou[54], S. Kandel[8], N. Kanellos[10], N. J. Kang[138], D. Kar[34j], E. Karentzos[25], K. Karki[8], O. Karkout[116], S. N. Karpov[39], Z. M. Karpova[39], V. Kartvelishvili[92,154b], A. N. Karyukhin[38], E. Kasimi[157], J. Katzy[48], S. Kaur[35], K. Kawade[145], M. P. Kawale[122], C. Kawamoto[88], T. Kawamoto[62], E. F. Kay[37], S. Kazakos[108], V. F. Kazanin[38], J. M. Keaveney[34a], R. Keeler[170], G. V. Kehris[61], J. S. Keller[35], J. M. Kelly[170], J. J. Kempster[151], O. Kepka[133], J. Kerr[161b], B. P. Kerridge[136], B. P. Kerševan[94], L. Keszeghova[29a], R. A. Khan[131], A. Khanov[123], A. G. Kharlamov[38], T. Kharlamova[38], E. E. Khoda[141], M. Kholodenko[132a], T. J. Khoo[19], G. Khoriauli[171], Y. Khoulaki[36a], Y. A. R. Khwaira[129], B. Kibirige[34j], D. Kim[6], D. W. Kim[18b], Y. K. Kim[40], N. Kimura[97], M. K. Kingston[55], A. Kirchhoff[55], C. Kirfel[25], F. Kirfel[25], J. Kirk[136], A. E. Kiryunin[111], S. Kita[162], O. Kivernyk[25], M. Klassen[163], C. Klein[35], L. Klein[171], M. H. Klein[45], S. B. Klein[56], U. Klein[93], A. Klimentov[30], T. Klioutchnikova[37], P. Kluit[116], S. Kluth[111], E. Kneringer[79], T. M. Knight[160], A. Knue[49], M. Kobel[50], D. Kobylianskii[174], S. F. Koch[128], M. Kocian[148], P. Kodyš[135], D. M. Koeck[125], T. Koffas[35], O. Kolay[50], I. Koletsou[4], T. Komarek[87], K. Köneke[55], A. X. Y. Kong[1], T. Kono[120],

N. Konstantinidis[97], P. Kontaxakis[56], B. Konya[99], R. Kopeliansky[42], S. Koperny[86a], R. Koppenhofer[54], K. Korcyl[87], K. Kordas[157,d], A. Korn[97], S. Korn[55], I. Korolkov[13], N. Korotkova[38], B. Kortman[116], O. Kortner[111], S. Kortner[111], W. H. Kostecka[117], M. Kostov[29a], V. V. Kostyukhin[146], A. Kotsokechagia[37], A. Kotwal[51], A. Koulouris[37], A. Kourkoumeli-Charalampidi[73a,73b], C. Kourkoumelis[9], E. Kourlitis[111], O. Kovanda[125], R. Kowalewski[170], W. Kozanecki[125], A. S. Kozhin[38], V. A. Kramarenko[38], G. Kramberger[94], P. Kramer[25], M. W. Krasny[129], A. Krasznahorkay[104], A. C. Kraus[117], J. W. Kraus[176], J. A. Kremer[48], N. B. Krengel[146], T. Kresse[50], L. Kretschmann[176], J. Kretzschmar[93], P. Krieger[160], K. Krizka[21], K. Kroeninger[49], H. Kroha[111], J. Kroll[133], J. Kroll[130], K. S. Krowpman[108], U. Kruchonak[39], H. Krüger[25], N. Krumnack[80], M. C. Kruse[51], O. Kuchinskaia[39], S. Kuday[3a], S. Kuehn[37], R. Kuesters[54], T. Kuhl[48], V. Kukhtin[39], Y. Kulchitsky[39], S. Kuleshov[139b,139d], J. Kull[1], E. V. Kumar[110], M. Kumar[34j], N. Kumari[48], P. Kumari[161b], A. Kupco[133], A. Kupich[38], O. Kuprash[54], H. Kurashige[85], L. L. Kurchaninov[161a], O. Kurdysh[4], A. Kurova[38], M. Kuze[140], A. K. Kvam[104], J. Kvita[124], N. G. Kyriacou[141], M. Laassiri[30], C. Lacasta[168], F. Lacava[75a,75b], H. Lacker[19], D. Lacour[129], N. N. Lad[97], E. Ladygin[39], A. Lafarge[41], B. Laforge[129], T. Lagouri[177], F. Z. Lahbabi[36a], S. Lai[37,55], W. S. Lai[97], I. K. Lakomiec[55], J. E. Lambert[170], S. Lammers[68], W. Lampl[7], C. Lampoudis[157,d], G. Lamprinoudis[171], A. N. Lancaster[117], E. Lançon[30], U. Landgraf[54], M. P. J. Landon[95], V. S. Lang[54], A. J. Lankford[164], F. Lanni[37], C. S. Lantz[167], K. Lantzsch[25], A. Lanza[73a], M. Lanzac Berrocal[168], J. F. Laporte[137], T. Lari[71a], D. Larsen[17], L. Larson[11], F. Lasagni Manghi[24b], M. Lassnig[37], S. D. Lawlor[144], R. Lazaridou[164], M. Lazzaroni[71a,71b], E. T. T. Le[164], H. D. M. Le[108], E. M. Le Boulicaut[177], L. T. Le Pottier[18a], B. Leban[24a,24b], F. Ledroit-Guillon[60], T. F. Lee[161b], L. L. Leeuw[34c], M. Lefebvre[170], C. Leggett[18a], G. Lehmann Miotto[37], M. Leigh[56], W. A. Leight[104], W. Leinonen[115], A. Leisos[157,u], M. A. L. Leite[82c], C. E. Leitgeb[19], R. Leitner[135], K. J. C. Leney[45], T. Lenz[25], S. Leone[74a], C. Leonidopoulos[52], A. Leopold[149], J. LePage Bourbonnais[35], R. Les[108], C. G. Lester[33], M. Levchenko[38], J. Levêque[4], L. J. Levinson[174], G. Levrini[24a,24b], M. P. Lewicki[87], C. Lewis[141], D. J. Lewis[4], L. Lewitt[144], A. Li[30], B. Li[142a], C. Li[107], C.-Q. Li[111], H. Li[142a], H. Li[102], H. Li[15], H. Li[62], H. Li[142a], J. Li[143a], K. Li[14], L. Li[143a], R. Li[177], S. Li[14,113c], S. Li[143a,143b], T. Li[5], X. Li[105], Y. Li[14], Z. Li[158], Z. Li[14,113c], Z. Li[62], S. Liang[14,113c], Z. Liang[14], M. Liberatore[137], B. Liberti[76a], G. B. Libotte[82d], K. Lie[64c], J. Lieber Marin[82e], H. Lien[68], H. Lin[107], S. F. Lin[150], L. Linden[110], R. E. Lindley[7], J. H. Lindon[37], J. Ling[61], E. Lipeles[130], A. Lipniacka[17], A. Lister[169], J. D. Little[68], B. Liu[14], B. X. Liu[113b], D. Liu[155], D. Liu[138], E. H. L. Liu[21], J. K. K. Liu[119], K. Liu[143b], K. Liu[143a,143b], M. Liu[62], M. Y. Liu[62], P. Liu[14], Q. Liu[148], S. Liu[150], X. Liu[142a], Y. Liu[113b,113c], Y. Liu[167], Y. L. Liu[142a], Y. W. Liu[62], Z. Liu[66,k], S. L. Lloyd[95], E. M. Lobodzinska[48], P. Loch[7], E. Lodhi[160], K. Lohwasser[144], E. Loiacono[48], J. D. Lomas[21], J. D. Long[42], I. Longarini[164], R. Longo[167], A. Lopez Solis[13], N. A. Lopez-canelas[7], N. Lorenzo Martinez[4], A. M. Lory[110], M. Losada[118a], G. Löschcke Centeno[4], X. Lou[47a,47b], X. Lou[14,113c], A. Lounis[66], P. A. Love[92], M. Lu[66], S. Lu[130], Y. J. Lu[153], H. J. Lubatti[141], C. Luci[75a,75b], F. L. Lucio Alves[113a], F. Luehring[68], B. S. Lunday[130], O. Lundberg[149], J. Lunde[37], N. A. Luongo[6], M. S. Lutz[37], A. B. Lux[26], D. Lynn[30], R. Lysak[133], V. Lysenko[134], E. Lytken[99], V. Lyubushkin[39], T. Lyubushkina[39], M. M. Lyukova[150], H. Ma[30], K. Ma[62], L. L. Ma[142a], W. Ma[62], Y. Ma[123], J. C. MacDonald[101], P. C. Machado De Abreu Farias[82e], D. Macina[37], R. Madar[41], T. Madula[97], J. Maeda[85], T. Maeno[30], P. T. Mafa[34c,j], H. Maguire[144], M. Maheshwari[33], V. Maiboroda[66], A. Maio[132a,132b,132d], K. Maj[86a], O. Majersky[48], S. Majewski[125], R. Makhmanazarov[38], N. Makovec[66], V. Maksimovic[16], B. Malaescu[129], J. Malamant[127], Pa. Malecki[87], V. P. Maleev[38], F. Malek[60,o], M. Mali[94], D. Malito[96], A. Maloizel[5], S. Maltezos[10], A. Malvezzi Lopes[82d], S. Malyukov[39], J. Mamuzic[94], G. Mancini[53], M. N. Mancini[27], G. Manco[73a,73b], J. P. Mandalia[95], S. S. Mandarry[151], I. Mandić[94], L. Manhaes de Andrade Filho[82a], I. M. Maniatis[174], J. Manjarres Ramos[90], D. C. Mankad[174], A. Mann[110], T. Manoussos[37], M. N. Mantinan[40], S. Manzoni[37], L. Mao[143a], X. Mapekula[34c], A. Marantis[157], R. R. Marcelo Gregorio[95], G. Marchiori[5], C. Marcon[71a], E. Maricic[16], M. Marinescu[48], S. Marium[48], M. Marjanovic[122], A. Markhoos[54], M. Markovitch[66], M. K. Maroun[104], M. C. Marr[147], G. T. Marsden[102], E. J. Marshall[92], Z. Marshall[18a], S. Marti-Garcia[168], J. Martin[97], T. A. Martin[136], V. J. Martin[52], B. Martin dit Latour[17], L. Martinelli[75a,75b], M. Martinez[13,x], P. Martinez Agullo[168], V. I. Martinez Outschoorn[104], P. Martinez Suarez[37], S. Martin-Haugh[136], G. Martinovicova[135], V. S. Martoiu[28b], A. C. Martyniuk[97], A. Marzin[37], D. Mascione[78a,78b], L. Masetti[101], J. Masik[102], A. L. Maslennikov[39], S. L. Mason[42], P. Massarotti[72a,72b], P. Mastrandrea[74a,74b], A. Mastroberardino[44a,44b], T. Masubuchi[126], T. T. Mathew[125], J. Matousek[135], D. M. Mattern[49], K. Mauer[48], J. Maurer[28b], T. Maurin[59],

A. J. Maury[66], B. Maček[94], C. Mavungu Tsava[103], D. A. Maximov[38], A. E. May[102], E. Mayer[41], R. Mazini[34j], I. Maznas[117], S. M. Mazza[138], E. Mazzeo[37], J. P. Mc Gowan[170], S. P. Mc Kee[107], C. A. Mc Lean[6], C. C. McCracken[169], E. F. McDonald[106], A. E. McDougall[116], L. F. Mcelhinney[92], J. A. Mcfayden[151], R. P. McGovern[130], R. P. Mckenzie[34j], T. C. Mclachlan[48], D. J. Mclaughlin[97], S. J. McMahon[136], C. M. Mcpartland[93], R. A. McPherson[170,ab], S. Mehlhase[110], A. Mehta[93], D. Melini[168], B. R. Mellado Garcia[34j], A. H. Melo[55], F. Meloni[48], A. M. Mendes Jacques Da Costa[102], L. Meng[92], S. Menke[111], M. Mentink[37], E. Meoni[44a,44b], G. Mercado[117], S. Merianos[157], C. Merlassino[69a,69c], C. Meroni[71a,71b], J. Metcalfe[6], A. S. Mete[6], E. Meuser[101], C. Meyer[68], J-P. Meyer[137], Y. Miao[113a], R. P. Middleton[136], M. Mihovilovic[66], L. Mijović[52], G. Mikenberg[174], M. Mikestikova[133], M. Mikuž[94], H. Mildner[101], A. Milic[37], D. W. Miller[40], E. H. Miller[148], A. Milov[174], D. A. Milstead[47a,47b], T. Min[113a], A. A. Minaenko[38], I. A. Minashvili[154b], A. I. Mincer[119], B. Mindur[86a], M. Mineev[39], Y. Mino[88], L. M. Mir[13], M. Miralles Lopez[59], M. Mironova[18a], M. Missio[41], A. Mitra[172], V. A. Mitsou[168], Y. Mitsumori[112], O. Miu[160], P. S. Miyagawa[95], T. Mkrtchyan[37], M. Mlinarevic[97], T. Mlinarevic[97], M. Mlynarikova[135], L. Mlynarska[86a], C. Mo[143a], S. Mobius[20], M. H. Mohamed Farook[114], S. Mohapatra[42], M. F. Mohd Soberi[52], S. Mohiuddin[123], G. Mokgatitswane[34j], L. Moleri[174], U. Molinatti[128], L. G. Mollier[20], B. Mondal[133], S. Mondal[134], K. Mönig[48], E. Monnier[103], L. Monsonis Romero[168], J. Montejo Berlingen[13], A. Montella[47a,47b], M. Montella[121], F. Montereali[77a,77b], F. Monticelli[91], S. Monzani[69a,69c], A. Morancho Tarda[43], N. Morange[66], A. L. Moreira De Carvalho[48], M. Moreno Llácer[168], C. Moreno Martinez[56], J. M. Moreno Perez[23b], P. Morettini[57b], S. Morgenstern[37], M. Morii[61], M. Morinaga[158], M. Moritsu[89], F. Morodei[75a,75b], P. Moschovakos[37], B. Moser[54], M. Mosidze[154b], T. Moskalets[45], P. Moskvitina[115], J. Moss[32], P. Moszkowicz[86a], T. Motta Quirino[82d], A. Moussa[36d], Y. Moyal[174], H. Moyano Gomez[13], E. J. W. Moyse[104], T. G. Mroz[87], S. Muanza[103], M. Mucha[25], J. Mueller[131], G. A. Mullier[166], A. J. Mullin[33], J. J. Mullin[51], A. C. Mullins[45], A. E. Mulski[61], D. P. Mungo[160], D. Munoz Perez[168], F. J. Munoz Sanchez[102], W. J. Murray[136,172], M. Muškinja[94], C. Mwewa[48], A. G. Myagkov[38,a], A. J. Myers[8], G. Myers[107], M. Myska[134], B. P. Nachman[148], K. Nagai[128], K. Nagano[83], R. Nagasaka[158], J. L. Nagle[30,al], E. Nagy[103], A. M. Nairz[37], Y. Nakahama[83], K. Nakamura[83], K. Nakkalil[5], A. Nandi[63b], H. Nanjo[126], E. A. Narayanan[45], Y. Narukawa[158], I. Naryshkin[38], L. Nasella[71a,71b], S. Nasri[118b], C. Nass[25], G. Navarro[23a], A. Nayaz[19], P. Y. Nechaeva[38], S. Nechaeva[24a,24b], F. Nechansky[133], L. Nedic[128], T. J. Neep[21], A. Negri[73a,73b], M. Negrini[24b], C. Nellist[116], C. Nelson[105], K. Nelson[107], S. Nemecek[133], M. Nessi[37,g], M. S. Neubauer[167], J. Newell[93], P. R. Newman[21], Y. W. Y. Ng[167], B. Ngair[118a], H. D. N. Nguyen[109], J. D. Nichols[122], R. B. Nickerson[128], R. Nicolaidou[137], J. Nielsen[138], M. Niemeyer[55], J. Niermann[37], N. Nikiforou[37], V. Nikolaenko[38,a], I. Nikolic-Audit[129], P. Nilsson[30], I. Ninca[48], G. Ninio[156], A. Nisati[75a], R. Nisius[111], N. Nitika[174], E. K. Nkadimeng[34b], T. Nobe[158], D. Noll[148], T. Nommensen[152], M. B. Norfolk[144], B. J. Norman[35], L. C. Nosler[18a], M. Noury[36a], J. Novak[94], T. Novak[94], P. Novotny[174], R. Novotny[134], L. Nozka[124], K. Ntekas[164], D. Ntounis[148], N. M. J. Nunes De Moura Junior[82b], J. Ocariz[129], I. Ochoa[132a], A. Odella Rodriguez[13], S. Oerdek[48], J. T. Offermann[40], A. Ogrodnik[87], A. Oh[102], C. C. Ohm[149], H. Oide[83], M. L. Ojeda[37], Y. Okumura[158], L. F. Oleiro Seabra[132a], I. Oleksiyuk[56], G. Oliveira Correa[13], D. Oliveira Damazio[30], J. L. Oliver[1], R. Omar[68], Ö. O. Öncel[54], A. P. O'Neill[20], Y. Onoda[140], A. Onofre[132a,132e,e], P. U. E. Onyisi[11], M. J. Oreglia[40], D. Orestano[77a,77b], R. Orlandini[77a,77b], R. S. Orr[160], L. M. Osojnak[42], Y. Osumi[112], G. Otero y Garzón[31], H. Otono[89], M. Ouchrif[36d], F. Ould-Saada[127], T. Ovsiannikova[141], M. Owen[59], R. E. Owen[136], V. E. Ozcan[22a], F. Ozturk[87], N. Ozturk[8], S. Ozturk[81], H. A. Pacey[128], K. Pachal[161a], A. Pacheco Pages[13], C. Padilla Aranda[13], G. Padovano[75a,75b], S. Pagan Griso[18a], J. Pampel[25], J. Pan[177], D. K. Panchal[11], C. E. Pandini[60], J. G. Panduro Vazquez[136], H. D. Pandya[1], H. Pang[137], P. Pani[48], G. Panizzo[69a,69c], L. Panwar[129], L. Paolozzi[56], S. Parajuli[167], A. Paramonov[6], C. Paraskevopoulos[53], D. Paredes Hernandez[64b], S. R. Paredes Saenz[52], A. Pareti[73a,73b], K. R. Park[42], T. H. Park[111], F. Parodi[57b], J. A. Parsons[42], U. Parzefall[54], B. Pascual Dias[41], L. Pascual Dominguez[100], E. Pasqualucci[75a], S. Passaggio[57b], F. Pastore[96], P. Patel[87], U. M. Patel[51], J. R. Pater[102], T. Pauly[37], F. Pauwels[135], C. I. Pazos[163], M. Pedersen[127], R. Pedro[132a], S. V. Peleganchuk[38], O. Penc[133], S. Peng[15], G. D. Penn[177], K. E. Penski[110], M. Penzin[38], B. S. Peralva[82d], A. P. Pereira Peixoto[141], L. Pereira Sanchez[148], D. V. Perepelitsa[30,al], G. Perera[104], E. Perez Codina[37], M. Perganti[10], H. Pernegger[37], S. Perrella[75a,75b], K. Peters[48], R. F. Y. Peters[102], B. A. Petersen[37], T. C. Petersen[43], E. Petit[103], V. Petousis[134], A. R. Petri[71a,71b], C. Petridou[157,d], T. Petru[135], M. Pettee[18a], A. Petukhov[81], K. Petukhova[37], R. Pezoa[139g], L. Pezzotti[24a,24b], G. Pezzullo[177],

L. Pfaffenbichler[37], A. J. Pfleger[79], T. M. Pham[175], T. Pham[106], P. W. Phillips[136], G. Piacquadio[150], E. Pianori[18a], F. Piazza[125], R. Piegaia[31], D. Pietreanu[28b], A. D. Pilkington[102], M. Pinamonti[69a,69c], J. L. Pinfold[2], G. Pinheiro Matos[42], B. C. Pinheiro Pereira[132a], J. Pinol Bel[13], A. E. Pinto Pinoargote[129], L. Pintucci[69a,69c], K. M. Piper[151], A. Pirttikoski[56], D. A. Pizzi[35], L. Pizzimento[64b], A. Plebani[33], M.-A. Pleier[30], V. Pleskot[135], E. Plotnikova[39], G. Poddar[95], R. Poettgen[99], L. Poggioli[129], S. Polacek[135], G. Polesello[73a], A. Poley[147], A. Polini[24b], C. S. Pollard[172], Z. B. Pollock[121], E. Pompa Pacchi[122], N. I. Pond[97], D. Ponomarenko[68], L. Pontecorvo[37], S. Popa[28a], G. A. Popeneciu[28d], A. Poreba[37], D. M. Portillo Quintero[161a], S. Pospisil[134], M. A. Postill[144], P. Postolache[28c], K. Potamianos[172], P. A. Potepa[86a], I. N. Potrap[39], C. J. Potter[33], H. Potti[152], J. Poveda[168], M. E. Pozo Astigarraga[37], R. Pozzi[37], A. Prades Ibanez[76a,76b], S. R. Pradhan[144], J. Pretel[170], D. Price[102], M. Primavera[70a], L. Primomo[69a,69c], M. A. Principe Martin[100], R. Privara[124], T. Procter[86b], M. L. Proffitt[141], N. Proklova[130], K. Prokofiev[64c], G. Proto[111], J. Proudfoot[6], M. Przybycien[86a], W. W. Przygoda[86b], A. Psallidas[46], J. E. Puddefoot[144], D. Pudzha[53], H. I. Purnell[1], D. Pyatiizbyantseva[115], J. Qian[107], R. Qian[108], D. Qichen[128], Y. Qin[13], T. Qiu[52], A. Quadt[55], M. Queitsch-Maitland[102], G. Quetant[56], R. P. Quinn[169], G. Rabanal Bolanos[61], D. Rafanoharana[111], F. Raffaeli[76a,76b], F. Ragusa[71a,71b], J. L. Rainbolt[40], S. Rajagopalan[30], E. Ramakoti[39], L. Rambelli[57a,57b], I. A. Ramirez-Berend[35], K. Ran[107,113c], D. S. Rankin[130], N. P. Rapheeha[34j], H. Rasheed[28b], A. Rastogi[18a], S. Rave[101], S. Ravera[57a,57b], B. Ravina[37], I. Ravinovich[174], M. Raymond[37], A. L. Read[127], N. P. Readioff[144], D. M. Rebuzzi[73a,73b], A. S. Reed[59], K. Reeves[27], D. Reikher[37], A. Rej[49], C. Rembser[37], H. Ren[62], M. Renda[28b], F. Renner[48], A. G. Rennie[59], M. Repik[56], A. L. Rescia[57a,57b], S. Resconi[71a], M. Ressegotti[57b], S. Rettie[116], W. F. Rettie[35], M. M. Revering[33], E. Reynolds[18a], O. L. Rezanova[39], P. Reznicek[135], H. Riani[36d], N. Ribaric[51], B. Ricci[69a,69c], E. Ricci[78a,78b], R. Richter[111], S. Richter[47a,47b], E. Richter-Was[86b], M. Ridel[129], S. Ridouani[36d], P. Rieck[119], P. Riedler[37], E. M. Riefel[47a,47b], J. O. Rieger[116], M. Rijssenbeek[150], M. Rimoldi[34c], L. Rinaldi[24a,24b], P. Rincke[55,166], G. Ripellino[166], I. Riu[13], J. C. Rivera Vergara[170], F. Rizatdinova[123], E. Rizvi[95], B. R. Roberts[40], S. S. Roberts[138], D. Robinson[33], A. Robson[59], A. Rocchi[76a,76b], C. Roda[74a,74b], F. A. Rodriguez[117], S. Rodriguez Bosca[37], Y. Rodriguez Garcia[23a], A. M. Rodríguez Vera[117], S. Roe[37], J. T. Roemer[37], O. Røhne[127], R. A. Rojas[37], C. P. A. Roland[129], A. Romaniouk[79], E. Romano[73a,73b], M. Romano[24b], A. C. Romero Hernandez[167], N. Rompotis[93], L. Roos[129], S. Rosati[75a], B. J. Rosser[40], E. Rossi[128], E. Rossi[72a,72b], L. P. Rossi[61], L. Rossini[54], R. Rosten[121], M. Rotaru[28b], R. Roth[37], D. Rousseau[66], D. Rousso[48], S. Roy-Garand[160], A. Rozanov[103], Z. M. A. Rozario[59], Y. Rozen[155], A. Rubio Jimenez[168], V. H. Ruelas Rivera[19], T. A. Ruggeri[1], A. Ruggiero[128], A. Ruiz-Martinez[168], A. Rummler[37], G. B. Rupnik Boero[37], Z. Rurikova[54], N. A. Rusakovich[39], S. Ruscelli[49], H. L. Russell[170], G. Russo[75a,75b], J. P. Rutherfoord[7], S. Rutherford Colmenares[33], M. Rybar[135], P. Rybczynski[86a], A. Ryzhov[45], H. F.-W. Sadrozinski[138], F. Safai Tehrani[75a], S. Saha[1], M. Sahinsoy[81], B. Sahoo[174], A. Saibel[168], B. T. Saifuddin[122], M. Saimpert[137], G. T. Saito[82c], M. Saito[158], T. Saito[158], A. Sala[71a,71b], A. Salnikov[148], J. Salt[168], A. Salvador Salas[156], F. Salvatore[151], A. Salzburger[37], D. Sammel[54], E. Sampson[92], D. Sampsonidis[157,d], D. Sampsonidou[125], M. A. A. Samy[59], J. Sánchez[168], V. Sanchez Sebastian[168], H. Sandaker[127], C. O. Sander[48], J. A. Sandesara[175], M. Sandhoff[176], C. Sandoval[23b], L. Sanfilippo[63a], D. P. C. Sankey[136], T. Sano[88], A. Sansoni[53], M. Santana Queiroz[18b], L. Santi[37], C. Santoni[41], H. Santos[132a,132b], A. Santra[174], E. Sanzani[24a,24b], K. A. Saoucha[84b], J. G. Saraiva[132a,132d], J. Sardain[7], O. Sasaki[83], K. Sato[162], C. Sauer[37], E. Sauvan[4], P. Savard[160,ai], R. Sawada[158], C. Sawyer[136], L. Sawyer[98], A. M. Sayed[27], C. Sbarra[24b], A. Sbrizzi[24a,24b], T. Scanlon[97], J. Schaarschmidt[141], U. Schäfer[101], A. C. Schaffer[45,66], D. Schaile[110], R. D. Schamberger[150], C. Scharf[19], M. M. Schefer[20], V. A. Schegelsky[38], D. Scheirich[135], M. Schernau[139f], C. Scheulen[56], C. Schiavi[57a,57b], M. Schioppa[44a,44b], B. Schlag[148], S. Schlenker[37], J. Schmeing[176], E. Schmidt[111], M. A. Schmidt[176], K. Schmieden[25], C. Schmitt[101], N. Schmitt[101], S. Schmitt[48], N. A. Schneider[110], L. Schoeffel[137], A. Schoening[63b], P. G. Scholer[35], E. Schopf[146], M. Schott[25], S. Schramm[56], T. Schroer[56], H.-C. Schultz-Coulon[63a], M. Schumacher[54], B. A. Schumm[138], Ph. Schune[137], H. R. Schwartz[7], A. Schwartzman[148], T. A. Schwarz[107], Ph. Schwemling[137], R. Schwienhorst[108], F. G. Sciacca[20], A. Sciandra[30], G. Sciolla[27], F. Scuri[74a], C. D. Sebastiani[37], K. Sedlaczek[117], S. C. Seidel[114], A. Seiden[138], B. D. Seidlitz[42], C. Seitz[48], J. M. Seixas[82b], G. Sekhniaidze[72a], L. Selem[60], N. Semprini-Cesari[24a,24b], A. Semushin[178], D. Sengupta[56], V. Senthilkumar[168], L. Serin[66], M. Sessa[72a,72b], H. Severini[122], F. Sforza[57a,57b], A. Sfyrla[56], Q. Sha[14], H. Shaddix[117], A. H. Shah[33], R. Shaheen[149], J. D. Shahinian[130], M. Shamim[37], L. Y. Shan[14],

M. Shapiro[18a], A. Sharma[37], A. S. Sharma[169], P. Sharma[30], P. B. Shatalov[38], K. Shaw[151], S. M. Shaw[102], Q. Shen[14], D. J. Sheppard[147], P. Sherwood[97], L. Shi[97], X. Shi[14], S. Shimizu[83], I. P. J. Shipsey[128,*], S. Shirabe[89], M. Shiyakova[39,z], M. J. Shochet[40], D. R. Shope[127], B. Shrestha[122], S. Shrestha[121,an], I. Shreyber[39], M. J. Shroff[170], P. Sicho[133], A. M. Sickles[167], E. Sideras Haddad[34j,165], A. C. Sidley[116], A. Sidoti[24b], F. Siegert[50], Dj. Sijacki[16], F. Sili[62], J. M. Silva[52], I. Silva Ferreira[82b], M. V. Silva Oliveira[30], S. B. Silverstein[47a], S. Simion[66], R. Simoniello[37], E. L. Simpson[102], H. Simpson[151], L. R. Simpson[6], S. Simsek[81], S. Sindhu[55], P. Sinervo[160], S. N. Singh[27], S. Singh[30], S. Sinha[48], S. Sinha[102], M. Sioli[24a,24b], K. Sioulas[9], I. Siral[37], E. Sitnikova[48], J. Sjölin[47a,47b], A. Skaf[55], E. Skorda[21], P. Skubic[122], M. Slawinska[87], I. Slazyk[17], I. Sliusar[127], V. Smakhtin[174], B. H. Smart[136], S. Yu. Smirnov[139b], Y. Smirnov[34c], L. N. Smirnova[38,a], O. Smirnova[99], A. C. Smith[42], D. R. Smith[164], J. L. Smith[102], M. B. Smith[35], R. Smith[148], H. Smitmanns[101], M. Smizanska[92], K. Smolek[134], P. Smolyanskiy[134], A. A. Snesarev[39], H. L. Snoek[116], R. M. Snyder[51], S. Snyder[30], R. Sobie[170,ab], A. Soffer[156], C. A. Solans Sanchez[37], E. Yu. Soldatov[39], U. Soldevila[168], A. A. Solodkov[34j], S. Solomon[27], A. Soloshenko[39], K. Solovieva[54], O. V. Solovyanov[41], P. Sommer[50], A. Sonay[13], A. Sopczak[134], A. L. Sopio[52], F. Sopkova[29b], J. D. Sorenson[114], I. R. Sotarriva Alvarez[140], V. Sothilingam[63a], O. J. Soto Sandoval[139b,139c], S. Sottocornola[68], R. Soualah[84a], Z. Soumaimi[36e], D. South[48], N. Soybelman[174], S. Spagnolo[70a,70b], D. Sperlich[54], B. Spisso[72a,72b], D. P. Spiteri[59], L. Splendori[103], M. Spousta[135], E. J. Staats[35], R. Stamen[63a], E. Stanecka[87], W. Stanek-Maslouska[48], M. V. Stange[50], B. Stanislaus[18a], M. M. Stanitzki[48], E. A. Starchenko[38], G. H. Stark[138], J. Stark[90], P. Staroba[133], P. Starovoitov[84b], R. Staszewski[87], C. Stauch[110], G. Stavropoulos[46], A. Stefl[37], A. Stein[101], P. Steinberg[30], B. Stelzer[147,161a], H. J. Stelzer[131], O. Stelzer[161a], H. Stenzel[58], T. J. Stevenson[151], G. A. Stewart[37], J. R. Stewart[123], G. Stoicea[28b], M. Stolarski[132a], S. Stonjek[111], A. Straessner[50], J. Strandberg[149], S. Strandberg[47a,47b], M. Stratmann[176], M. Strauss[122], T. Strebler[103], P. Strizenec[29b], R. Ströhmer[171], D. M. Strom[125], R. Stroynowski[45], A. Strubig[47a,47b], S. A. Stucci[30], B. Stugu[17], J. Stupak[122], N. A. Styles[48], D. Su[148], S. Su[62], X. Su[62], D. Suchy[29a], A. D. Sudhakar Ponnu[55], L. Sudit[174], K. Sugizaki[130], V. V. Sulin[38], D. M. S. Sultan[128], L. Sultanaliyeva[25], S. Sultansoy[3b], S. Sun[175], W. Sun[14], N. Sur[99], N. Suri Jr[177], M. R. Sutton[151], M. Svatos[133], P. N. Swallow[33], M. Swiatlowski[161a], A. Swoboda[37], I. Sykora[29a], M. Sykora[135], T. Sykora[135], D. Ta[101], K. Tackmann[48,y], A. Taffard[164], R. Tafirout[161a], Y. Takubo[83], M. Talby[103], A. A. Talyshev[38], K. C. Tam[64b], N. M. Tamir[156], A. Tanaka[158], J. Tanaka[158], R. Tanaka[66], M. Tanasini[150], Z. Tao[169], S. Tapia Araya[139g], S. Tapprogge[101], A. Tarek Abouelfadl Mohamed[37], S. Tarem[155], K. Tariq[14], G. Tarna[37], G. F. Tartarelli[71a], M. J. Tartarin[90], P. Tas[135], M. Tasevsky[133], E. Tassi[44a,44b], A. C. Tate[167], Y. Tayalati[36e,aa], G. N. Taylor[106], W. Taylor[161b], R. J. Taylor Vara[168], A. S. Tegetmeier[90], P. Teixeira-Dias[96], J. J. Teoh[160], K. Terashi[158], J. Terron[100], S. Terzo[13], M. Testa[53], R. J. Teuscher[160,ab], A. Thaler[79], O. Theiner[56], T. Theveneaux-Pelzer[103], D. W. Thomas[96], J. P. Thomas[21], E. A. Thompson[18a], P. D. Thompson[21], E. Thomson[130], R. E. Thornberry[45], C. Tian[62], Y. Tian[56], V. Tikhomirov[81], Yu. A. Tikhonov[39], S. Timoshenko[38], D. Timoshyn[135], E. X. L. Ting[1], P. Tipton[177], A. Tishelman-Charny[30], K. Todome[140], S. Todorova-Nova[135], L. Toffolin[69a,69c], M. Togawa[83], J. Tojo[89], S. Tokár[29a], O. Toldaiev[68], G. Tolkachev[103], M. Tomoto[83], L. Tompkins[148,n], E. Torrence[125], H. Torres[90], D. I. Torres Arza[139g], E. Torró Pastor[168], M. Toscani[31], C. Tosciri[40], M. Tost[11], D. R. Tovey[144], T. Trefzger[171], P. M. Tricarico[13], A. Tricoli[30], I. M. Trigger[161a], S. Trincaz-Duvoid[129], D. A. Trischuk[170], A. Tropina[39], D. Truncali[76a,76b], L. Truong[34c], M. Trzebinski[87], A. Trzupek[87], F. Tsai[150], M. Tsai[107], A. Tsiamis[157], P. V. Tsiareshka[39], S. Tsigaridas[161a], A. Tsirigotis[157,u], V. Tsiskaridze[154a], E. G. Tskhadadze[154a], Y. Tsujikawa[88], I. I. Tsukerman[38], V. Tsulaia[18a], S. Tsuno[83], K. Tsuri[120], D. Tsybychev[150], Y. Tu[64b], A. Tudorache[28b], V. Tudorache[28b], S. B. Tuncay[128], S. Turchikhin[57a,57b], I. Turk Cakir[3a], R. Turra[71a], T. Turtuvshin[39,ac], P. M. Tuts[42], S. Tzamarias[157,d], Y. Uematsu[83], F. Ukegawa[162], P. A. Ulloa Poblete[139b,139c], E. N. Umaka[30], G. Unal[37], A. Undrus[30], G. Unel[164], J. Urban[29b], P. Urrejola[139e], G. Usai[8], R. Ushioda[159], M. Usman[109], F. Ustuner[52], Z. Uysal[81], V. Vacek[134], B. Vachon[105], T. Vafeiadis[37], A. Vaitkus[97], C. Valderanis[110], E. Valdes Santurio[47a,47b], M. Valente[37], S. Valentinetti[24a,24b], A. Valero[168], E. Valiente Moreno[168], A. Vallier[90], J. A. Valls Ferrer[168], D. R. Van Arneman[116], A. Van Der Graaf[49], H. Z. Van Der Schyf[34j], P. Van Gemmeren[6], M. Van Rijnbach[37], S. Van Stroud[97], I. Van Vulpen[116], P. Vana[135], M. Vanadia[76a,76b], U. M. Vande Voorde[149], W. Vandelli[37], E. R. Vandewall[148], D. Vannicola[156], L. Vannoli[53], R. Vari[75a], M. Varma[177], E. W. Varnes[7], C. Varni[79], D. Varouchas[66], L. Varriale[168], K. E. Varvell[152], M. E. Vasile[28b], L. Vaslin[83], M. D. Vassilev[148], A. Vasyukov[39], L. M. Vaughan[123], R. Vavricka[135], T. Vazquez Schroeder[13], J. Veatch[32], V. Vecchio[102], M. J. Veen[104], I. Veliscek[30],

I. Velkovska[94], L. M. Veloce[160], F. Veloso[132a,132c], A. G. Veltman[52], S. H. Venetianer[163], S. Veneziano[75a], A. Ventura[70a,70b], A. Verbytskyi[111], M. Verducci[74a,74b], C. Vergis[95], M. Verissimo De Araujo[82b], W. Verkerke[116], J. C. Vermeulen[116], C. Vernieri[148], M. Vessella[164], M. C. Vetterli[147,ai], A. Vgenopoulos[101], N. Viaux Maira[139g,af], T. Vickey[144], O. E. Vickey Boeriu[144], G. H. A. Viehhauser[128], L. Vigani[63b], M. Vigl[111], M. Villa[24a,24b], M. Villaplana Perez[168], E. M. Villhauer[40], E. Vilucchi[53], M. Vincent[168], M. G. Vincter[35], A. Visibile[116], A. Visive[116], C. Vittori[37], I. Vivarelli[24a,24b], M. I. Vivas Albornoz[48], E. Voevodina[111], F. Vogel[110], J. C. Voigt[50], P. Vokac[134], Yu. Volkotrub[86b], L. Vomberg[25], E. Von Toerne[25], B. Vormwald[37], K. Vorobev[51], M. Vos[168], K. Voss[146], M. Vozak[37], L. Vozdecky[122], N. Vranjes[16], M. Vranjes Milosavljevic[16], M. Vreeswijk[116], N. K. Vu[143a,143b], R. Vuillermet[37], O. Vujinovic[101], I. Vukotic[40], I. K. Vyas[35], J. F. Wack[33], S. Wada[162], C. Wagner[148], J. M. Wagner[18a], W. Wagner[176], S. Wahdan[176], H. Wahlberg[91], C. H. Waits[122], J. Walder[136], R. Walker[110], K. Walkingshaw Pass[59], W. Walkowiak[146], A. Wall[130], E. J. Wallin[99], T. Wamorkar[18a], K. Wandall-Christensen[168], A. Wang[62], A. Z. Wang[138], C. Wang[48], C. Wang[11], H. Wang[18a], J. Wang[64c], P. Wang[102], P. Wang[97], R. Wang[61], R. Wang[6], S. M. Wang[153], S. Wang[14], T. Wang[115], T. Wang[62], W. T. Wang[128], W. Wang[14], X. Wang[167], X. Wang[143a], X. Wang[48], Y. Wang[150], Y. Wang[114], Z. Wang[107], Z. Wang[143b], Z. Wang[107], C. Wanotayaroj[83], A. Warburton[105], A. L. Warnerbring[146], S. Waterhouse[96], A. T. Watson[21], H. Watson[52], M. F. Watson[21], E. Watton[37], G. Watts[141], B. M. Waugh[97], J. M. Webb[54], C. Weber[30], M. S. Weber[20], S. M. Weber[63a], C. Wei[62], Y. Wei[54], A. R. Weidberg[128], E. J. Weik[119], J. Weingarten[49], C. Weiser[54], C. J. Wells[48], T. Wenaus[30], T. Wengler[37], N. S. Wenke[111], N. Wermes[25], M. Wessels[63a], A. M. Wharton[92], A. S. White[61], A. White[8], M. J. White[1], D. Whiteson[164], L. Wickremasinghe[126], W. Wiedenmann[175], M. Wielers[136], R. Wierda[149], C. Wiglesworth[43], H. G. Wilkens[37], J. J. H. Wilkinson[33], D. M. Williams[42], H. H. Williams[130], S. Williams[33], S. Willocq[104], B. J. Wilson[102], D. J. Wilson[102], P. J. Windischhofer[40], F. I. Winkel[31], F. Winklmeier[125], B. T. Winter[54], M. Wittgen[148], M. Wobisch[98], T. Wojtkowski[60], Z. Wolffs[116], J. Wollrath[37], M. W. Wolter[87], H. Wolters[132a,132c], M. C. Wong[138], E. L. Woodward[42], S. D. Worm[48], B. K. Wosiek[87], K. W. Woźniak[87], S. Wozniewski[55], K. Wraight[59], C. Wu[160], C. Wu[21], J. Wu[158], M. Wu[113b], M. Wu[115], S. L. Wu[175], S. Wu[14,ak], X. Wu[62], Y. Q. Wu[160], Y. Wu[62], Z. Wu[4], Z. Wu[113a], J. Wuerzinger[111], T. R. Wyatt[102], B. M. Wynne[52], S. Xella[43], L. Xia[113a], M. Xie[62], A. Xiong[125], D. Xu[14], H. Xu[62], L. Xu[62], R. Xu[130], T. Xu[107], W. Xu[113a], Y. Xu[141], Z. Xu[52], R. Xue[131], B. Yabsley[152], S. Yacoob[34a], Y. Yamaguchi[83], E. Yamashita[158], H. Yamauchi[162], T. Yamazaki[18a], Y. Yamazaki[85], S. Yan[59], Z. Yan[104], H. J. Yang[143a,143b], H. T. Yang[62], S. Yang[62], T. Yang[64c], X. Yang[37], X. Yang[14], Y. Yang[158], Y. Yang[62], W.-M. Yao[18a], C. L. Yardley[151], J. Ye[14], S. Ye[30], X. Ye[62], Y. Yeh[97], I. Yeletskikh[39], B. Yeo[18b], M. R. Yexley[97], T. P. Yildirim[128], K. Yorita[173], C. J. S. Young[37], C. Young[148], I. N. L. Young[59], N. D. Young[125], Y. Yu[62], J. Yuan[14,113c,ak], M. Yuan[107], R. Yuan[143b], L. Yue[97], M. Zaazoua[62], B. Zabinski[87], I. Zahir[36a], A. Zaio[57a,57b], Z. K. Zak[87], T. Zakareishvili[168], S. Zambito[56], J. A. Zamora Saa[139d], J. Zang[158], R. Zanzottera[71a,71b], O. Zaplatilek[134], C. Zeitnitz[176], H. Zeng[14], D. T. Zenger Jr[27], O. Zenin[38], T. Ženiš[29a], S. Zenz[95], D. Zerwas[66], B. Zhang[172], D. F. Zhang[144], G. Zhang[14,ak], J. Zhang[142a], J. Zhang[6], L. Zhang[62], L. Zhang[113a], P. Zhang[14,113c], R. Zhang[113a], S. Zhang[90], T. Zhang[158], Y. Zhang[141], Y. Zhang[97], Y. Zhang[62], Y. Zhang[113a], Z. Zhang[18a], Z. Zhang[142a], Z. Zhang[66], H. Zhao[141], T. Zhao[142a], Y. Zhao[35], Z. Zhao[62], Z. Zhao[62], A. Zhemchugov[39], J. Zheng[113a], K. Zheng[167], X. Zheng[62], Z. Zheng[148], D. Zhong[167], B. Zhou[107], B. Zhou[143a,143b], H. Zhou[7], N. Zhou[143a], Y. Zhou[15], Y. Zhou[113a], Y. Zhou[7], J. Zhu[107], X. Zhu[143b], Y. Zhu[143a], Y. Zhu[62], X. Zhuang[14], K. Zhukov[68], N. I. Zimine[39], J. Zinsser[63b], M. Ziolkowski[146], L. Živković[16], A. Zoccoli[24a,24b], K. Zoch[61], A. Zografos[37], T. G. Zorbas[144], O. Zormpa[46], L. Zwalinski[37]

[1] Department of Physics, University of Adelaide, Adelaide, Australia
[2] Department of Physics, University of Alberta, Edmonton, AB, Canada
[3] [(a)]Department of Physics, Ankara University, Ankara, Türkiye; [(b)]Division of Physics, TOBB University of Economics and Technology, Ankara, Türkiye
[4] LAPP, CNRS/IN2P3, Université Savoie Mont Blanc, Annecy, France
[5] APC, CNRS/IN2P3, Université Paris Cité, Paris, France
[6] High Energy Physics Division, Argonne National Laboratory, Argonne, IL, USA
[7] Department of Physics, University of Arizona, Tucson, AZ, USA
[8] Department of Physics, University of Texas at Arlington, Arlington, TX, USA

[9] Physics Department, National and Kapodistrian University of Athens, Athens, Greece
[10] Physics Department, National Technical University of Athens, Zografou, Greece
[11] Department of Physics, University of Texas at Austin, Austin, TX, USA
[12] Institute of Physics, Azerbaijan Academy of Sciences, Baku, Azerbaijan
[13] Institut de Física d'Altes Energies (IFAE), Barcelona Institute of Science and Technology, Barcelona, Spain
[14] Institute of High Energy Physics, Chinese Academy of Sciences, Beijing, China
[15] Physics Department, Tsinghua University, Beijing, China
[16] Institute of Physics, University of Belgrade, Belgrade, Serbia
[17] Department for Physics and Technology, University of Bergen, Bergen, Norway
[18] [(a)]Physics Division, Lawrence Berkeley National Laboratory, Berkeley, CA, USA; [(b)]University of California, Berkeley, CA, USA
[19] Institut für Physik, Humboldt Universität zu Berlin, Berlin, Germany
[20] Albert Einstein Center for Fundamental Physics and Laboratory for High Energy Physics, University of Bern, Bern, Switzerland
[21] School of Physics and Astronomy, University of Birmingham, Birmingham, UK
[22] [(a)]Department of Physics, Bogazici University, Istanbul, Türkiye; [(b)]Department of Physics Engineering, Gaziantep University, Gaziantep, Türkiye; [(c)]Department of Physics, Istanbul University, Istanbul, Türkiye
[23] [(a)]Facultad de Ciencias y Centro de Investigaciónes, Universidad Antonio Nariño, Bogotá, Colombia; [(b)]Departamento de Física, Universidad Nacional de Colombia, Bogotá, Colombia
[24] [(a)]Dipartimento di Fisica e Astronomia A. Righi, Università di Bologna, Bologna, Italy; [(b)]INFN Sezione di Bologna, Bologna, Italy
[25] Physikalisches Institut, Universität Bonn, Bonn, Germany
[26] Department of Physics, Boston University, Boston, MA, USA
[27] Department of Physics, Brandeis University, Waltham, MA, USA
[28] [(a)]Transilvania University of Brasov, Brasov, Romania; [(b)]Horia Hulubei National Institute of Physics and Nuclear Engineering, Bucharest, Romania; [(c)]Department of Physics, Alexandru Ioan Cuza University of Iasi, Iasi, Romania; [(d)]National Institute for Research and Development of Isotopic and Molecular Technologies, Physics Department, Cluj-Napoca, Romania; [(e)]National University of Science and Technology Politechnica, Bucharest, Romania; [(f)]West University in Timisoara, Timisoara, Romania; [(g)]Faculty of Physics, University of Bucharest, Bucharest, Romania
[29] [(a)]Faculty of Mathematics, Physics and Informatics, Comenius University, Bratislava, Slovakia; [(b)]Department of Subnuclear Physics, Institute of Experimental Physics of the Slovak Academy of Sciences, Kosice, Slovak Republic
[30] Physics Department, Brookhaven National Laboratory, Upton, NY, USA
[31] Facultad de Ciencias Exactas y Naturales, Departamento de Física, y CONICET, Instituto de Física de Buenos Aires (IFIBA), Universidad de Buenos Aires, Buenos Aires, Argentina
[32] California State University, Long Beach, CA, USA
[33] Cavendish Laboratory, University of Cambridge, Cambridge, UK
[34] [(a)]Department of Physics, University of Cape Town, Cape Town, South Africa; [(b)]iThemba Labs, Western Cape, South Africa; [(c)]Department of Mechanical Engineering Science, University of Johannesburg, Johannesburg, South Africa; [(d)]National Institute of Physics, University of the Philippines Diliman (Philippines), Quezon City, Philippines; [(e)]Department of Physics, Stellenbosch University, Matieland, Stellenbosch, South Africa; [(f)]School of Agriculture and Science, Mathematics, University of KwaZulu-Natal, Westville, Durban, South Africa; [(g)]Department of Physics, University of South Africa, Pretoria, South Africa; [(h)]Department of Mechanical and Aeronautical Engineering, University of Pretoria, Pretoria, South Africa; [(i)]University of Zululand, KwaDlangezwa, Ongoye, South Africa; [(j)]School of Physics, University of the Witwatersrand, Johannesburg, South Africa
[35] Department of Physics, Carleton University, Ottawa, ON, Canada
[36] [(a)]Faculté des Sciences Ain Chock, Université Hassan II de Casablanca, Casablanca, Morocco; [(b)]Faculté des Sciences, Université Ibn-Tofail, Kénitra, Morocco; [(c)]Faculté des Sciences Semlalia, LPHEA-Marrakech, Université Cadi Ayyad, Marrakech, Morocco; [(d)]LPMR, Faculté des Sciences, Université Mohamed Premier, Oujda, Morocco; [(e)]Faculté des Sciences, Université Mohammed V, Rabat, Morocco; [(f)]Institute of Applied Physics, Mohammed VI Polytechnic University, Ben Guerir, Morocco
[37] CERN, Geneva, Switzerland
[38] Institute Formerly Covered by a Cooperation Agreement with CERN, Geneva, Switzerland

[39] International Laboratory Covered by a Cooperation Agreement with CERN, Geneva, Switzerland
[40] Enrico Fermi Institute, University of Chicago, Chicago, IL, USA
[41] LPC, CNRS/IN2P3, Université Clermont Auvergne, Clermont-Ferrand, France
[42] Nevis Laboratory, Columbia University, Irvington, NY, USA
[43] Niels Bohr Institute, University of Copenhagen, Copenhagen, Denmark
[44] [(a)]Dipartimento di Fisica, Università della Calabria, Rende, Italy; [(b)]Laboratori Nazionali di Frascati, INFN Gruppo Collegato di Cosenza, Cosenza, Italy
[45] Physics Department, Southern Methodist University, Dallas, TX, USA
[46] National Centre for Scientific Research Demokritos, Agia Paraskevi, Greece
[47] [(a)]Department of Physics, Stockholm University, Stockholm, Sweden; [(b)]Oskar Klein Centre, Stockholm, Sweden
[48] Deutsches Elektronen-Synchrotron DESY, Hamburg and Zeuthen, Germany
[49] Fakultät Physik, Technische Universität Dortmund, Dortmund, Germany
[50] Institut für Kern- und Teilchenphysik, Technische Universität Dresden, Dresden, Germany
[51] Department of Physics, Duke University, Durham, NC, USA
[52] SUPA-School of Physics and Astronomy, University of Edinburgh, Edinburgh, UK
[53] INFN e Laboratori Nazionali di Frascati, Frascati, Italy
[54] Physikalisches Institut, Albert-Ludwigs-Universität Freiburg, Freiburg, Germany
[55] II. Physikalisches Institut, Georg-August-Universität Göttingen, Göttingen, Germany
[56] Département de Physique Nucléaire et Corpusculaire, Université de Genève, Geneva, Switzerland
[57] [(a)]Dipartimento di Fisica, Università di Genova, Genoa, Italy; [(b)]INFN Sezione di Genova, Genoa, Italy
[58] II. Physikalisches Institut, Justus-Liebig-Universität Giessen, Giessen, Germany
[59] SUPA-School of Physics and Astronomy, University of Glasgow, Glasgow, UK
[60] LPSC, CNRS/IN2P3, Grenoble INP, Université Grenoble Alpes, Grenoble, France
[61] Laboratory for Particle Physics and Cosmology, Harvard University, Cambridge, MA, USA
[62] Department of Modern Physics and State Key Laboratory of Particle Detection and Electronics, University of Science and Technology of China, Hefei, China
[63] [(a)]Kirchhoff-Institut für Physik, Ruprecht-Karls-Universität Heidelberg, Heidelberg, Germany; [(b)]Physikalisches Institut, Ruprecht-Karls-Universität Heidelberg, Heidelberg, Germany
[64] [(a)]Department of Physics, Chinese University of Hong Kong, Shatin, N.T., Hong Kong, China; [(b)]Department of Physics, University of Hong Kong, Hong Kong, China; [(c)]Department of Physics and Institute for Advanced Study, Hong Kong University of Science and Technology, Clear Water Bay, Kowloon, Hong Kong, China
[65] Department of Physics, National Tsing Hua University, Hsinchu, Taiwan
[66] IJCLab, CNRS/IN2P3, Université Paris-Saclay, 91405 Orsay, France
[67] Centro Nacional de Microelectrónica (IMB-CNM-CSIC), Barcelona, Spain
[68] Department of Physics, Indiana University, Bloomington, IN, USA
[69] [(a)]INFN Gruppo Collegato di Udine, Sezione di Trieste, Udine, Italy; [(b)]ICTP, Trieste, Italy; [(c)]Dipartimento Politecnico di Ingegneria e Architettura, Università di Udine, Udine, Italy
[70] [(a)]INFN Sezione di Lecce, Lecce, Italy; [(b)]Dipartimento di Matematica e Fisica, Università del Salento, Lecce, Italy
[71] [(a)]INFN Sezione di Milano, Milan, Italy; [(b)]Dipartimento di Fisica, Università di Milano, Milan, Italy
[72] [(a)]INFN Sezione di Napoli, Naples, Italy; [(b)]Dipartimento di Fisica, Università di Napoli, Naples, Italy
[73] [(a)]INFN Sezione di Pavia, Pavia, Italy; [(b)]Dipartimento di Fisica, Università di Pavia, Pavia, Italy
[74] [(a)]INFN Sezione di Pisa, Pisa, Italy; [(b)]Dipartimento di Fisica E. Fermi, Università di Pisa, Pisa, Italy
[75] [(a)]INFN Sezione di Roma, Rome, Italy; [(b)]Dipartimento di Fisica, Sapienza Università di Roma, Rome, Italy
[76] [(a)]INFN Sezione di Roma Tor Vergata, Rome, Italy; [(b)]Dipartimento di Fisica, Università di Roma Tor Vergata, Rome, Italy
[77] [(a)]INFN Sezione di Roma Tre, Rome, Italy; [(b)]Dipartimento di Matematica e Fisica, Università Roma Tre, Rome, Italy
[78] [(a)]INFN-TIFPA, Povo, Italy; [(b)]Università degli Studi di Trento, Trento, Italy
[79] Department of Astro and Particle Physics, Universität Innsbruck, Innsbruck, Austria
[80] Department of Physics and Astronomy, Iowa State University, Ames, IA, USA
[81] Istinye University, Sariyer, Istanbul, Türkiye
[82] [(a)]Departamento de Engenharia Elétrica, Universidade Federal de Juiz de Fora (UFJF), Juiz de Fora,

Brazil; [b]Universidade Federal do Rio de Janeiro COPPE/EE/IF, Rio de Janeiro, Brazil; [c]Instituto de Física, Universidade de São Paulo, São Paulo, Brazil; [d]Rio de Janeiro State University, Rio de Janeiro, Brazil; [e]Federal University of Bahia, Bahia, Brazil
[83] KEK, High Energy Accelerator Research Organization, Tsukuba, Japan
[84] [a]Khalifa University of Science and Technology, Abu Dhabi, United Arab Emirates; [b]University of Sharjah, Sharjah, United Arab Emirates
[85] Graduate School of Science, Kobe University, Kobe, Japan
[86] [a]Faculty of Physics and Applied Computer Science, AGH University of Krakow, Kraków, Poland; [b]Marian Smoluchowski Institute of Physics, Jagiellonian University, Kraków, Poland
[87] Institute of Nuclear Physics Polish Academy of Sciences, Kraków, Poland
[88] Faculty of Science, Kyoto University, Kyoto, Japan
[89] Research Center for Advanced Particle Physics and Department of Physics, Kyushu University, Fukuoka , Japan
[90] L2IT, CNRS/IN2P3, UPS, Université de Toulouse, Toulouse, France
[91] Instituto de Física La Plata, Universidad Nacional de La Plata and CONICET, La Plata, Argentina
[92] Physics Department, Lancaster University, Lancaster, UK
[93] Oliver Lodge Laboratory, University of Liverpool, Liverpool, UK
[94] Department of Experimental Particle Physics, Jožef Stefan Institute and Department of Physics, University of Ljubljana, Ljubljana, Slovenia
[95] Department of Physics and Astronomy, Queen Mary University of London, London, UK
[96] Department of Physics, Royal Holloway University of London, Egham, UK
[97] Department of Physics and Astronomy, University College London, London, UK
[98] Louisiana Tech University, Ruston, LA, USA
[99] Fysiska institutionen, Lunds universitet, Lund, Sweden
[100] Departamento de Física Teorica C-15 and CIAFF, Universidad Autónoma de Madrid, Madrid, Spain
[101] Institut für Physik, Universität Mainz, Mainz, Germany
[102] School of Physics and Astronomy, University of Manchester, Manchester, UK
[103] CPPM, CNRS/IN2P3, Aix-Marseille Université, Marseille, France
[104] Department of Physics, University of Massachusetts, Amherst, MA, USA
[105] Department of Physics, McGill University, Montreal, QC, Canada
[106] School of Physics, University of Melbourne, Victoria, Australia
[107] Department of Physics, University of Michigan, Ann Arbor, MI, USA
[108] Department of Physics and Astronomy, Michigan State University, East Lansing, MI, USA
[109] Group of Particle Physics, University of Montreal, Montreal, QC, Canada
[110] Fakultät für Physik, Ludwig-Maximilians-Universität München, Munich, Germany
[111] Max-Planck-Institut für Physik (Werner-Heisenberg-Institut), Munich, Germany
[112] Graduate School of Science and Kobayashi-Maskawa Institute, Nagoya University, Nagoya, Japan
[113] [a]Department of Physics, Nanjing University, Nanjing, China; [b]School of Science, Shenzhen Campus of Sun Yat-sen University, Guangzhou, China; [c]University of Chinese Academy of Science (UCAS), Beijing, China
[114] Department of Physics and Astronomy, University of New Mexico, Albuquerque, NM, USA
[115] Institute for Mathematics, Astrophysics and Particle Physics, Radboud University/Nikhef, Nijmegen, Netherlands
[116] Nikhef National Institute for Subatomic Physics, University of Amsterdam, Amsterdam, Netherlands
[117] Department of Physics, Northern Illinois University, DeKalb, IL, USA
[118] [a]New York University Abu Dhabi, Abu Dhabi, United Arab Emirates; [b]United Arab Emirates University, Al Ain, United Arab Emirates
[119] Department of Physics, New York University, New York, NY, USA
[120] Ochanomizu University, Otsuka, Bunkyo-ku, Tokyo, Japan
[121] Ohio State University, Columbus, OH, USA
[122] Homer L. Dodge Department of Physics and Astronomy, University of Oklahoma, Norman, OK, USA
[123] Department of Physics, Oklahoma State University, Stillwater, OK, USA
[124] Palacký University, Joint Laboratory of Optics, Olomouc, Czech Republic
[125] Institute for Fundamental Science, University of Oregon, Eugene, OR, USA
[126] Graduate School of Science, University of Osaka, Osaka, Japan
[127] Department of Physics, University of Oslo, Oslo, Norway

[128] Department of Physics, Oxford University, Oxford, UK
[129] LPNHE, CNRS/IN2P3, Sorbonne Université, Université Paris Cité, Paris, France
[130] Department of Physics, University of Pennsylvania, Philadelphia, PA, USA
[131] Department of Physics and Astronomy, University of Pittsburgh, Pittsburgh, PA, USA
[132] [(a)]Laboratório de Instrumentação e Física Experimental de Partículas-LIP, Lisbon, Portugal; [(b)]Departamento de Física, Faculdade de Ciências, Universidade de Lisboa, Lisbon, Portugal; [(c)]Departamento de Física, Universidade de Coimbra, Coimbra, Portugal; [(d)]Centro de Física Nuclear da Universidade de Lisboa, Lisbon, Portugal; [(e)]Departamento de Física, Escola de Ciências, Universidade do Minho, Braga, Portugal; [(f)]Departamento de Física Teórica y del Cosmos, Universidad de Granada, Granada, Spain; [(g)]Departamento de Física, Instituto Superior Técnico, Universidade de Lisboa, Lisbon, Portugal
[133] Institute of Physics of the Czech Academy of Sciences, Prague, Czech Republic
[134] Czech Technical University in Prague, Prague, Czech Republic
[135] Faculty of Mathematics and Physics, Charles University, Prague, Czech Republic
[136] Particle Physics Department, Rutherford Appleton Laboratory, Didcot, UK
[137] IRFU, CEA, Université Paris-Saclay, Gif-sur-Yvette, France
[138] Santa Cruz Institute for Particle Physics, University of California Santa Cruz, Santa Cruz, CA, USA
[139] [(a)]Departamento de Física, Pontificia Universidad Católica de Chile, Santiago, Chile; [(b)]Millennium Institute for Subatomic physics at high energy frontier (SAPHIR), Santiago, Chile; [(c)]Instituto de Investigación Multidisciplinario en Ciencia y Tecnología, y Departamento de Física, Universidad de La Serena, La Serena, Chile; [(d)]Universidad Andres Bello, Department of Physics, Santiago, Chile; [(e)]Universidad San Sebastian, Recoleta, Chile; [(f)]Instituto de Alta Investigación, Universidad de Tarapacá, Arica, Chile; [(g)]Departamento de Física, Universidad Técnica Federico Santa María, Valparaiso, Chile
[140] Department of Physics, Institute of Science, Tokyo, Japan
[141] Department of Physics, University of Washington, Seattle, WA, USA
[142] [(a)]Institute of Frontier and Interdisciplinary Science and Key Laboratory of Particle Physics and Particle Irradiation (MOE), Shandong University, Qingdao, China; [(b)]School of Physics, Zhengzhou University, Zhengzhou, China
[143] [(a)]State Key Laboratory of Dark Matter Physics, School of Physics and Astronomy, Shanghai Jiao Tong University, Key Laboratory for Particle Astrophysics and Cosmology (MOE), SKLPPC, Shanghai, China; [(b)]State Key Laboratory of Dark Matter Physics, Tsung-Dao Lee Institute, Shanghai Jiao Tong University, Shanghai, China
[144] Department of Physics and Astronomy, University of Sheffield, Sheffield, UK
[145] Department of Physics, Shinshu University, Nagano, Japan
[146] Department Physik, Universität Siegen, Siegen, Germany
[147] Department of Physics, Simon Fraser University, Burnaby, BC, Canada
[148] SLAC National Accelerator Laboratory, Stanford, CA, USA
[149] Department of Physics, Royal Institute of Technology, Stockholm, Sweden
[150] Departments of Physics and Astronomy, Stony Brook University, Stony Brook, NY, USA
[151] Department of Physics and Astronomy, University of Sussex, Brighton, UK
[152] School of Physics, University of Sydney, Sydney, Australia
[153] Institute of Physics, Academia Sinica, Taipei, Taiwan
[154] [(a)]E. Andronikashvili Institute of Physics, Iv. Javakhishvili Tbilisi State University, Tbilisi, Georgia; [(b)]High Energy Physics Institute, Tbilisi State University, Tbilisi, Georgia; [(c)]University of Georgia, Tbilisi, Georgia
[155] Department of Physics, Technion, Israel Institute of Technology, Haifa, Israel
[156] Raymond and Beverly Sackler School of Physics and Astronomy, Tel Aviv University, Tel Aviv, Israel
[157] Department of Physics, Aristotle University of Thessaloniki, Thessaloníki, Greece
[158] Department of Physics, International Center for Elementary Particle Physics, University of Tokyo, Tokyo, Japan
[159] Graduate School of Science and Technology, Tokyo Metropolitan University, Tokyo, Japan
[160] Department of Physics, University of Toronto, Toronto, ON, Canada
[161] [(a)]TRIUMF, Vancouver, BC, Canada; [(b)]Department of Physics and Astronomy, York University, Toronto, ON, Canada
[162] Division of Physics and Tomonaga Center for the History of the Universe, Faculty of Pure and Applied Sciences, University of Tsukuba, Tsukuba, Japan
[163] Department of Physics and Astronomy, Tufts University, Medford, MA, USA
[164] Department of Physics and Astronomy, University of California Irvine, Irvine, CA, USA
[165] University of West Attica, Athens, Greece

[166] Department of Physics and Astronomy, University of Uppsala, Uppsala, Sweden
[167] Department of Physics, University of Illinois, Urbana, IL, USA
[168] Instituto de Física Corpuscular (IFIC), Centro Mixto Universidad de Valencia-CSIC, Valencia, Spain
[169] Department of Physics, University of British Columbia, Vancouver, BC, Canada
[170] Department of Physics and Astronomy, University of Victoria, Victoria, BC, Canada
[171] Fakultät für Physik und Astronomie, Julius-Maximilians-Universität Würzburg, Würzburg, Germany
[172] Department of Physics, University of Warwick, Coventry, UK
[173] Waseda University, Tokyo, Japan
[174] Department of Particle Physics and Astrophysics, Weizmann Institute of Science, Rehovot, Israel
[175] Department of Physics, University of Wisconsin, Madison, WI, USA
[176] Fakultät für Mathematik und Naturwissenschaften, Fachgruppe Physik, Bergische Universität Wuppertal, Wuppertal, Germany
[177] Department of Physics, Yale University, New Haven, CT, USA
[178] Yerevan Physics Institute, Yerevan, Armenia

[a] Also at Affiliated with an Institute Formerly Covered by a Cooperation Agreement with CERN, Geneva, Switzerland
[b] Also at An-Najah National University, Nablus, Palestine
[c] Also at Borough of Manhattan Community College, City University of New York, New York, NY, USA
[d] Also at Center for Interdisciplinary Research and Innovation (CIRI-AUTH), Thessaloníki, Greece
[e] Also at Centre of Physics of the Universities of Minho and Porto (CF-UM-UP), Porto, Portugal
[f] Also at CERN, Geneva, Switzerland
[g] Also at Département de Physique Nucléaire et Corpusculaire, Université de Genève, Geneva, Switzerland
[h] Also at Departament de Fisica de la Universitat Autonoma de Barcelona, Barcelona, Spain
[i] Also at Department of Financial and Management Engineering, University of the Aegean, Chios, Greece
[j] Also at Department of Mathematical Sciences, University of South Africa, Johannesburg, South Africa
[k] Also at Department of Modern Physics and State Key Laboratory of Particle Detection and Electronics, University of Science and Technology of China, Hefei, China
[l] Also at Department of Physics, Bolu Abant Izzet Baysal University, Bolu, Türkiye
[m] Also at Department of Physics, King's College London, London, UK
[n] Also at Department of Physics, Stanford University, Stanford, CA, USA
[o] Also at Department of Physics, Stellenbosch University, Stellenbosch, South Africa
[p] Also at Department of Physics, University of Fribourg, Fribourg, Switzerland
[q] Also at Department of Physics, University of Thessaly, Volos, Greece
[r] Also at Department of Physics, Westmont College, Santa Barbara, USA
[s] Also at Faculty of Physics, Sofia University, 'St. Kliment Ohridski', Sofia, Bulgaria
[t] Also at Faculty of Physics, University of Bucharest, Bucharest, Romania
[u] Also at Hellenic Open University, Patras, Greece
[v] Also at Henan University, Kaifeng, China
[w] Also at Imam Mohammad Ibn Saud Islamic University, Riyadh, Saudi Arabia
[x] Also at Institucio Catalana de Recerca i Estudis Avancats, ICREA, Barcelona, Spain
[y] Also at Institut für Experimentalphysik, Universität Hamburg, Hamburg, Germany
[z] Also at Institute for Nuclear Research and Nuclear Energy (INRNE) of the Bulgarian Academy of Sciences, Sofia, Bulgaria
[aa] Also at Institute of Applied Physics, Mohammed VI Polytechnic University, Ben Guerir, Morocco
[ab] Also at Institute of Particle Physics (IPP), Toronto, Canada
[ac] Also at Institute of Physics and Technology, Mongolian Academy of Sciences, Ulaanbaatar, Mongolia
[ad] Also at Institute of Physics, Azerbaijan Academy of Sciences, Baku, Azerbaijan
[ae] Also at Institute of Theoretical Physics, Ilia State University, Tbilisi, Georgia
[af] Also at Millennium Institute for Subatomic Physics at High Energy Frontier (SAPHIR), Santiago, Chile
[ag] Also at National Institute of Physics, University of the Philippines Diliman (Philippines), Quezon City, Philippines
[ah] Also at The Collaborative Innovation Center of Quantum Matter (CICQM), Beijing, China
[ai] Also at TRIUMF, Vancouver, BC, Canada
[aj] Also at Università di Napoli Parthenope, Naples, Italy

[ak] Also at University of Chinese Academy of Sciences (UCAS), Beijing, China
[al] Also at Department of Physics , University of Colorado Boulder, Colorado, USA
[am] Also at University of Siena, Siena, Italy
[an] Also at Washington College, Chestertown, MD, USA
[ao] Also at Physics Department, Yeditepe University, Istanbul, Türkiye
*Deceased